AN ABSTRACT OF THE DISSERTATION OF

George Francis Neuhaus for the degree of Doctor of Philosophy in Chemistry presented on May 28, 2020.

Title: Gene Expression, Structure Elucidation, and Bioactivity of *Aspergillus* Natural Products.

Abstract approved:

_____

Sandra Loesgen

The study of natural products (NPs) and their application has shaped humanity. Starting with the idea of using plants as medicine, it has now grown into the science of purifying and identifying organic molecules from nature to study their inherent biological activities. Understanding the molecular structures of NPs is the first critical step in their application. Along with many organisms, fungi have a record of producing a multitude of small organic molecules that have impacted society. The ubiquitous

genus *Aspergillus* is known to taint crops with mycotoxins but is also able to produce the lifesaving cholesterol lowering statins. In this thesis, known and new NPs from *Aspergillus* were studied. The research is set out over three chapters. Chapter two utilizes LCMS-based metabolomics and RNA sequencing to explore the differential regulation of NPs in *Aspergillus nidulans* spores. Mutant strains that lack transcription factors critical for conidiation exhibited greatly varied NP production, which may indicate a specific function for NPs in sporulation and fungal development. Chapter three focuses on the discovery and structure elucidation of five new drimane sesquiterpenes from *Aspergillus ustus*. Following bioactivity-guided fractionation, antibiotic synergism was found between the newly discovered metabolite named ustusoic acid B (**3.5**) and stromemycin (**3.6**). Chapter four highlights the structure elucidation of four new polyketides from *Aspergillus porosus*. Here, the absolute configuration of these flexible polyketides was supported by guiding the DFT-based conformational search with experimental parameters. Together, this thesis explores both the function and application of fungal NPs and introduces newly discovered metabolites, from their structure determination to their bioactivity.

Gene Expression, Structure Elucidation, and Bioactivity of *Aspergillus* Natural Products

By

George Francis Neuhaus

A DISSERTATION

submitted to

Oregon State University

in partial fulfillment of
the requirements for the
degree of

Doctor of Philosophy

Presented May 28, 2020
Commencement June 2020

Doctor of Philosophy dissertation of George Francis Neuhaus presented on May 28, 2020

APPROVED:

Major Professor, representing Chemistry

Head of the Department of Chemistry

Dean of the Graduate School

I understand that my dissertation will become part of the permanent collection of Oregon State University libraries. My signature below authorizes release of my dissertation to any reader upon request.

George Francis Neuhaus, Author

ACKNOWLEDGEMENTS

My initial thanks go to my advisor, Prof. Sandra Loesgen. Thank you for your dedication in guiding me though graduate school and for motivating me to achieve my highest potential. Your passion and curiosity for chemistry, along with your endless support and positivity, will continue to inspire and motivate me throughout my future endeavors.

In addition, I need to thank Prof. Kerry McPhail. I admire your dedication and support for not only your own students, but for all students here at Oregon State. You have been an outstanding role model and you will continue to influence my career.

I must also thank my friends and my lab members. My friends were with me throughout graduate school and I thank them for all the support. I also had the pleasure to work with the greatest laboratory members one could ask for. Thank you for providing me with an inspiring and supporting environment. Special thanks to Dr. Ross Overacker, Dr. Birte Plitzko, Dr. Donovon Adpressa, Dr. Chenxi (Zoe) Zhu, Paige Mandelare, and Elizabeth Kaweesa. May we remain close throughout the future.

My family offered endless support throughout my graduate career. I need to thank my parents, John and Elaine Neuhaus, and my sister, Katie Neuhaus, for their endless love. Most importantly, I need to thank my wife, Nikita Neuhaus. She has been right by my side for all graduate school offering her love and support. Thank you, Nikita, for all you have done.

CONTRIBUTION OF AUTHORS

Prof. Sandra Loesgen was the major advisor on all projects and assisted with the design and writing of all chapters contained herein. In Chapter two, genetic mutants of *A. nidulans* were generated by Dr. Ming-Yueh Wu and Dr. Jae-Hyuk Yu. RNA sequencing and relative gene expression analysis of secondary metabolite gene clusters were generated by Dr. Ming-Yueh Wu, Dr. Matthew E. Mead and Dr. Antonis Rokas. Dr. Mi-Kyung Lee and Dr. Hee-Soo Park performed the genome-wide analyses of genetic mutants, including Venn diagram analysis and the Gene Ontology term enrichment analysis. Dr. Donovon Adpressa assisted in organic extraction and metabolomics analysis of spore extracts in Chapter two, as well as with the computation of ECD spectra and NMR chemical shift values presented in Chapter four. Dr. Torsten Bruhn aided in reevaluation of the conformer ensemble for porosuphenol A and assisted in the examination of various levels of theory and basis set pairs for energy minimization calculations presented in Chapter four.

TABLE OF CONTENTS

TABLE OF CONTENTS (Continued)

LIST OF FIGURES

LIST OF FIGURES (Continued)

LIST OF FIGURES (Continued)

LIST OF TABLES

Table Page

LIST OF APPENDIX FIGURES

Figure Page

LIST OF APPENDEX FIGURES (Continued)

LIST OF APPENDEX FIGURES (Continued)

LIST OF APPENDEX FIGURES (Continued)

LIST OF APPENDEX FIGURES (Continued)

LIST OF APPENDIX TABLES

Chapter One: General Introduction

George F. Neuhaus

1.1 History of natural products

Natural Products (NPs), also referred to as secondary metabolites (SMs), are organic molecules produced by organisms that are not required for growth, but offer an evolutionary advantage.[1] Humans have been utilising these small molecules since long before the establishment of chemical sciences.[2] The first records of using NPs are found in traditional medicine where people recorded that certain plants are effective in treating illness. For example, in 2600 BC, ancient Mesopotamians recorded that the oils of cedar, cypress, and myrrh, among others, could be used to treat a range of ailments including coughs, colds, inflammation, and parasite infections.[3] From the ancient Egyptians, we also inherited texts describing the use of plants, animal organs, and minerals to treat various diseases dating back as far as 2900 BC, with the most famous record being "Ebers Papyrus" from 1500 BC.[4] Additionally, traditional Chinese medicine dates back to 1100 BC, with *Materia Medica*, Shennong Herbal, and the Tang Herbal documenting many herbal medicines.[5] Around 300 BC, the ancient western world began to document the first herbal drugs in literary works with the earliest coming from the Greek philosopher Theophrastus in 'History of Plants'.[3a, 6] These documented medicinal plants and natural remedies set the foundation for medicine and medical treatments as we know them today.

The idea of purifying the active components within remedies began to take shape much later. In the 1800's, with the transition from alchemy to systematic chemical

sciences, many NPs were isolated from various therapeutically relevant plants. One of the first was morphine (**1.1**), isolated from the opium poppy in 1806 (Figure 1.1). Morphine went on to be one of the first commercially pure NPs sold as a medicine in 1826 by E. Merck and is still extensively used today as an analgesic despite its addictive effects.[7] Morphine's discovery heralded the identification of numerous additional

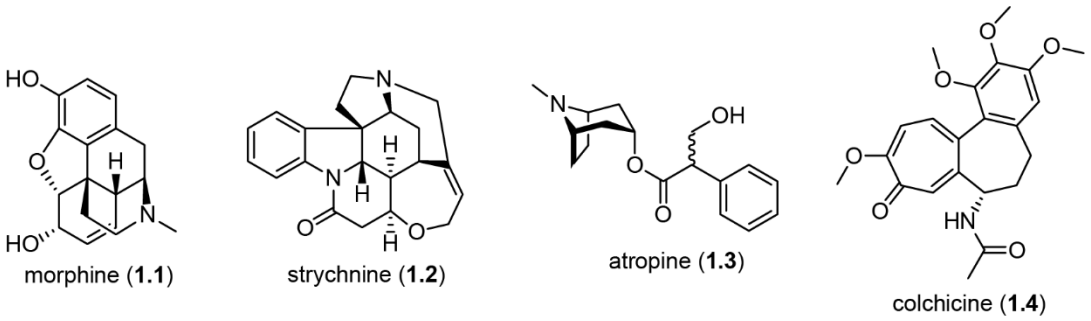

Figure 1.1: Structures of some of the first NPs isolated from nature

NPs including strychnine (**1.2**), atropine (**1.3**), and colchicine (**1.4**),[3a] thus forever changing medicine and shaping organic chemistry as we know it today (Figure 1.1). Even in 2020, NPs have continued to inspire half of all the FDA approved small molecule drugs used to treat illness in the US.[8] In addition, NPs are relevant to applications beyond medicine. In agriculture, it was found that compounds such as strobilurin,[9] azadirachtin, and rotenone could protect crops by acting as fungicides and insecticides.[10] Additionally, NPs have had a long history of use in cosmetics and personal healthcare products as fragrances and ointments,[11] as well as in foods as flavorings and coloring agents. Finally, NP chemistry can provide insight into the

chemical ecology of plants, animals, and microorganisms.[12] Altogether, the ability to isolate pure chemical components from nature has provided countless benefits to society and lead to an influx of interest in solving the unique molecular structures of these useful compounds.

1.2 Structure elucidation

By 1860, the conceptual framework for determining the molecular structure of a NP started to take shape. With the advent of structural theory, chemists started to implement early chemical techniques to gain information about a molecular structure, such as for **1.1** or **1.2**.[13] These initial approaches were time-consuming, involving early spectroscopic techniques along with degradation and derivatization reactions. During this time, there were great advances in synthetic organic approaches,[13a] which allowed chemists to build NPs from scratch and with more material, they enabled better evidence of their molecular structures. Considering the limitations in spectral analysis, chemical synthesis, and chemical knowledge at the time, determining a molecular structure often required years of intellectually demanding work. For example strychnine was isolated in 1818, but it took over 100 years, until 1956 to reveal its correct structure (Figure 1.2).[13a] At the heart of every structure elucidation, from small molecules to macromolecules like proteins and DNA, is the gathering of adequate experimental evidence in support of the proposed structure, which historically was linked to the development of various analytical techniques.

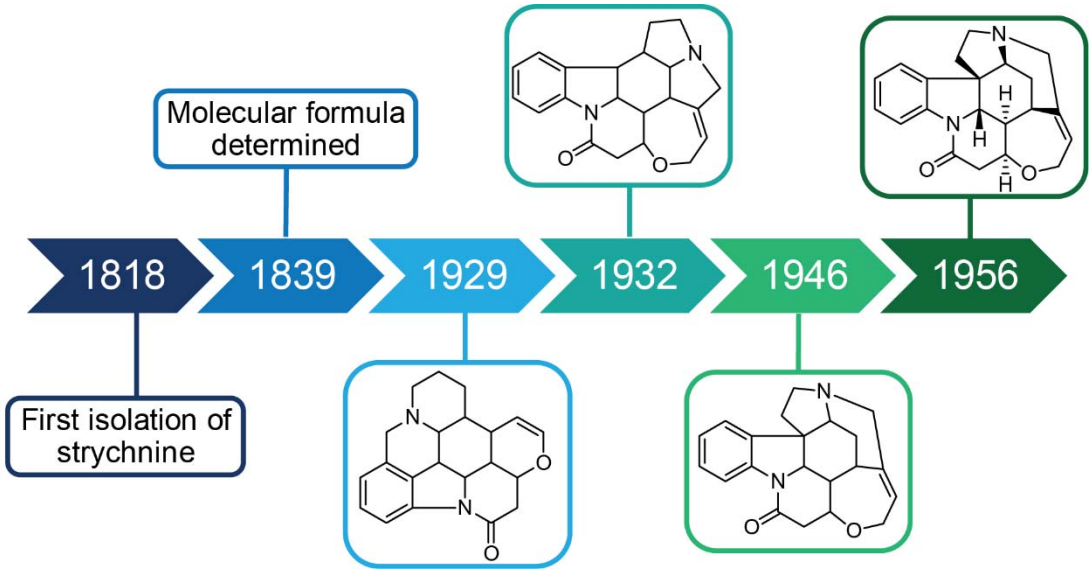

Figure 1.2: Timeline for structure elucidation and subsequent corrections of the NP strychnine

Today, chemists have advanced spectroscopic and chromatographic techniques to aid in the isolation and structural elucidation process for a given NP. The introduction and further advances in mass spectrometry (MS),[14] X-ray crystallography,[15], electron diffraction,[16] and nuclear magnetic resonance (NMR)[17] have allowed chemists to quickly elucidate structures on increasingly smaller amounts of material. Despite all the advances, there are still challenges inherent in the structure determination of an unknown compound, and recent reviews predict that at modest predictions, at least two percent of NPs published actually require structural revisions (Figure 1.3).[18] A good practice approach should include multiple lines of evidence to support a structural assignment, and combine the analysis of NMR, mass spectrometry, X-ray, and

chiroptical data. In recent years, modelling experimental data with computations has provided additional evidence to support experimental data.[19] Roughly 1600 new NPs are introduced into the world on average every year, with many of them featuring novel structural entities.[18a] The determination of the absolute structure of a NP remains an art and a necessary challenge to make use of the full benefits that NPs can bring to society.

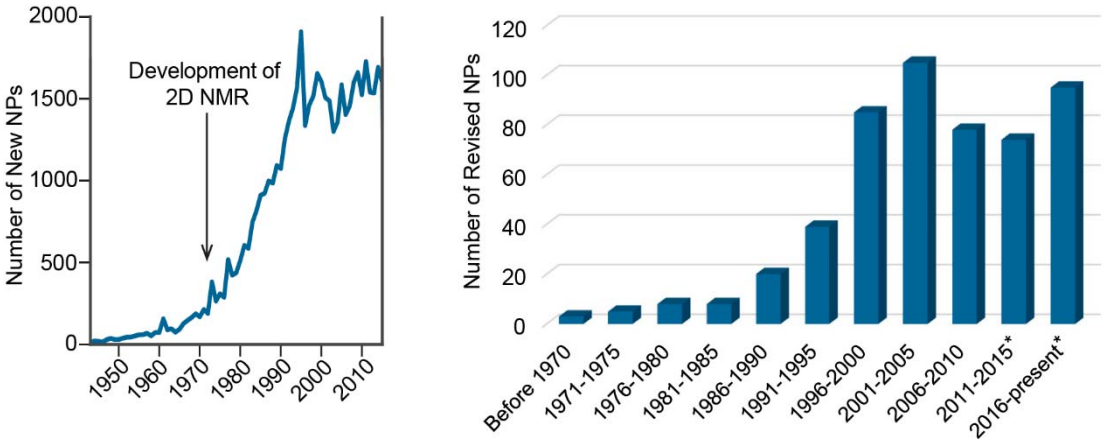

Figure 1.3: Left) Total number of new natural products (recreated from ref [18a]). Right) Number of NP revisions per 5-year period (recreated from ref [18e]). *Extrapolated from 2010 to present with Scifinder search for natural product revisions.

1.3 Natural products and chemical ecology of *Aspergillus* fungi

The study of fungal NPs gained momentum in the 1920's with the discovery of the antibiotic penicillin (**1.8**)[20] and the application of the medically useful ergot alkaloids.[21] This early success triggered great interest in fungi and focus was put on the ubiquitous genus *Aspergillus.* This saprophytic mold, with species such as *A. fumigatus* that is known to cause aspergillosis in humans and animals,[22] has been identified to grow in

most ecological niches around the world, even found aboard the international space station recently.[23] All species of *Aspergillus* are well known to produce a large array of NPs that impact humanity in both positive and negative ways (Figure 1.4). Some, like *A. terreus*, produce lifesaving pharmaceuticals such as the statins (**1.7**),[24] while others, such as *A. flavus*, are contaminants of food stocks and can synthesize carcinogenic compounds like the aflatoxins (**1.5**).[25]

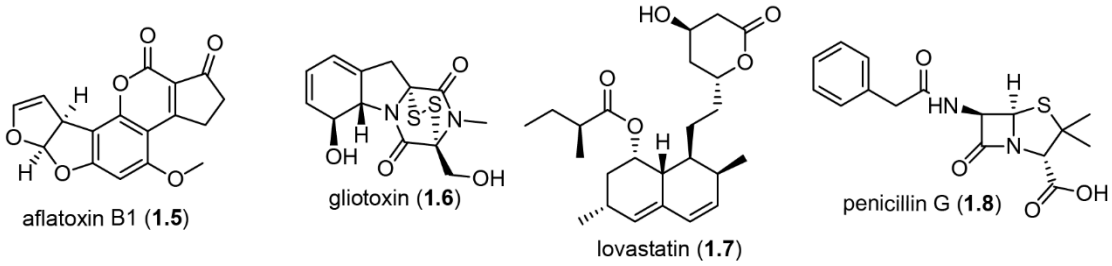

Figure 1.4: NPs from genus *Aspergillus*

With numerous applications in human health and wellbeing, it is no doubt that fungal NPs are useful to society. But why have fungi evolved to produce NPs in the first place? Early studies have shown NPs from plant associated fungi can enhance competitiveness of the plant and the fungus by acting as feeding deterrents against insects and vertebrates.[26] Recent work with *A. fumigatus* has shown that NPs such as gliotoxin (**1.6**) can combat a host's immune system to aid in infection.[27] The fungus then uses an arsenal of other NPs to gather nutrients and fight off competitors.[27] From communicating with other organisms to sequestering nutrients from the environment, fungal NPs have allowed these eukaryotes to thrive in almost every ecological niche.

1.4 Fungal natural product discovery today: genetics and metabolomics

In the United States there are more than 2.8 million antibiotic-resistant infections per year, with more than 35,000 deaths per year attributed.[28] As we now find ourselves in the 'post-antibiotic era',[28] facing a global viral pandemic in 2020 with threatening bacterial co-infections, the need for new antibiotics is dire. Despite having already mined fungal NPs for bioactivity for the last 100 years, with great success in the area of antibiotics,[29] current estimates show that there is still a great potential of finding new bioactive fungal NPs.[30] Currently, about 100,000 fungal species are known, but it is estimated that over a million species inhabit our planet, meaning most fungi have not been subjected to chemical analysis.[30a] Furthermore, advances in genome sequencing indicate that fungi harbor a vast biosynthetic potential to produce more NPs then what has been discovered.[30c] With genetic information as a road map, many silent or cryptic gene clusters have been targeted with an array of genetic or elicitation techniques and expressed, resulting in the discovery of new fungal NPs.[25b, 31] The well of structural diversity that remains within the fungal genome may be holding the next antibiotics that can help in the fight against antibiotic resistance.

In recent years, aside from genetic techniques, advances in metabolomic analysis of mass spectroscopic data has facilitated the discovery of novel fungal NPs.[25b, 30b, 32] This technique is particularly useful when comparing two or more growth conditions as it allows for rapid detection and dereplication of any metabolic changes. Utilizing

LCMS based multivariate techniques, such as molecular networking or relative abundance analysis, have been greatly beneficial to discover new NPs.[33] Pairing LCMS-based metabolomics approaches with genetic approaches such as use of genetic mutants generated by gene deletion, gene overexpression, or heterologous expression, or non-genetic elicitation approaches, such as epigenetic perturbation or the OSMAC approach (one strain many compounds), has resulted in the discovery of new NPs.[32a, 34] A recent example used LCMS-guided metabolomics to track metabolic changes between a genetic mutant of *Fusarium graminearum*, in which histone modifying enzyme Kmt6 was deleted, and the wildtype strain. This resulted in the discovery of three new NPs, protofusarin, tricinolone, and tricinolonoic acid, from the extensively studied *F. graminearum*.[34b] OMICS techniques have shown us that fungi have many more NPs to offer and continue to inspire the chemical sciences and applications.

1.5 Chapter overview

My thesis work is focused on the analysis and discovery of known and new NPs from *Aspergillus* species. In the following chapters I describe work done by myself and in collaboration to analyze gene regulation of known NPs and determine the absolute structure of newly discovered NPs. To accomplish this, I utilized LCMS-based metabolomics (chapter two) along with state-of-the art NMR and DFT-based computational techniques (chapters three and four).

Chapter two is focused on understanding the role of the transcription factors WetA, VosA, and VelB in the development of *Aspergillus nidulans*, particularly in conidiation and secondary metabolite biosynthesis. Knockout mutants of these transcription factors were generated, and the transcriptome and secondary metabolome of the mutant spores were compared to the wildtype. Almost half of the *A. nidulans* genome was differentially regulated in each null mutant. In addition, each mutant had differential expression of austinol (**2.1**), sterigmatocystin (**2.3**), and the emericellamides (**2.7**) in spores. This chapter is written in manuscript form and is currently in preparation for submission.

In chapter three, bioactivity-guided fractionation lead to the discovery of five new fungal sesquiterpenes along with eight known metabolites from *Aspergillus ustus*. The new structures were determined using conventional 1D and 2D NMR techniques while their absolute configuration was determined by a comparison of experimental and computational NMR chemical shifts and chiroptical properties. Bioactivity-guided fractionation revealed that three of the isolated compounds exhibit weak activity against Gram-positive bacterial pathogens. Synergism could be shown when ustusoic acid B (**3.5**) was combined with equal amounts (μg/mL) of stromemycin (**3.6**), which was isolated from the same fungus. This chapter is written in manuscript form and is currently in preparation for submission.

Chapter four recounts the discovery of four new polyketides and two known diterpenes from *Aspergillus porosus*. The planar structures were solved from 1D and 2D NMR data. The absolute configuration was determined using a range of techniques, including Mosher ester analysis, a *J*-based conformational analysis, and DFT-based computation of NMR and chiroptical properties. Due to the conformational freedom of the linear polyketides, a new approach utilizing experimental parameters to guide the conformational search was implemented. In addition, the cytotoxic activity of the known diterpene sphaeropsidin A (**4.4**) was confirmed, while its co-isolated congener aspergiloid E (**4.5**) was inactive. This chapter is adapted from the published article Neuhaus, G.F.; Adpressa, D.A.; Bruhn, T.; Loesgen, S. 'Polyketides from Marine-Derived *Aspergillus porosus*: Challenges and Opportunities for Determining Absolute Configuration" *Journal of Natural Products* **2019**, *82*, 2780-2789 (DOI 10.1021/acs.jnatprod.9b00416).

The final chapter presents a conclusion of the works presented, including a summary of the methods used to analyze the secondary metabolism of a gene knockout variant of *A. nidulans* and to elucidate new fungal NPs from *Aspergillus* sp. and determine their bioactivity. In addition, it offers a brief perspective on the future of structure elucidation and fungal NP discovery.

1.6 References

(1) Dewick, P. M., *Medicinal Natural Products: A Biosynthetic Approach, 3rd Edition*. John Wiley & Sons, Ltd.: The Atrium, Southern Gate, Chichester, West Sussex, PO19 8SQ, United Kingdom, 2009.

(2) Sneader, W., *Drug Discovery: A History*. John Wiley & Sons Ltd: The Atrium, Southern Gate, Chichester, West Sussex Po19 8SQ, England, 2005.

(3) (a) Newman, D. J.; Cragg, G. M.; Snader, K. M. *Natural Product Reports* **2000**, *17*, 215. (b) Borchardt, J. *Drug News & Perspectives* **2002**, *15*, 187.

(4) (a) Cragg, G. M.; Newman, D. J. *Biochimica et Biophysica Acta* **2013**, *1830*, 3670. (b) Abou El-Soud, N. *Journal of Medicinal Plants Research* **2010**, *4*, 82.

(5) (a) Cragg, G. M.; Newman, D. J. *Pure and Applied Chemistry* **2005**, *77*, 7. (b) Zhu, Y.-P.; Woerdenbag, H. J. *Pharmacy World and Science* **1995**, *17*, 103.

(6) Scarborough, J. *Journal of the History of Biology* **1978**, *11*, 353.

(7) Brownstein, M. J. *Proceedings of the National Academy of Sciences* **1993**, *90*, 5391.

(8) Newman, D. J.; Cragg, G. M. *Journal of Natural Products* **2020**, *83*, 770.

(9) Nofiani, R.; de Mattos-Shipley, K.; Lebe, K. E.; Han, L.-C.; Iqbal, Z.; Bailey, A. M.; Willis, C. L.; Simpson, T. J.; Cox, R. J. *Nature Communications* **2018**, *9*, 3940.

(10) Dayan, F. E.; Cantrell, C. L.; Duke, S. O. *Bioorganic & Medicinal Chemistry* **2009**, *17*, 4022.

(11) Carvalho, I. T.; Estevinho, B. N.; Santos, L. *International Journal of Cosmetic Science* **2016**, *38*, 109.

(12) (a) Dean, L. J.; Prinsep, M. R. *Natural Product Reports* **2017**, *34*, 1359. (b) Spiteller, P. *Natural Product Reports* **2015**, *32*, 971. (c) Eisner, T. *Proceedings of the National Academy of Sciences* **2003**, *100*, 14517.

(13) (a) Hoffmann, R. W., *Classical Methods in Structure Elucidation of Natural Products*. Wiley: 2018. (b) Staab, H. A. *Angewandte Chemie* **1958**, *70*, 37.

(14) Bouslimani, A.; Sanchez, L. M.; Garg, N.; Dorrestein, P. C. *Natural Product Reports* **2014**, *31*, 718.

(15) (a) Wagner, U.; Kratky, C. *Progress in the Chemistry of Organic Natural Products* **2015**, *100*, 1. (b) Hoshino, M.; Khutia, A.; Xing, H.; Inokuma, Y.; Fujita, M. *IUCrJ* **2016**, *3*, 139.

(16) De Carlo, S.; Gruene, T. *Angewandte Chemie International Edition* **2018**, *57*, 16313.

(17) (a) Breton, R. C.; Reynolds, W. F. *Natural Product Reports* **2013**, *30*, 501. (b) Aue, W. P.; Bartholdi, E.; Ernst, R. R. *The Journal of Chemical Physics* **1976**,

64, 2229. (c) Halabalaki, M.; Vougogiannopoulou, K.; Mikros, E.; Skaltsounis, A. L. *Current Opinion in Biotechnology* **2014**, *25*, 1.
(18) (a) Pye, C. R.; Bertin, M. J.; Lokey, R. S.; Gerwick, W. H.; Linington, R. G. *Proceedings of the National Academy of Sciences* **2017**, *114*, 5601. (b) Nicolaou, K. C.; Snyder, S. A. *Angewandte Chemie International Edition* **2005**, *44*, 1012. (c) Maier, M. E. *Natural Product Reports* **2009**, *26*, 1105. (d) Usami, Y. *Marine Drugs* **2009**, *7*, 314. (e) Suyama, T. L.; Gerwick, W. H.; McPhail, K. L. *Bioorganic & Medicinal Chemistry* **2011**, *19*, 6675. (f) Chhetri, B. K.; Lavoie, S.; Sweeney-Jones, A. M.; Kubanek, J. *Natural Product Reports* **2018**, *35*, 514.
(19) (a) Nugroho, A. E.; Morita, H. *Journal of Natural Medicines* **2019**, *73*, 687. (b) Grauso, L.; Teta, R.; Esposito, G.; Menna, M.; Mangoni, A. *Natural Product Reports* **2019**, *36*, 1005. (c) Lodewyk, M. W.; Siebert, M. R.; Tantillo, D. J. *Chemical Reviews* **2012**, *112*, 1839.
(20) Alharbi, S. A.; Wainwright, M.; Alahmadi, T. A.; Salleeh, H. B.; Faden, A. A.; Chinnathambi, A. *Saudi Journal of Biological Sciences* **2014**, *21*, 289.
(21) Schiff, P. L. *American Journal of Pharmaceutical Education* **2006**, *70*, 98.
(22) Latgé, J.-P. *Clinical Microbiology Reviews* **1999**, *12*, 310.
(23) Knox, B. P.; Blachowicz, A.; Palmer, J. M.; Romsdahl, J.; Huttenlocher, A.; Wang, C. C. C.; Keller, N. P.; Venkateswaran, K. *mSphere* **2016**, *1*, e00227.
(24) Tobert, J. A. *Nature Reviews Drug Discovery* **2003**, *2*, 517.
(25) (a) Rushing, B. R.; Selim, M. I. *Food and Chemical Toxicology* **2019**, *124*, 81. (b) Sanchez, J. F.; Somoza, A. D.; Keller, N. P.; Wang, C. C. C. *Natural Product Reports* **2012**, *29*, 351. (c) Amare, M. G.; Keller, N. P. *Fungal Genetics and Biology* **2014**, *66*, 11.
(26) (a) Kempken, F.; Rohlfs, M. *Fungal Ecology* **2010**, *3*, 107. (b) Kusari, S.; Hertweck, C.; Spiteller, M. *Chemistry & Biology* **2012**, *19*, 792.
(27) Raffa, N.; Keller, N. P. *PLOS Pathogens* **2019**, *15*, e1007606.
(28) CDC, Antibiotic Resistance Threats in the United States. Services, U. S. D. o. H. a. H., Ed. CDC: Atlanta, GA, 2019.
(29) Hutchings, M.; Truman, A.; Wilkinson, B. *Current Opinion in Microbiology* **2019**, *51*, 72.
(30) (a) Schueffler, A.; Anke, T. *Natural Product Reports* **2014**, *31*, 1425. (b) Hautbergue, T.; Jamin, E. L.; Debrauwer, L.; Puel, O.; Oswald, I. P. *Natural Product Reports* **2018**, *35*, 147. (c) Rutledge, P. J.; Challis, G. L. *Nature Reviews Microbiology* **2015**, *13*, 509.
(31) (a) Romsdahl, J.; Wang, C. C. C. *MedChemComm* **2019**, *10*, 840. (b) Scherlach, K.; Hertweck, C. *Organic & Biomolecular Chemistry* **2009**, *7*, 1753. (c) Guo, C.-J.; Wang, C. C. C. *Frontiers in Microbiology* **2014**, *5*. (d) Bok, J. W.;

Hoffmeister, D.; Maggio-Hall, L. A.; Murillo, R.; Glasner, J. D.; Keller, N. P. *Chemistry & Biology* **2006**, *13*, 31.

(32) (a) Albright, J. C.; Henke, M. T.; Soukup, A. A.; McClure, R. A.; Thomson, R. J.; Keller, N. P.; Kelleher, N. L. *ACS Chemical Biology* **2015**, *10*, 1535. (b) Covington, B. C.; McLean, J. A.; Bachmann, B. O. *Natural Product Reports* **2017**, *34*, 6.

(33) (a) Bader, C. D.; Panter, F.; Müller, R. *Biotechnology Advances* **2020**, *39*, 107480. (b) Adpressa, D. A.; Loesgen, S. *Chemistry & Biodiversity* **2016**, *13*, 253. (c) Sproule, A.; Correa, H.; Decken, A.; Haltli, B.; Berrué, F.; Overy, D. P.; Kerr, R. G. *Marine Drugs* **2019**, *17*, 347. (d) Macintyre, L.; Zhang, T.; Viegelmann, C.; Martinez, I. J.; Cheng, C.; Dowdells, C.; Abdelmohsen, U. R.; Gernert, C.; Hentschel, U.; Edrada-Ebel, R. *Marine Drugs* **2014**, *12*, 3416. (e) Roullier, C.; Bertrand, S.; Blanchet, E.; Peigné, M.; Robiou du Pont, T.; Guitton, Y.; Pouchus, Y. F.; Grovel, O. *Marine Drugs* **2016**, *14*, 103.

(34) (a) Clevenger, K. D.; Bok, J. W.; Ye, R.; Miley, G. P.; Verdan, M. H.; Velk, T.; Chen, C.; Yang, K.; Robey, M. T.; Gao, P.; Lamprecht, M.; Thomas, P. M.; Islam, M. N.; Palmer, J. M.; Wu, C. C.; Keller, N. P.; Kelleher, N. L. *Nature Chemical Biology* **2017**, *13*, 895. (b) Adpressa, D. A.; Connolly, L. R.; Konkel, Z. M.; Neuhaus, G. F.; Chang, X. L.; Pierce, B. R.; Smith, K. M.; Freitag, M.; Loesgen, S. *Fungal Genetics and Biology* **2019**, *132*, 103256. (c) Henke, M. T.; Soukup, A. A.; Goering, A. W.; McClure, R. A.; Thomson, R. J.; Keller, N. P.; Kelleher, N. L. *ACS Chemical Biology* **2016**, *11*, 2117. (d) Nguyen, Q.-T.; Merlo, M. E.; Medema, M. H.; Jankevics, A.; Breitling, R.; Takano, E. *FEBS Letters* **2012**, *586*, 2177.

Chapter Two: The Role of WetA, VosA, and VelB in the Regulation of Secondary Metabolism in *Aspergillus nidulans* Conidia

Ming-Yueh Wu, Matthew E. Mead, Mi-Kyung Lee, George F. Neuhaus, Donovon A. Adpressa, Julia I. Martien, Ye-Eun Son, Heungyun Moon, Daniel Amador-Noguez, Kap-Hoon Han, Antonis Rokas, Sandra Loesgen, Jae-Hyuk Yu, Hee-Soo Park

2.1 Abstract

Asexual sporulation is a fundamental reproductive mode in filamentous fungi, particularly among ascomycetes, the largest phylum of fungi. Formation of resilient spores (conidia) aids in fungal ecology and lifestyle, including infection of plants and humans. *Aspergillus nidulans* has emerged as a leading model for understanding conidiogenesis. Fungal development and production of conidia is tightly regulated, and progress has been made in recent years on understanding the genetic regulatory networks (GRNs) that govern asexual spore formation. WetA, VosA, and VelB are three transcription factors that have a role in regulating spore maturation and have been shown to affect secondary metabolism. Using *Aspergillus nidulans* as a model organism, this study explores the role WetA, VosA, and VelB play in secondary metabolite (SM) biosynthesis in conidia. RNA sequencing (RNAseq) of null mutant (Δ*wetA*, Δ*vosA*, Δ*velB*) derived conidia showed that almost half of the genes in *A. nidulans* genome were differentially regulated, especially SM biosynthesis. LCMS-based metabolomics analysis of spore extracts revealed strikingly different SM profiles for mutant and wildtype strains. The meroterpenoid austinol (**2.1**) was found to be down regulated in all three null mutants, while the mycotoxin sterigmatocystin (**2.3**) was found to be down regulated only in Δ*velB*. Emericellamides (**2.7**), mixed polyketide-peptide derived metabolites, were overproduced in the Δ*vosA* and Δ*velB* mutant spores. This study reveals that WetA, VosA, and VelB regulate the production of SMs in the

conidia of *A. nidulans* and hints that these secondary metabolites play a role in fungal development.

2.2 Introduction

The formation of asexual spores (conidia) is the most common reproductive method for filamentous fungi.[1] Conidiation contributes to the fecundity and fitness of many ascomycetes, allowing highly efficient protection of the genome for survival and propagation.[2] Many pathogenic fungi rely on conidia as the primary means of infecting host organisms,[3] and it has been shown that morphological development of conidia is coordinated with toxic secondary metabolite (SM) production.[4]

The ubiquitous fungal genus *Aspergillus*[5] has had an immense impact on society and all produce conidia as the main means of reproduction. Some species within this genus, such as *A. fumigatus*, act as plant and human pathogens causing aspergillosis,[6] while others like *A. flavus* can spoil food stocks by producing mycotoxins. Conversely, many *Aspergilli* have had a positive impact on society. *A. terreus* is known for producing important pharmaceuticals, such as lovastatin, while *A. oryzae's* role in fermentation for the production of soy sauce and sake in East Asian cuisine is well documented.[6-7]

Aspergillus nidulans has served as a model organism for over 60 years, helping to establish an understanding of many eukaryotic processes from genetic aspects to cell biology. It has recently emerged as the leading model for understanding conidiation.[6] *A. nidulans*, like other *Aspergilli*, is well known for producing NPs, including the mycotoxin sterigmatocystin (**2.3**), and the antibacterial compound penicillin.[7-8] This

SM production, along with the well understood sexual reproductive cycle, make *A. nidulans* an excellent model to study the regulation of conidiation and SM production.

The process of conidiation can be split into three stages. First, budding of the conidiophore, formation of metulae and phialides, and finally conidia formation and maturation.[9] This sequence is orchestrated by the central regulatory cascade *brlA*→*adaA*→*wetA*, with each gene acting as the central regulator for each step.[2b, 10] WetA is a transcription factor that governs the last step in conidiation, conidia formation and maturation and has been shown to greatly affect secondary metabolism in the conidia as well.[2, 4b, 11] Along with the central regulatory cascade, there are other levels of regulation in conidiation. For example, the *velvet* regulators are named for the lack of a velvety appearance in mutant strains lacking these transcription factors.[12] Two specific *velvet* proteins, VosA and VelB, work together in the conidia to confer spore maturation and dormancy.[13] They are also known to have a role in regulation of both fungal development and secondary metabolism.[13b, 14] Understanding how secondary metabolism is regulated in relation to conidiation would shed light on the function of SMs in conidia.

This study aims to explore the role of WetA, VosA, and VelB in the regulation of secondary metabolism in conidia. Using *Aspergillus nidulans* conidia from three null mutants, Δ*wetA*, Δ*vosA*, and Δ*velB*, gene expression was monitored using RNA sequencing. Next, secondary metabolism was analyzed by LCMS-based metabolomics.

These techniques together allow rapid detection and identification of SMs, enabling insights into how secondary metabolism is regulated during conidiation.

2.3 Results and discussion

A comparative analysis of gene expression differences between the wildtype (WT) and the three null mutants was performed to understand the roles of VosA, VelB, and WetA in *A. nidulans* (strain FGSC4) conidia (Figure 2.1A). Of the 10988 genes in the *A. nidulans* genome,[2b] it was found that 2649 genes were down regulated, and 3076 genes were up regulated in the Δ*wetA* null mutant when compared to the WT. Additionally, the Δ*vosA* null mutant had 1979 genes down regulated and 2520 genes up regulated as compared to the WT. Finally, in the Δ*velB* null mutant, 2359 genes were down regulated, and 2649 genes were up regulated compared to the WT. This indicates that all three transcription factors play a significant role in regulating conidiation, each differentially regulating roughly half of the genes in the *A. nidulans* genome. A closer look reveals that the Δ*wetA* null mutant solely regulates a substantial number of genes (1435 down regulated and 1357 up regulated). This matches the function of WetA as one of the transcription factors in the central regulatory cascade of conidiation, playing a major role in coordinating conidia maturation. Conversely, Δ*vosA* and Δ*velB* only have a small number of uniquely regulated genes but have large numbers of genes that are co-regulated with one or more of the other transcription

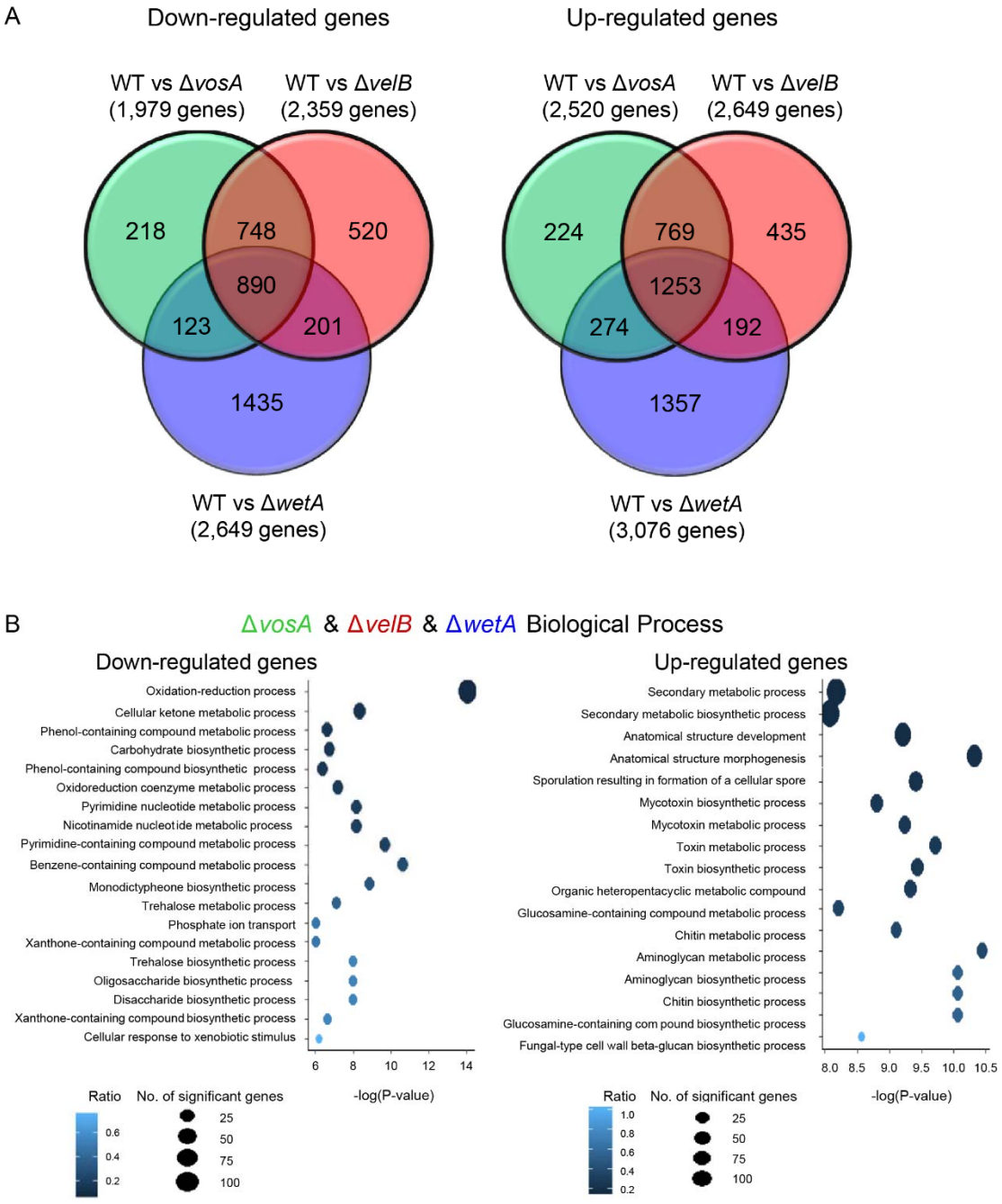

Figure 2.1: Genome-wide analyses of VosA, VelB, WetA-dependent genes in *A. nidulans* conidia. (A) Venn diagram showing VosA, VelB, and WetA-dependent genes in conidia. (B) Gene Ontology (GO) term enrichment analysis of differentially expressed genes in the Δ*vosA*, Δ*velB*, and Δ*wetA* conidia.

factors. This speaks to a more specialized role of VosA and VelB in conidiation, indicating they usually work in coordination with other transcription factors to regulate genes. [12, 13b, 14a]

Next, functional category analyses by determining Gene Ontology (GO) terms was performed to gain more insight into the regulatory roles of VosA, VelB, and WetA (Figure 2.1B). GO is a bioinformatics process to classify and group genes based on their function or their GO term. Figure 2.1B is displaying the GO terms (functions) that are most differentially regulated in the null mutants as compared to the WT. When looking at the GO terms that are down regulated in the null mutants, many genes involved with primary metabolism are differentially expressed. Specifically, genes involved in carbohydrate metabolism, nucleotide metabolism, and aromatic compound metabolism. The most down regulated genes are involved in oxidation and reduction processes. Conversely, the GO terms that are the most up regulated when compared to the WT are involved in secondary metabolism. Other functions that were up regulated are involved in forming anatomical structures, such as sporulation or cell wall biosynthesis.

To better understand the effects of transcription factor deletion on the secondary metabolism in the conidia, organic extracts of the conidia were prepared in biological triplicate. LCMS profiles (technical triplicate in both negative and positive mode) were imported into MZMine 2.38[15] for peak picking and generation of mass and retention

time pairs (m/z value and RT). First, a principal component analysis (PCA) was generated to visualize the variability amongst LCMS profiles of the conidia extracts (Figure A.1, Appendix A). The PCA indicates that there is great variability in the chemical makeup of the three null mutant derived extracts. The closest to the wildtype are Δ*wetA* spores, implying that these produce the most similar abundances and types of secondary metabolites. The Δ*velB* and Δ*vosA* extracts are distant, suggesting they are the most chemically unique. Next, to understand what accounts for these differences, an analysis of variance (ANOVA) was applied to the m/z value and RT pairs to generate relative expression plots (Figure 2.2).

The meroterpenoids austinol (**2.1**) and dehydroaustinol (**2.2**) were found to be down regulated in all three null mutants (Figure 2.3). These SMs are synthesized by coordination of two separate gene clusters.[16] Gene *ausA* (AN8383) encodes a nonreducing polyketide synthase that is responsible for synthesis of 3,5-dimethylorsellinic acid, a proposed precursor for the biosynthesis of these meroterpenoids. RNAseq reveals *ausA* is down regulated in Δ*velB*, with transcripts reduced by a factor of four when compared to the wildtype, and in Δ*wetA*. This is supported by these mutant spore extracts having the lowest ion abundance of austinol when compared to the wildtype. The *ausD* (AN8384) gene, encoding a protein with

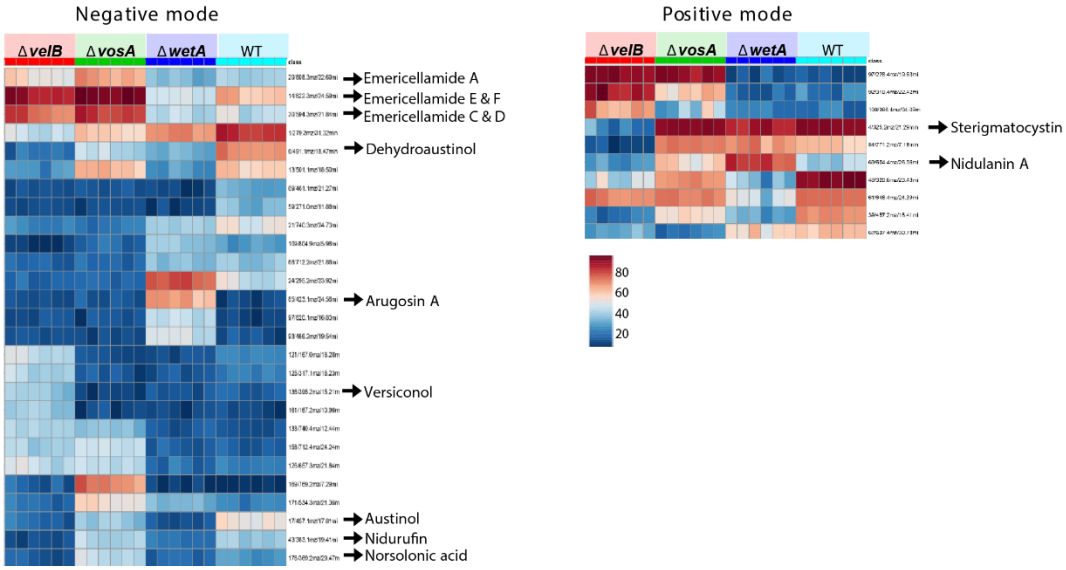

Figure 2.2: Relative expression plots of ion/retention time pairs detected in the WT, Δ*vosA*, Δ*velB*, and Δ*wetA* conidia extracts by LCMS analysis. The heatmap is color coded and represents high ion abundance (red) or low ion abundance (blue).

unknown function, is shown to be required in **2.1** biosynthesis.[16] It is down regulated in both Δ*wetA* and Δ*velB* mutants, supporting the secondary metabolite abundance data. Finally, a cytochrome P450 oxygenase, encoded by *ausG* (AN9248), is required in the last step of **2.1** biosynthesis and is down regulated in all three null mutants, by half to one quarter, depending on mutant, compared to the wildtype. The data set corroborates that WetA, VosA, and VelB play an important role in regulating the biosynthesis of **2.1** and **2.2** and may hint to a function for these meroterpenes in fungal development.

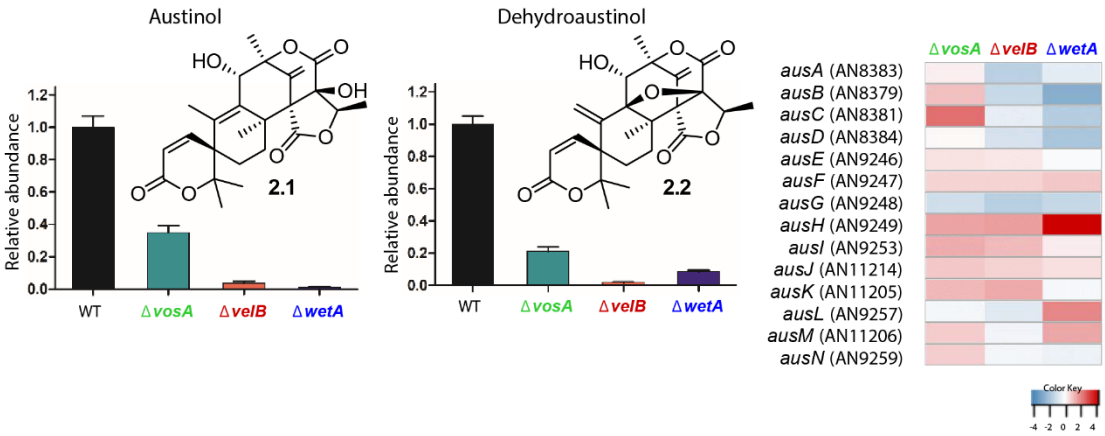

Figure 2.3: Left panel: The ion abundance of **2.1** and **2.2** in the WT, Δ*vosA*, Δ*velB*, and Δ*wetA* conidia with their structures. Right panel: The mRNA expression relative to the wildtype of genes associated with the austinol biosynthesis in the Δ*vosA*, Δ*velB*, and Δ*wetA* conidia.

Sterigmatocystin (**2.3**) is a precursor to the aflatoxins, some of the most toxic and carcinogenic compounds among all fungal mycotoxins.[17] The **2.3** gene cluster contains 25 genes.[18] Compared to the wildtype, the ion abundance of **2.3** in the conidia extract was greatly reduced in Δ*velB*, while Δ*wetA* and Δ*vosA* displayed similar ion abundances compared to the wildtype (Figure 2.4). Levels of **2.3** precursors also varied in abundance across the null mutants. First, norsolorinic acid (**2.4**) and nidurufin (**2.5**)[19] were over abundant in Δ*vosA* spore extract. This correlated with high levels of mRNA for almost all genes in the cluster in both the Δ*vosA* and Δ*wetA* conidia. There was an average of an 8-fold increase in transcripts across the gene cluster in Δ*vosA*, while Δ*wetA* had an average of 3.5-fold increase. Next, versiconol (**2.6**), a shunt metabolite,[19b, 20] was found to be most abundant in Δ*velB* spore extract and in general,

RNAseq data for the Δ*velB* mutant indicated that many genes were down regulated in comparison to the wildtype, especially the mRNA levels of *stcL*, *stcN*, *stcQ*, *stcT*, *stcU*, *stcV*, and *stcW*. Most of these genes are downstream of **2.6**,[17b, 18] helping explain the abundance of **2.6** in the Δ*velB* conidia. Overall the expression data corroborates that WetA, VosA, and VelB regulate **2.3** biosynthesis,[8] and suggests that VosA and VelB play opposing roles in the regulatory mechanism.

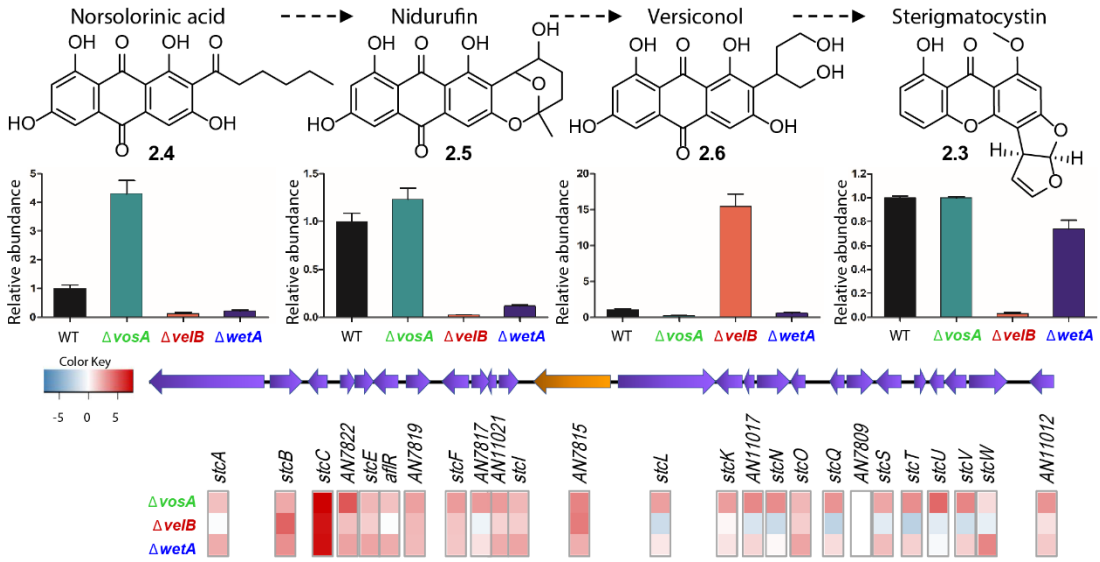

Figure 2.4: Top panel: Intermediates of the aflatoxin biosynthesis found in this study. Middle panel: The ion abundance of **2.4**, **2.5**, **2.6**, and **2.3** in the WT, Δ*vosA*, Δ*velB*, and Δ*wetA* conidia. Bottom panel: The sterigmatocystin gene cluster and mRNA expression levels relative to the wildtype for genes associated with sterigmatocystin biosynthesis in Δ*vosA*, Δ*velB*, and Δ*wetA* conidia.

Several *Aspergillus* species are known to make the emericellamides, cyclic peptides of mixed polyketide-nonribosomal peptide synthetase (NRPS) origin.[21] The gene cluster encoding these SMs contains both a highly reducing polyketide synthase and a

NRPS.[22] Emericellamide A (**2.7**), and congeners, were highly abundant in the spore extracts of Δ*vosA* and Δ*velB*. This was supported by high mRNA expression levels for all four required genes, *easA* (NRPS), *easB* (polyketide synthase), *easC* (acyltransferase), and *easD* (acyl-CoA ligase) (Figure 2.5). Interestingly, despite higher mRNA levels for Δ*wetA* as compared to the wildtype, the ion abundance of **2.7** was similar to the wildtype. This suggests a more complex regulatory mechanism in the Δ*wetA* conidia for the biosynthesis of the emericellamides.

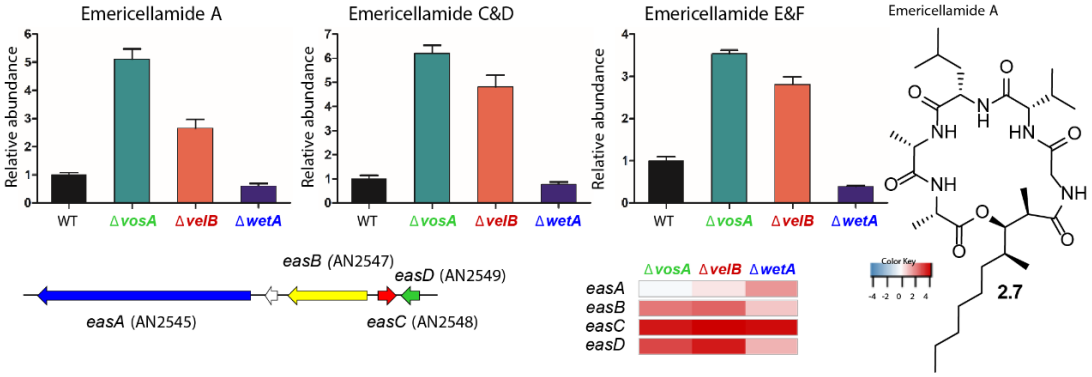

Figure 2.5: Top panel: Ion abundance of emericellamides (structure shown for **2.7**) in the WT, Δ*vosA*, Δ*velB*, and Δ*wetA* conidia. Bottom panel: The emericellamide gene cluster and the mRNA expression of genes relative to the wildtype associated with emericellamide biosynthesis in the Δ*vosA*, Δ*velB*, and Δ*wetA* conidia.

This study presents the comparative analysis of gene regulation and SM biosynthesis in the conidia of three null mutants of *Aspergillus nidulans*, Δ*wetA*, Δ*vosA*, and Δ*velB*, and the wildtype. These genes encoding for transcription factors have been found to broadly regulate about half of the genes in the genome. One area that was especially affected was SM biosynthesis. First, **2.1** and **2.2** were found in low

amounts in all mutants compared to the wildtype, suggesting all three, WetA, VosA, and VelB, highly affect the meroterpenoid production in the conidia. Second, **2.3**, a highly carcinogenic mycotoxin, was absent from Δ*velB*, but found in equal amounts in Δ*wetA* and Δ*vosA* when compared to the wildtype. This, along with the presence of the shunt metabolite **2.6** in Δ*velB* shows that VelB has a specialized and indispensable role in sterigmatocystin biosynthesis, regulating the downstream portion of the biosynthesis. Many sterigmatocystin (**2.3**) intermediates were found in high amounts in Δ*vosA* spores, suggesting this transcription factor has an opposing role in regulating the biosynthesis. Finally, the emericellamides had higher ion abundance in Δ*vosA* and Δ*velB* null mutant conidia compared to the wildtype. This suggests that VosA and VelB control the expression levels of these cyclic peptides. In summary, RNAseq data combined with comparative metabolomics revealed the regulation of individual SM biosynthetic pathways in conidia. Taken together, this study corroborates that WetA, VosA, and VelB form a complex regulatory network for the production of SMs in the conidia of *A. nidulans* and may indicated a role for these secondary metabolites in fungal development.

2.4 Experimental

Strains, media, and culture conditions

Fungal strains used in this study are listed in Table A.1 (Appendix A). Fungal strains were grown on solid or liquid minimal media with 1% glucose (MMG) (7 mM

KCl, 2 mM MgSO4, 70 mM NaNO3, 11.2 mM KH2PO4, 0.1% trace element solution pH 5.5) and appropriate supplements for general purposes as previously described.[2b, 14d, 23] For conidia samples, WT and mutant conidia were inoculated onto solid MMG plates and incubated for 48 h. Then, conidia were collected from plates using Miracloth (Calbiochem, San Diego, CA, USA) and stored at -80 °C.

Generation of *wetA*, *vosA* and *velB* deletion and complementation strains

We generated the deletion (Δ) and complementation (complement) strains of *wetA* in *A. nidulans* (*AniwetA*). The oligonucleotides used in this study are listed in Table A.2 (Appendix A). Briefly, the deletion construct containing the *A. fumigatus pyrG* marker with 5' and 3' flanking regions of *AniwetA* was introduced into recipient strain RJMP1.59.[24] To generate complemented strains, a WT *AniwetA* gene region, including its 2-kb upstream region, was cloned into plasmid pHS13.[13b] The resulting pMY1 plasmid was then introduced into recipient Δ*AniwetA* strain TMY3, resulting in isolation of strain TMY4. Multiple Δ*AniwetA* strains were generated, and all behaved the same. Multiple complement *AniwetA* strains were generated, and also behaved identically to one another. The *velB* and *vosA* delete mutants were generated in analogous ways.[13b]

Nucleic acid manipulation

The isolation of genomic DNA and total RNA for WetA RNA-seq and ChIP-seq was performed as previously described[2b, 25] and the same protocol was performed for

the *velB* and *vosA* mutant strains in this manuscript. Briefly, genomic DNA of all strains was isolated by adding ~0.3-0.5 mL of silica/zirconium beads, 0.5 mL of breaking buffer [2% Triton X-100, 1% SDS, 100 mM NaCl 10 mM Tris-HCl (pH 8.0), 1 mM EDTA], and 0.5 mL of phenol:chloroform:isoamylalcohol (25:24:1) to the mycelial samples followed by homogenizing in a Mini Bead Beater for 2 min. DNA in the aqueous phase was collected and ethanol precipitated. The purified genomic DNA in 50 µl of Tris-EDTA buffer was diluted 10 times for PCR reactions.

RNA sequencing (RNA-seq)

To isolate total RNA for RNA-seq analysis, total RNA from WT and mutant conidia was extracted using Trizol Reagent (Invitrogen, USA) according to the manufacturer's instructions with modification. To remove DNA contamination from RNA samples, DNase I (Promega, USA) was used and the RNA was purified using RNeasy Mini kit (Qiagen, USA). Three technical replicates of each sample were analyzed. RNA sequencing was performed as previous described.[26] RNA samples were submitted to the University of Wisconsin Gene Expression Center (Madison, WI, USA) for library preparation and sequencing. A strand-specific library was prepared using an Illumina TruSeq strand-specific RNA sample preparation system. The libraries of all the replicates were sequenced using an Illumina HiSeq 2500 system.

Data analysis of the *A. nidulans* WetA RNA-seq experiment was previously described and published[2b] and the same analysis pipeline was used for the *velB* and

vosA experiments described here. RNA isolated from wildtype conidia was compared to RNA isolated from a knockout mutant (either Δ*velB* or Δ*vosA*). Three technical replicates of each sample (WT, Δ*velB*, and Δ*vosA*) were analyzed. RNA samples were submitted to the University of Wisconsin Gene Expression Center (Madison, WI) for library preparation and sequencing. A strand-specific library was prepared using an Illumina TruSeq strand-specific RNA sample preparation system. The libraries of all the replicates were sequenced using an Illumina HiSeq 2500 system. Reads were mapped to the *A. nidulans* A4 transcriptome using Tophat2 version 2.1.1[27] and the parameter "--max-intron-length 4000". On average, 19.9 million reads per sample mapped to the genome, and the number of reads aligning to each gene was counted with HTseq-Count version 0.9.1.[28] DESeq version 1.14.1[29] was used to determine significantly differentially expressed genes, and genes were considered regulated if they exhibited an adjusted p-value less than 0.05 and either a log2 fold-change greater than one or less than negative one.

Functional enrichment analysis

Functional enrichment analyses including "GO Biological Process", "KEGG", "InterPro", and "Pfam" were carried out using the tool available at AspGD,[30] FungiDB, [31] and ShinyGO v0.60.[32] Unless otherwise stated, default settings were used in ShinyGO v0.60. The settings are as following: (Database: *Emericella nidulans* STRINGdb, P-value cutoff (FDR): 0.05, # of most significant terms to show: 30).

Secondary metabolites analysis[2b]

The conidia (7-16 mg) from WT, Δ*wetA*, Δ*velB*, and Δ*vosA* strains were extracted by adding 1.5 mL of methanol/acetonitrile (2:1) mixture followed by sonication for 60 min. The suspension was then left overnight, supernatant was separated from spores by centrifugation at 14,000 rpm for 15 mins. 1 mL of supernatant was removed, filtered and evaporated to dryness in vacuo. Extracts for the metabolomics analysis were normalized to 10 mg/mL in methanol for LCMS analysis because this concentration provided adequate signal to noise for the analysis.

Analytical HPLC was performed using an Agilent 1100 HPLC system equipped with a photodiode array detector. The mobile phase consisted of ultra-pure water (A) and acetonitrile (B) with 0.05% formic acid in each solvent. A gradient method from 10% B to 100% B in 35 min at a flow rate of 0.8 mL/min was used. The column (Phenomenex Kinetex C18, 5 µm x 150 mm x 4.6 mm) was re-equilibrated before each injection and the column compartment was maintained at 30˚C throughout each run. All samples were filtered through a 0.45 µm nylon filter before LCMS analysis.

Extracts (10 µL of 10 mg/mL) from each WT and null mutant conidia were analyzed in duplicate on an Agilent 1100 series LCMS platform. All samples were run on the same day in the same batch to minimize RT drift. Blank injections were run between each set of biological duplicates to minimize column bleed over. Negative mode ionization was found to detect most metabolites. The first 5 min of every run was

removed due to a large amount of co-eluting, low molecular weight, polar metabolites. Data sets were exported from Agilent's Chemstation software as .netCDF files and imported into MZmine 2.38.[33] Peak picking was performed with established protocols[34] resulting in 123 marker ions. Briefly, mass detection was centroid with 5E2 minimum height. Chromatogram building was limited to peaks greater that 0.1 min with 0.05 m/z tolerance and 1E3 minimum height. Data smoothing performed at a filter width of 5. Chromatogram deconvolution utilized local minimum search with a chromatographic threshold of 95%, minimum relative height of 10%, min absolute height of 3E3, minimum ratio of peak to edge of 1, and a peak duration range of 0.1-5.0 min. Isotopic peaks were removed with a m/z 1 ppm tolerance before all treatments were aligned and duplicate peaks combined with a tolerance of m/z 0.1 and 3.0 minutes RT. Peak finder gap filling was performed with 50% intensity tolerance and m/z 0.1 tolerance. Peak lists were exported to Metaboanalyst[35] where missing values were replaced with half the minimum positive value, data was filtered by interquartile range, and log transformation of the data was employed.

2.5 References

(1) (a) Adams, T. H., Asexual Sporulation in Higher Fungi. In *The Growing Fungus*, Gow, N. A. R.; Gadd, G. M., Eds. Springer Netherlands: Dordrecht, 1995; pp 367. (b) Park, H.-S.; Lee, M.-K.; Han, K.-H.; Kim, M.-J.; Yu, J.-H., Developmental Decisions in Aspergillus nidulans. In *Biology of the Fungal Cell*, Hoffmeister, D.; Gressler, M., Eds. Springer International Publishing: Cham, 2019; pp 63.

(2) (a) Park, H.-S.; Yu, J.-H., 1 Molecular Biology of Asexual Sporulation in Filamentous Fungi. In *Biochemistry and Molecular Biology*, Hoffmeister, D.,

Ed. Springer International Publishing: Cham, 2016; pp 3. (b) Wu, M.-Y.; Mead, M. E.; Lee, M.-K.; Ostrem Loss, E. M.; Kim, S.-C.; Rokas, A.; Yu, J.-H. *mBio* **2018**, *9*, e01130.

(3) Ebbole, D. J., The Conidium. In *Cellular and Molecular Biology of Filamentous Fungi*, American Society of Microbiology: 2010.

(4) (a) Calvo, A. M.; Wilson, R. A.; Bok, J. W.; Keller, N. P. *Microbiology and Molecular Biology Reviews* **2002**, *66*, 447. (b) Yu, J.-H.; Keller, N. *Annual Review of Phytopathology* **2005**, *43*, 437.

(5) Samson, R. A.; Visagie, C. M.; Houbraken, J.; Hong, S. B.; Hubka, V.; Klaassen, C. H.; Perrone, G.; Seifert, K. A.; Susca, A.; Tanney, J. B.; Varga, J.; Kocsube, S.; Szigeti, G.; Yaguchi, T.; Frisvad, J. C. *Studies in Mycology* **2014**, *78*, 141.

(6) Scazzocchio, C., Aspergillus: A Multifaceted Genus. In *Encyclopedia of Microbiology*, Elsevier: 2009; pp 401.

(7) Sanchez, J. F.; Somoza, A. D.; Keller, N. P.; Wang, C. C. C. *Natural Product Reports* **2012**, *29*, 351.

(8) Kato, N.; Brooks, W.; Calvo, A. M. *Eukaryotic Cell* **2003**, *2*, 1178.

(9) Adams, T. H.; Wieser, J. K.; Yu, J.-H. *Microbiology and Molecular Biology Reviews* **1998**, *62*, 35.

(10) (a) de Vries, R. P.; Riley, R.; Wiebenga, A.; Aguilar-Osorio, G.; Amillis, S.; Uchima, C. A.; Anderluh, G.; Asadollahi, M.; Askin, M.; Barry, K.; Battaglia, E.; Bayram, Ö.; Benocci, T.; Braus-Stromeyer, S. A.; Caldana, C.; Cánovas, D.; Cerqueira, G. C.; Chen, F.; Chen, W.; Choi, C.; Clum, A.; dos Santos, R. A. C.; Damásio, A. R. d. L.; Diallinas, G.; Emri, T.; Fekete, E.; Flipphi, M.; Freyberg, S.; Gallo, A.; Gournas, C.; Habgood, R.; Hainaut, M.; Harispe, M. L.; Henrissat, B.; Hildén, K. S.; Hope, R.; Hossain, A.; Karabika, E.; Karaffa, L.; Karányi, Z.; Kraševec, N.; Kuo, A.; Kusch, H.; LaButti, K.; Lagendijk, E. L.; Lapidus, A.; Levasseur, A.; Lindquist, E.; Lipzen, A.; Logrieco, A. F.; MacCabe, A.; Mäkelä, M. R.; Malavazi, I.; Melin, P.; Meyer, V.; Mielnichuk, N.; Miskei, M.; Molnár, Á. P.; Mulé, G.; Ngan, C. Y.; Orejas, M.; Orosz, E.; Ouedraogo, J. P.; Overkamp, K. M.; Park, H.-S.; Perrone, G.; Piumi, F.; Punt, P. J.; Ram, A. F. J.; Ramón, A.; Rauscher, S.; Record, E.; Riaño-Pachón, D. M.; Robert, V.; Röhrig, J.; Ruller, R.; Salamov, A.; Salih, N. S.; Samson, R. A.; Sándor, E.; Sanguinetti, M.; Schütze, T.; Sepčić, K.; Shelest, E.; Sherlock, G.; Sophianopoulou, V.; Squina, F. M.; Sun, H.; Susca, A.; Todd, R. B.; Tsang, A.; Unkles, S. E.; van de Wiele, N.; van Rossen-Uffink, D.; Oliveira, J. V. d. C.; Vesth, T. C.; Visser, J.; Yu, J.-H.; Zhou, M.; Andersen, M. R.; Archer, D. B.; Baker, S. E.; Benoit, I.; Brakhage, A. A.; Braus, G. H.; Fischer, R.; Frisvad, J. C.; Goldman, G. H.; Houbraken, J.; Oakley, B.; Pócsi, I.; Scazzocchio, C.; Seiboth, B.; vanKuyk, P. A.; Wortman, J.; Dyer, P. S.;

Grigoriev, I. V. *Genome Biology* **2017**, *18*, 28. (b) Mirabito, P. M.; Adams, T. H.; Timberlake, W. E. *Cell* **1989**, *57*, 859. (c) Boylan, M. T.; Mirabito, P. M.; Willett, C. E.; Zimmerman, C. R.; Timberlake, W. E. *Molecular and Cellular Biology* **1987**, *7*, 3113.

(11) Wu, M. Y.; Mead, M. E.; Kim, S. C.; Rokas, A.; Yu, J. H. *PLoS One* **2017**, *12*, e0179571.

(12) Hee-Soo, P.; Jae-Hyuk, Y. *Microbiology and Biotechnology Letters* **2016**, *44*, 409.

(13) (a) Park, H.-S.; Yu, J.-H. *Current Opinion in Microbiology* **2012**, *15*, 669. (b) Park, H.-S.; Ni, M.; Jeong, K. C.; Kim, Y. H.; Yu, J.-H. *PLoS One* **2012**, *7*, e45935.

(14) (a) Bayram, O.; Krappmann, S.; Ni, M.; Bok, J. W.; Helmstaedt, K.; Valerius, O.; Braus-Stromeyer, S.; Kwon, N. J.; Keller, N. P.; Yu, J. H.; Braus, G. H. *Science* **2008**, *320*, 1504. (b) Bayram, Ö.; Feussner, K.; Dumkow, M.; Herrfurth, C.; Feussner, I.; Braus, G. H. *Fungal Genetics and Biology* **2016**, *87*, 30. (c) Park, H.-S.; Lee, M.-K.; Kim, S. C.; Yu, J.-H. *PLoS One* **2017**, *12*, e0177099. (d) Thieme, K. G.; Gerke, J.; Sasse, C.; Valerius, O.; Thieme, S.; Karimi, R.; Heinrich, A. K.; Finkernagel, F.; Smith, K.; Bode, H. B.; Freitag, M.; Ram, A. F. J.; Braus, G. H. *PLOS Genetics* **2018**, *14*, e1007511. (e) Gerke, J.; Braus, G. H. *Applied Microbiology and Biotechnology* **2014**, *98*, 8443.

(15) Pluskal, T.; Castillo, S.; Villar-Briones, A.; Orešič, M. *BMC Bioinformatics* **2010**, *11*, 395.

(16) Lo, H.-C.; Entwistle, R.; Guo, C.-J.; Ahuja, M.; Szewczyk, E.; Hung, J.-H.; Chiang, Y.-M.; Oakley, B. R.; Wang, C. C. C. *Journal of the American Chemical Society* **2012**, *134*, 4709.

(17) (a) Rushing, B. R.; Selim, M. I. *Food and Chemical Toxicology* **2019**, *124*, 81. (b) Yu, J.; Chang, P. K.; Ehrlich, K. C.; Cary, J. W.; Bhatnagar, D.; Cleveland, T. E.; Payne, G. A.; Linz, J. E.; Woloshuk, C. P.; Bennett, J. W. *Applied and Environmental Microbiology* **2004**, *70*, 1253.

(18) Brown, D. W.; Yu, J. H.; Kelkar, H. S.; Fernandes, M.; Nesbitt, T. C.; Keller, N. P.; Adams, T. H.; Leonard, T. J. *Proceedings of the National Academy of Sciences of the United States of America* **1996**, *93*, 1418.

(19) (a) Shier, W. T.; Lao, Y.; Steele, T. W. J.; Abbas, H. K. *Bioorganic Chemistry* **2005**, *33*, 426. (b) Grau, M. F.; Entwistle, R.; Oakley, C. E.; Wang, C. C. C.; Oakley, B. R. *ACS Chemical Biology* **2019**, *14*, 1643.

(20) Chang, P.-K.; Yabe, K.; Yu, J. *Applied and Environmental Microbiology* **2004**, *70*, 3593.

(21) Oh, D.-C.; Kauffman, C. A.; Jensen, P. R.; Fenical, W. *Journal of Natural Products* **2007**, *70*, 515.

(22) Chiang, Y.-M.; Szewczyk, E.; Nayak, T.; Davidson, A. D.; Sanchez, J. F.; Lo, H.-C.; Ho, W.-Y.; Simityan, H.; Kuo, E.; Praseuth, A.; Watanabe, K.; Oakley, B. R.; Wang, C. C. C. *Chemistry & Biology* **2008**, *15*, 527.
(23) Käfer, E., Meiotic and Mitotic Recombination in Aspergillus and Its Chromosomal Aberrations. In *Advances in Genetics*, Caspari, E. W., Ed. Academic Press: 1977; Vol. 19, pp 33.
(24) Shaaban, M. I.; Bok, J. W.; Lauer, C.; Keller, N. P. *Eukaryotic Cell* **2010**, *9*, 1816.
(25) Seo, J.-A.; Guan, Y.; Yu, J.-H. *Genetics* **2003**, *165*, 1083.
(26) Kim, M.-J.; Lee, M.-K.; Pham, H. Q.; Gu, M. J.; Zhu, B.; Son, S.-H.; Hahn, D.; Shin, J.-H.; Yu, J.-H.; Park, H.-S.; Han, K.-H. *Genes* **2020**, *11*, 103.
(27) Kim, D.; Pertea, G.; Trapnell, C.; Pimentel, H.; Kelley, R.; Salzberg, S. L. *Genome Biology* **2013**, *14*, R36.
(28) Anders, S.; Pyl, P. T.; Huber, W. *Bioinformatics* **2015**, *31*, 166.
(29) Love, M. I.; Huber, W.; Anders, S. *Genome Biology* **2014**, *15*, 550.
(30) Arnaud, M. B.; Chibucos, M. C.; Costanzo, M. C.; Crabtree, J.; Inglis, D. O.; Lotia, A.; Orvis, J.; Shah, P.; Skrzypek, M. S.; Binkley, G.; Miyasato, S. R.; Wortman, J. R.; Sherlock, G. *Nucleic Acids Research* **2010**, *38*, D420.
(31) Stajich, J. E.; Harris, T.; Brunk, B. P.; Brestelli, J.; Fischer, S.; Harb, O. S.; Kissinger, J. C.; Li, W.; Nayak, V.; Pinney, D. F.; Stoeckert, C. J., Jr.; Roos, D. S. *Nucleic Acids Research* **2012**, *40*, D675.
(32) Ge, S. X.; Jung, D.; Yao, R. *Bioinformatics* **2019**.
(33) Pluskal, T.; Castillo, S.; Villar-Briones, A.; Oresic, M. *BMC Bioinformatics* **2010**, *11*, 395.
(34) Abdelmohsen, U. R.; Cheng, C.; Viegelmann, C.; Zhang, T.; Grkovic, T.; Ahmed, S.; Quinn, R. J.; Hentschel, U.; Edrada-Ebel, R. *Marine Drugs* **2014**, *12*, 1220.
(35) Xia, J.; Sinelnikov, I. V.; Han, B.; Wishart, D. S. *Nucleic Acids Research* **2015**, *43*, W251.

Chapter Three: Antibacterial Drimane Sesquiterpenes from *Aspergillus ustus*

George F. Neuhaus and Sandra Loesgen

3.1 Abstract

Fungal natural products (NPs) have played a major role in shaping current modern medicine. Bioactivity-guided isolation of an organic extract from *Aspergillus ustus* lead to the discovery of five new drimane sesquiterpenes, ustusal A, ustusolate F and G, and ustusoic acid A and B, **3.1**-**3.5** respectively. Structural elucidation of these fungal terpenes relied on 1D and 2D NMR techniques, high-resolution mass spectrometry, and chiroptical properties. Their relative configuration was determined by NMR methods, while the absolute configuration was established using comparative analysis of computed and experimental NMR chemical shifts and ECD spectra. The sesquiterpenes only exhibited modest activity against Gram-positive pathogens, however the activity of **3.5** was drastically enhanced when equal amounts of stromemycin (**3.6**), a known metabolite isolated from the same fraction from *A. ustus*, was added.

3.2 Introduction

Fungal natural products (NPs) have been key players in fighting bacterial infections for the past century. The penicillins, cephalosporins, pleuromutilins, and fusidic acids have all contributed to extending the human life span.[1] Unfortunately, despite the great success of antibiotic discovery throughout the 1950's and 60's, we have entered the post-antibiotic era due to the rise of antimicrobial resistance (AR).[2] Pathogens such as vancomycin-resistant *Enterococcus faecium* and multidrug-resistant *Staphylococcus aureus*, which are on the CDC's list of serious threats,[2] could jeopardize our health care system because there are limited defenses against them[1, 3] and there is a potential of transferring chemical resistance to more dangerous pathogens.[4] More than 2.8 million antibiotic-resistant infections occur in the United States with more than 35,000 deaths per year.[2] This major health problem is predicted to get worse, with estimates of 10 million deaths to occur due to AR worldwide by 2050,[5] emphasizing the urgent need for new antibiotics to fight infection. One common method is to use combinatorial treatments that target multiple bacterial pathways to fight off infections, the most well-known being co-administration of amoxicillin and clavulanic acid to treat methicillin-resistant *S. aureus*.[6] Finding compounds that act in synergistic ways might improve our chances of fighting AR and in turn, our ability to combat infectious diseases.

During our search for new antibiotics from our in-house fungal strain library, we found cultures of *A. ustus* that produced strong antibacterial activity. *A. ustus* is well

known for producing bioactive NPs including meroterpenoids,[7] isochromanes,[8] drimane sesquiterpenes,[9] and ophiobolins.[10] During our bioactivity-guided isolation, we found eight known metabolites: deoxyuvidin B,[11] ustusol A and B,[12] strobilactone A,[13] mono(6-strobilactone-B) ester of (*E*,*E*)-2,4-hexadienedioic acid,[12b] two peptides, WIN 68577 and its deoxy derivative,[14] and stromemycin (**3.6**).[15] In addition, five new drimane sesquiterpenes (**3.1-3.5**) were isolated (Figure 3.1). Despite strong activity observed during the fractionation process, only weak activity was observed when compounds **3.4**, **3.5**, and **3.6** were tested separately. We suspected that two of the compounds were acting synergistically and indeed, when **3.5** and **3.6** were tested together, in a 1:1 ratio (μg/mL), strong activity was seen against Gram-positive

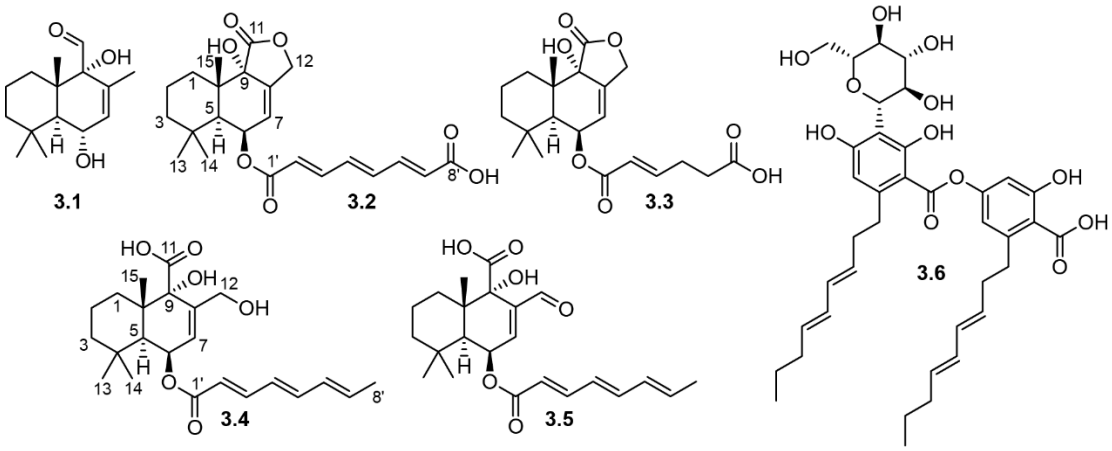

Figure 3.1: Structures of isolated NPs

bacteria, with MIC's of 8 μg/mL against *Bacillus subtilis* (ATCC 49343), 32 μg/mL against vancomycin-resistant *Enterococcus faecium* (ATCC 700221), and 64 μg/mL against multidrug-resistant *Staphylococcus aureus* (ATCC BAA-44). No anti-fungal or

cytotoxic affects were observed. Activity for the most active drimane ustusoic acid B (**3.5**) ranged from 38 to >128 μg/mL for the tested Gram-positive pathogens.

3.3 Results and discussion

From an in-house library of isolated Ascomycota, *A. ustus* (Spat_2017_*A. ustus*) was chosen for chemical analysis based on antimicrobial activity seen in an initial screen against multidrug-resistant *Staphylococcus aureus* (ATCC BAA-44). The fungus was identified by amplification of the complete internal transcribed spacer (ITS) regions 1 and 2 using primers ITS1 and ITS4.[16] Using the BLAST algorithm,[17] we found two matching *Aspergilli* within the section Usti,[18] namely *Aspergillus ustus* (strain ATCC 588983) and *Aspergillus insuetus* (strain IG 105) (Figure B.1, Appendix B). Both yielded 100% sequence coverage and 100% identity to our 438 bp amplified sequence. These strains are closely related, made distinct from one another in 2007.[18a] Our analysis of the ITS region could not distinguish between the two species, and we will refer to this strain as *A. ustus*. Members of section Usti are common filamentous fungi found in food, soil, and indoor air environments, with some considered to be rare human pathogens.[18-19]

Ustusal A (**3.1**) was isolated as an amorphous white solid (0.45 mg/L) and gave an *m/z* of 275.1615 ($[M+Na]^+$) in the HRESIMS. This provided a molecular formula of $C_{15}H_{24}O_3$ (calcd for $C_{15}H_{24}NaO_3$(+1) 275.162; Δ ppm = 1.0). The ^1H NMR spectrum

showed an aldehyde resonance (δ_H 9.71 ppm), an olefinic resonance (δ_H 5.56 ppm), three methylene, two methine, and four methyl resonances (Table 3.1). The ^{13}C NMR spectrum displayed one aldehyde carbon, two olefinic carbons and 12 aliphatic carbons (Table 3.1).

Table 3.1: ^{1}H and ^{13}C NMR spectroscopic data for compounds **3.1**-**3.5**

	ustusal A (**3.1**)[a]		ustusolate F (**3.2**)[b]		ustusolate G (**3.3**)[b,c]		ustusoic acid A (**3.4**)[b]		ustusoic acid B (**3.5**)[b]	
Position	δ_C, type	δ_H (J in Hz)	δ_C, type	δ_H (J in Hz)	δ_C, type	δ_H (J in Hz)	δ_C, type	δ_H (J in Hz)	δ_C, type	δ_H (J in Hz)
1a	33.8, CH_2	1.79, td (13.3, 3.1)	31.2, CH_2	2.02, m	31.0, CH_2	2.00, m	34.8, CH_2	1.87, m	33.8, CH_2	1.94, td (12.6, 4.0)
1b		0.88, d (12.8)						1.23, m		1.30, m
2a	17.8, CH_2	1.33, m	19.0, CH_2	1.73, m	18.8, CH_2	1.73, qt (13.8, 3.9)	19.6, CH_2	1.69, m	19.5, CH_2	1.69, m
2b		1.45, q (13.2)		1.55, m		1.54, dp (13.8, 3.6)		1.48, m		1.51, m
3a	43.1, CH_2	1.15, d (13.6)	46.2, CH_2	1.42, m	46.0, CH_2	1.41, br d (13.0)	46.0, CH_2	1.36, m	45.8, CH_2	1.38, m
3b		1.30, m		1.32, m		1.31, td (13.0, 2.9)		1.28, m		1.30, m
4	32.9, C		34.8, C		34.4, C		34.4, C		34.8, C	
5	47.3, CH	1.67, d (10.1)	46.2, CH	2.08, d (4.8)	46.0, CH	2.06, d (4.8)	46.4, CH	2.06, d (4.4)	46.7, CH	2.06, d (4.8)
6	66.9, CH	4.04, t (8.9)	67.9, CH	5.73, br s	67.5, CH	5.69, br s	68.5, CH	5.71, m	67.4, CH	5.89, t (4.8)
7	134.1, CH	5.56, br s	123.3, CH	5.86, br s	123.3, CH	5.83, br s	123.4, CH	5.93, d (4.9)	142.7, CH	6.70, d (4.8)
8	130.1, C		138.1, C		137.6, C		144.0, C		144.2, C	
9	82.0, C		75.2, C		75.0, C		81.4, C		78.1, C	
10	42.7, C		39.1, C		38.7, C		41.3, C		41.2, C	
11	207.2, C	9.71, s	176.7, C		176.4, C		178.5, C		177.5, C	
12a	18.4, CH_3	1.50, br s	70.0, CH_2	4.93, dt (12.6, 2.4)	69.8, CH_2	4.92, dt (12.6, 2.4)	63.3, CH_2	4.22, d (14.5)	194.4, C	9.40, s
12b				4.76, d (12.6)		4.75, dt (12.6, 1.3)		3.94, d (14.5)		
13	36.5, CH_3	1.11, s	25.2, CH_3	1.17, s	25.0, CH_3	1.15, s	25.3, CH_3	0.98, s	33.4, CH_3	1.00, s
14	22.7, CH_3	1.02, s	33.0, CH_3	1.00, s	32.8, CH_3	0.98, s	33.4, CH_3	1.15, s	25.4, CH_3	1.16, s
15	18.1, CH_3	1.05, s	19.1, CH_3	1.18, s	19.0, CH_3	1.15, s	20.6, CH_3	1.44, s	20.7, CH_3	1.37, s
OH-6		4.43, d (7.3)								
OH-9		5.19, s								
1'			167.5, C		167.0, C		168.5, C		168.0, C	
2'			123.4, CH	6.02, d (15.3)	122.0, CH	5.87, dt (15.6, 1.6)	121.3, CH	5.85, d (15.1)	120.6, CH	5.89, d (15.4)
3'			146.2, CH	7.34, dd (15.3, 11.0)	151.7, CH	7.03, dt (15.6, 6.8)	146.9, CH	7.27, dd (15.1, 11.3)	147.5, CH	7.32, dd (15.4, 11.2)
4'			134.8, CH	6.64, dd (14.9, 11.0)	30.7, CH_2	2.50, tdd (7.4, 6.8, 1.3)	128.8, CH	6.29, dd (14.8, 11.3)	128.7, CH	6.30, dd (14.7, 11.2)
5'			141.2, CH	6.75, dd (14.9, 11.0)	37.1, CH_2	2.28, t (7.4)	143.0, CH	6.59, dd (14.8, 10.8)	143.4, CH	6.62, dd (14.7, 10.6)
6'			139.8, CH	7.10, dd (15.2, 11.0)	180.4, C		132.6, CH	6.21, dd (15.0, 10.8)	132.6, CH	6.22, dd (14.8, 10.6)
7'			133.7, CH	6.13, d (15.2)			136.4, CH	6.00, dq (15.0, 7.0)	136.7, CH	6.02, dq (14.8, 6.9)
8'			174.3, C				18.7, CH_3	1.82, d (7.0)	18.7, CH_3	1.83, d (6.9)

a) Spectra recorded in DMSO-d_6

b) Spectra recorded in methanol-d_3

c) ^{13}C data measured indirectly from 2D spectrum

The structure of **3.1** was determined by conventional 2D NMR experiments. The COSY NMR spectrum exhibited two spin systems (Figure 3.2). The first consisted of three sets of diastereotopic methylene signals (H-1a, H-1b, H-2a, H-2b, H-3a, and H-3b). The second was made up of a shielded methine doublet (H-5), an oxygenated methine (H-6), an olefinic methine (H-7), and long range $^{4}J_{H\text{-}H}$ coupling between H_3-12 and H-7 (1-2 Hz).[20] Analysis of the HMBC NMR spectrum revealed **3.1** was a drimane sesquiterpene (Figure 3.2).[9] Connections between H_3-13 and H_3-14 and C-3, C-4, and C-5 placed the gem-dimethyl on C-4. Correlations between H_3-15 and C-1, C-5, and C-9, along with correlations from H-5, H_3-12, and H-11 to C-9 complete the decalin core and placed the aldehyde on C-9. The relative configuration of **3.1** was determined by NOE analysis (Figure 3.3). Correlations between H_3-15 and H-1b$_{(eq)}$, and between H-5 and H-1a$_{(ax)}$ established a *trans*-fused decalin ring system. Additional correlations between H-6 with H_3-14 and H_3-15, H-11 with H_3-15, and H-5 with OH-6, and OH-9 established a *cis*-configuration between H-6, H-11, and H_3-15, along with a *cis*-configuration between H-5, OH-6, and OH-9. The *cis*-configuration between H-5 and OH-6 is further supported by a large $^{3}J_{H5\text{-}H6}$ coupling constant of 10.2 Hz (Figure 3.3). Computational support for the relative configuration is discussed below.

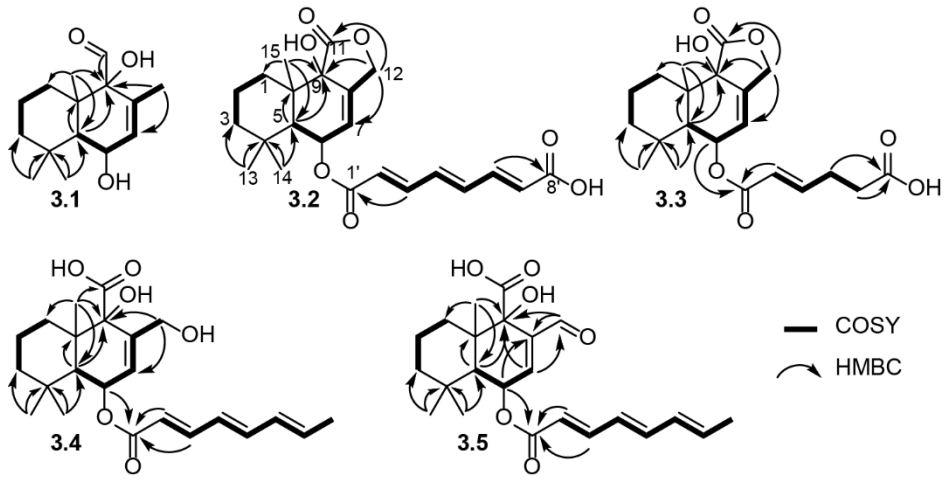

Figure 3.2: Key COSY and HMBC correlations of **3.1**-**3.5**

Despite multiple attempts, Mosher ester analysis to support the absolute configuration of C-6 in **3.1** failed due to degradation of the product. In lieu, we pursued a comparative analysis with computed chiroptical properties. Both the 5*S*,**6*R***,9*R*,10*S* and 5*S*,**6S**,9*R*,10*S* diastereomers were used to generate a suite of conformers by automatic sampling tools based on molecular mechanics with the Merck Molecular Force Field (MMFF) in Spartan. Next, the lowest energy conformers (>10 kcal/mol, seven in total) were reoptimized at the B3LYP/6-31G level of theory followed by a subsequent reoptimization at the M062X/TZVP level of theory with a solvation model based on density (SMD) variation of an integral equation formalism polarizable continuum model (IEFPCM) in methanol. Next, all conformers within 3 kcal/mol of the lowest energy conformer were submitted to time-dependent (TD)DFT calculations of ECD spectra (ECD spectra for the enantiomers were obtained by reflection). To

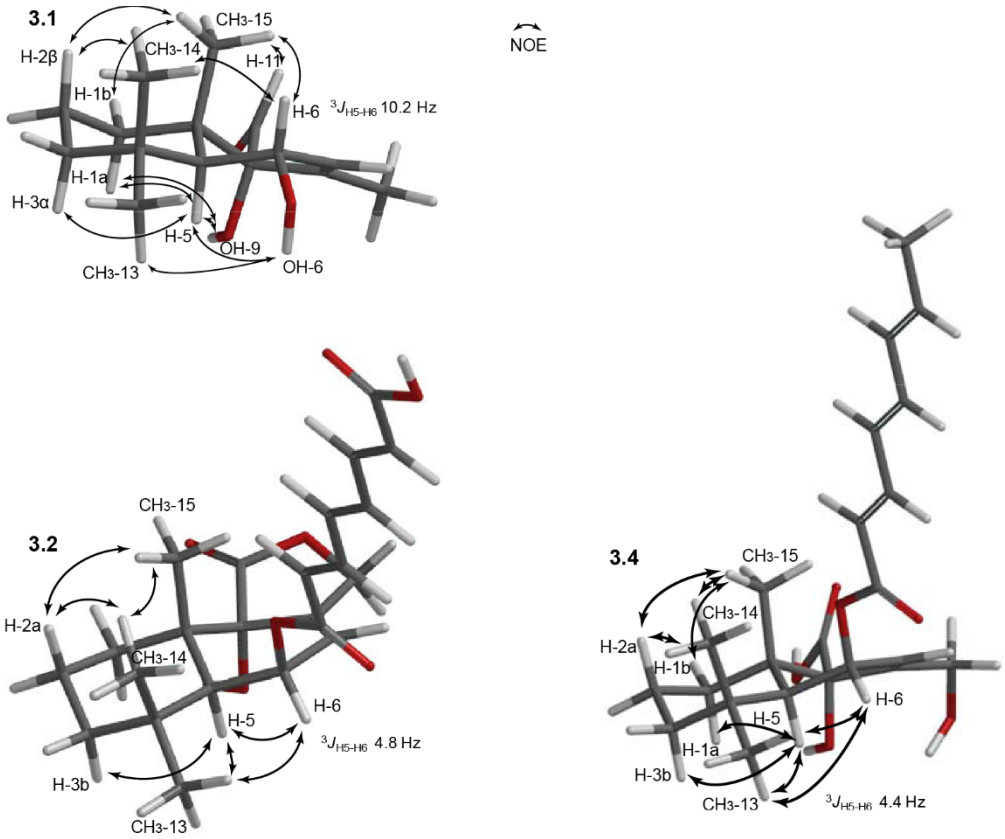

Figure 3.3: Lowest energy conformers from gas phase minimizations at B3LYP/6-31G level of theory with key NOE correlations and coupling constants of **3.1**, **3.2**, and **3.4**

maintain good computational practice, multiple levels of theory were tested using both hybrid and range-separated functionals: ωB97X/def2-TZVP (Figure 3.4), CAM-B3LYP/TZVP (Figure B.45, Appendix B), and M062X/def2-TZVP (Figure B.45, Appendix B). The 5*S*,6*R*,9*R*,10*S* diastereomer produced a poor fit to the experimental data and can therefore be excluded (Figure 3.4). The 5*S*,6*S*,9*R*,10*S* configuration

produced the best fit with the experimental data, with positive cotton effects around 210 and 300 nm. This supports the absolute configuration of **3.1** as 5*S*,6*S*,9*R*,10*S*.

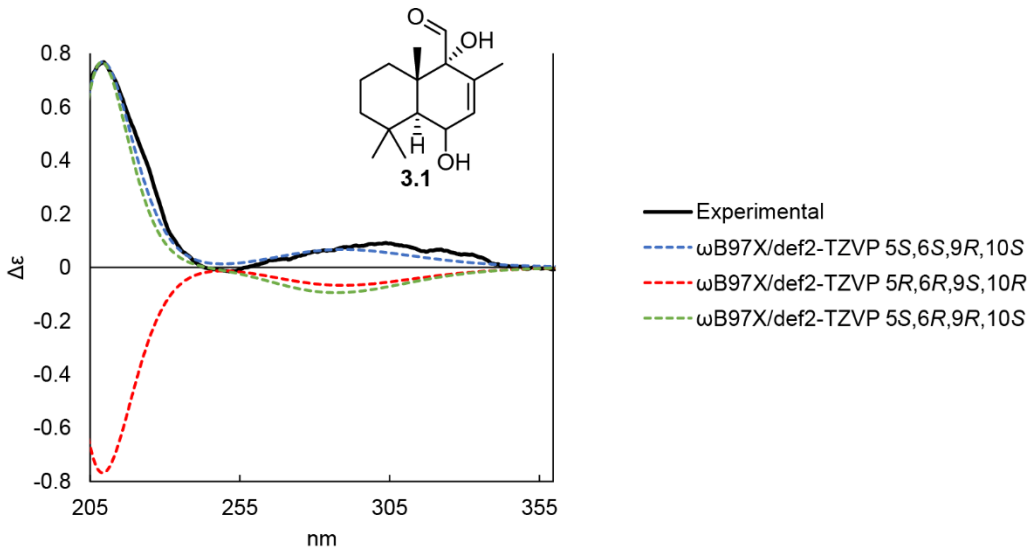

Figure 3.4: Experimental ECD spectrum of **3.1** (black) in methanol with computed spectra of the enantiomers 5*S*,6*S*,9*R*,10*S* and 5*R*,6*R*,9*S*,10*R* along with the diastereomer 5*S*,6*R*,9*R*,10*S* at the ωB97X/def2-TZVP level of theory. Blue dotted line: 5*S*,6*S*,9*R*,10*S* (shift: 15 nm; σ = 0.53 eV); red dotted line: 5*R*,6*R*,9*S*,10*R* (shift: 15 nm; σ = 0.53 eV); green dotted line: 5*S*,6*R*,9*R*,10*S* (shift: 14 nm; σ = 0.53 eV)

Ustusolate F (**3.2**) was isolated as an amorphous white solid. The HRESIMS gave an *m/z* value of 415.1770 ([M-H]$^-$), which provided a molecular formula of $C_{23}H_{28}O_7$ (calcd for $C_{23}H_{27}O_7$(-1) 415.176; Δ ppm = 1.9). The UV spectrum showed a maximum at 304 nm, indicating a conjugated system. The ^{13}C NMR spectrum showed 20 signals: two carbonyl shifts, six olefinic signals, and twelve aliphatic signals (Table 3.1) and three more were detected in 2D data sets, two olefinic signals and one carbonyl shift.

The ^{1}H NMR spectrum showed seven olefinic signals, four methylene signals, one methine, one oxygenated methine and three methyl singlets (Table 3.1).

With similar 1D and 2D NMR data to **3.1** (Figure 3.2), **3.2** was also determined to be a drimane sesquiterpene at its core. The structural differences can be accounted for in the northern portion of the molecule, chemical shifts of C-11 and C-12 indicate a γ-lactone. This is supported by diastereotopic methylene protons signals for H-12 (H-12a δ_H 4.93, H-12b δ_H 4,76 ppm) and a HMBC correlation between H-12 and C-11 (Figure 3.2). Additionally, eight more carbon signals and six olefinic protons where found in the ^{13}C and ^{1}H NMR spectrum, respectively. The additional olefinic protons belong to the same spin system as observed in the COSY spectrum (Figure 3.2). With HMBC correlations from H-3' to C-1' and H-6' to C-8', **3.2** exhibited an octatrienedioic acid sidechain linked through an ester bond. Large coupling constants ($^{3}J_{H2\text{-}H3}$ 15.3 Hz; $^{3}J_{H4\text{-}H5}$ 14.9 Hz; $^{3}J_{H6\text{-}H7}$ 15.2 Hz) are indicative of an *E* configuration for all three double bonds. The NMR data were recorded in MeOH-d_4 and therefore the carboxylic acid proton was not detected in the ^{1}H spectrum and we were unable to detect HMBC correlations connecting the triene moiety to the sesquiterpene core. To support our structural assignment, **3.2** was methylated in the presence of methyl iodide. Indeed, we were able to detect a new methoxy signal in the ^{1}H NMR spectrum in $CDCl_3$ (δ_C 51.9 ppm, δ_H 3.77 ppm), and observed HMBC correlations from H_3-9' to C-8', and from H-6 to C-1', supporting that OH-6 condenses with the acyl sidechain (Figure B.44,

Appendix B). This is in agreement with previously reported acylated drimane sesquiterpenes.[9, 12] The relative configuration of **3.2** was determined by NOE analysis and by comparative analysis of computed NMR chemical shifts to experimental spectra. A *trans*-fused decalin ring system was supported by NOE correlations between H_3-15 and H_3-$14_{(ax)}$ with H-$2a_{(ax)}$, H_3-15 with H_3-$14_{(ax)}$, and H-5 with H-$3b_{(ax)}$ and with H_3-$13_{(eq)}$ (Figure 3.3). A *cis*-configuration between H-5 and H-6 was supported by NOE correlations between H-5 with H-6 and H-6 with H_3-$13_{(eq)}$ as well as a small $^3J_{H5\text{-}H6}$ coupling of 4.8 Hz. For the relative configuration of C-9, a DP4+ based computation[21] of ^{1}H and ^{13}C chemical shifts with each possible configuration, 5*S*,6*R*,**9S,**10*S* and 5*S*,6*R*,**9*R***,10*S* was used. Briefly, conformer suites were generated using the method above. Next, gas phase minimizations were submitted directly to GIAO NMR calculations at mPW1PW91/6-311+g(2d,p) level of theory.[22] Applying the DP4+ algorithm to unscaled shielding tensors produced 100% confidence that 5*S*,6*R*,9*S*,10*S* best fits the experimental data (Table 3.2), supporting a *cis*-configuration between H-5 and OH-9. The absolute configuration of **3.2** was determined by the same means as **3.1**, through comparative analysis of computed ECD spectra to experimental spectra. Multiple levels of theory were used, and all agreed with an absolute configuration for **3.2** of 5*S*,6*R*,9*S*,10*S* (Figure 3.5), as seen from the negative cotton effects around 210 and 300 nm.

Table 3.2: DP4+ analysis of unscaled shielding tensors of **3.2**

	5*S*,6*R*,9*R*,10*S*	5*S*,6*R*,9*S*,10*S*
DP4+ (H data)	0.01%	99.99%
DP4+ (C data)	0.00%	100.00%
DP4+ (all data)	0.00%	100.00%

Ustusolate G (**3.3**) was isolated as a white amorphous solid and the HRESIMS gave an *m/z* value of 391.1771 ([M-H]$^-$). This provided a molecular formula of $C_{21}H_{28}O_7$ (calcd for $C_{21}H_{27}O$(-1) 319.176; Δ ppm = 2.2). The ^{1}H NMR spectrum of **3.3** had three olefinic resonances, six methylene resonances, one methine, one oxygenated methine, and three methyl resonances (Table 3.1). The ^{13}C spectrum showed 21 signals, three carbonyl, four olefinic, and 14 aliphatic.

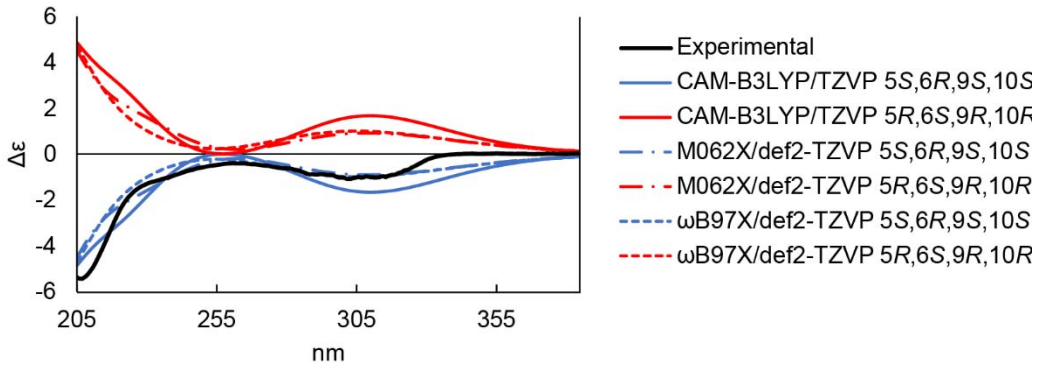

Figure 3.5: Experimental ECD spectrum of **3.2** (black) in methanol with computed spectra of the enantiomers 5*S*,6*R*,9*S*,10*S* (blue) and 5*R*,6*S*,9*R*,10*R* (red). Blue and red solid lines: CAM-B3LYP/TZVP (shift: 1 nm; σ = 0.48 eV); blue and red dashed lines: M062X/def2-TZVP (shift: 1 nm; σ = 0.57 eV); blue and red dotted lines: ωB97X/def2-TZVP (shift: 5 nm; σ = 0.62 eV)

Analysis of 2D NMR data showed that **3.3**[23] had the same sesquiterpene core as **3.2** and only differs in the acyl sidechain. The acyl group of **3.3** only had six carbons, two of which were methylene groups (Figure 3.2). The COSY spectrum revealed that H-2',

H-3', H-4' and H-5' make up a complete spin system. HMBC correlations from H-2' and H-6 to C-1' placed the double bond close to the ester linkage. With a $^{3}J_{H2'\text{-}H3'}$ coupling of 15.6 Hz, it was determined the olefin had an *E* configuration. HMBC correlations from H-4' and H-5' to C-6' placed the vicinal methylene groups close to the carboxylic acid. The relative and absolute configurations were extrapolated to be similar to compound **3.1** and **3.2** due to their shared biosynthetic origin. This is supported by an $[\alpha]_D^{22}$ -18 ($[\alpha]_D^{21}$ -75 for **3.2**) and a negative cotton effect at 210 in the ECD spectrum, similar to **3.2** (Figure B.19, Appendix B). We propose an absolute configuration for **3.3** of 5*S*,6*R*,9*S*,10*S*.

Ustusoic acid A (**3.4**) was isolated as a white amorphous solid. The HRESIMS gave an *m/z* value of 403.2136 ($[M\text{-}H]^-$), matching a molecular formula of $C_{23}H_{32}O_6$ (calcd for $C_{23}H_{31}O_6$(-1) 403.213; Δ ppm = 2.5). The UV spectra had a maximum at 308 nm, indicating a conjugated system. The ^{1}H NMR spectrum exhibited seven olefinic signals, four methylene signals, one oxygenated methine, one methine, and four methyl signals (Table 3.1). The ^{13}C NMR spectrum showed 23 signals: two carbonyl carbons, eight olefinic carbons, and 13 aliphatic signals.

Analysis of 2D NMR spectrum indicated that **3.4** is also a drimane sesquiterpene, with a similar core to **3.1** (Figure 3.2). Differences include a carboxylic acid at C-11, supported by a HMBC correlation from H_3-15 to C-11, and a hydroxylated methylene at C-12 that is supported by HMBC correlations from H-12 to C-9 and C-7. **3.4** also

includes an octatrienoate functionality, supported by a complete COSY spin system and HMBC correlations from H-6, H-2' and H-3' to C-1' (Figure 3.2). All double bonds in the acyl group were determined to be *E* configured based on large coupling constants: $^{3}J_{H2'\text{-}H3'}$ 15.1 Hz, $^{3}J_{H4'\text{-}H5'}$ 14.8 Hz, and $^{3}J_{H6'\text{-}H7'}$ 15.0 Hz. The relative configuration of **3.4** was determined by NOE analysis. NOE correlations between H_3-15 and H-1b$_{(eq)}$ and H-5 and H-1a$_{(ax)}$ supported a *trans*-fused decalin ring system. Next, correlations between H_3-13 with H-6 and H-5, along with a correlation between H-6 and H-5 supported a *cis*-configuration between H-5 and H-6. This is further supported by the $^{3}J_{H5\text{-}H6}$ coupling of 4.4 Hz (Figure 3.3). We propose the absolute configuration of **3.4** to be 5*S*,6*R*,9*S*,10*S*, as we assume the same biosynthetic origins as **3.1**, **3.2**, and **3.3**. This is further supported by negative cotton effects at 210 and at 305 nm in the ECD spectrum. (Figure B.25, Appendix B).

Ustusoic acid B (**3.5**) was isolated as a white amorphous solid. The HRESIMS gave an *m/z* value of 401.1978 ([M-H]$^{-}$), two mass units less than **3.4**. This matched a molecular formula of $C_{23}H_{30}O_6$ (calcd for $C_{23}H_{29}O_6$(-1) 401.197; Δ ppm = 2.1). Analysis of UV and NMR data supported that **3.5** is an oxidized version of **3.4**, with an aldehyde functionality at C-12, instead of a hydroxylated methylene group. This is further supported by HMBC correlations from H-12 to C-8 and C-9, along with H-7 to C-12. Due to a similar $[\alpha]_D^{22}$ -23 ($[\alpha]_D^{21}$ -29 for **3.4**) and negative cotton effects around 220 and 305 in the ECD spectrum (Figure B.33, Appendix B) to **3.4**, along with

biosynthetic considerations, the absolute configuration of **3.5** is proposed to be 5*S*,6*R*,9*S*,10*S*. Both compounds, **3.4** and **3.5**, were prone to oxidation and degradation. The addition of 5 µg of butylated hydroxytoluene (BHT), a known radical scavenger, to the HPLC collection flasks preserved compounds **3.4** and **3.5**. Initial samples used for NMR analysis did not include BHT while samples for bioactivity testing did. BHT was added to all control wells in bioassays at the same concentration.

Alongside the sesquiterpenes, the *C*-glycosidic depside stromemycin (**3.6**) was isolated. Stromemycin was first isolated and patented in 2001[15a] for its stromelysin inhibitory activity and cytotoxic properties. Analysis of spectroscopic data showed good agreement with literature values. In 2003, Bringmann et. al. determined the double bond geometry to be all *E* configured and identified the sugar as glucose.[15b]

Table 3.3: MIC's (µg/mL) of *A. ustus* extract, fraction, and pure compounds

	A. ustus Organic Extract	*A. ustus* Fraction 6	**3.5**	**3.4**	**3.6**
multidrug-resistant *S. aureus* (ATCC BAA-44)[a]	> 128	128	> 128	> 128	>128
vancomycin-resistant *E. faecium* (ATCC 700221)[b]	>128	128	67	128	>128
B. subtilis (ATCC 49343)[c]	>128	64	38	64	64

a) 100% growth inhibition with positive control vancomycin (125 µg/ml)
b) 99% growth inhibition with positive control nitrofurantoin (125 µg/ml)
c) 99% growth inhibition with positive control chloramphenicol (125 µg/ml)

All isolated compounds were screened for antimicrobial activity against three Gram-positive bacteria (*B. subtilis* ATCC 49343; vancomycin-resistant *E. faecium* ATCC 700221; and multidrug-resistant *S. aureus* ATCC BAA-44). Despite moderate

activity seen within fraction 6 (Table 3.3) after silica based fractionation (1:1 DCM:MeOH), surprisingly only weak activity was observed from compounds **3.4**, **3.5**, and **3.6** (Table 3.3). We were not able to detect any other active metabolites within fraction 6 and therefore thought of synergism between closely eluting metabolites, **3.5** and **3.6**, to be responsible for the fraction activity. Due to very limited amounts of **3.5**, checkerboard analysis or determination of the fractional inhibitory concentration (FIC) were prohibited.[24] Instead, compounds **3.5** and **3.6** were tested in a 1:1 ratio in MIC assays. Indeed, this combination produced moderate to strong activity against all three tested bacteria (Figure 3.6). From this assay, the coefficient of drug interaction (CDI) could be determined with CDI's less than one supporting synergism.[25] With combination treatment MIC's of 8 μg/mL (equals 19.9 μM of **3.5** and 11.5 μM of **3.6**) against *B. subtilis*, 32 μg/mL (equals 79.6 μM of **3.5** and 46.0 μM of **3.6**) against vancomycin-resistant *E. faecium*, and 64 μg/mL (equals 159.1 μM of **3.5** and 91.9 μM of **3.6**) against multi-drug resistant *S. aureus*, the CDI's were determined to be 9.0 x 10^{-4}, 1.3 x 10^{-4}, and 1.4 x 10^{-4} respectively, indictive of synergism. One hypothesis for the apparent synergism could be **3.6** acting as an antioxidant, thus stabilizing **3.5**, which is prone to degradation, or **3.6** aiding in membrane passage of the sesquiterpene. Both hypotheses are currently being explored.

In this study, we added five members to the drimane sesquiterpene family. State-of-the-art NMR experiments in combination with extensive computational methods

were used to determine the absolute configurations of new drimane sesquiterpenes. In addition, we report for the first time the antibacterial activity of ustusoic acid B (**3.5**) against clinically relevant pathogens like vancomycin-resistant *Enterococcus faecium* and multidrug-resistant *Staphylococcus aureus*, which was enhanced four-fold when combined with equimolar amounts of stromemycin (**3.6**), a known fungal metabolite produced by the same fungus. Future studies are planned to optimize the metabolite production in *Aspergillus ustus* in order to elaborate on the enhanced antibiotic activity of these co-eluted metabolites. Our study supports the notion that even well studied *Aspergilli* of the section Usti harbor interesting chemotypes and bioactivities that could inspire combination therapy to treat infectious diseases.

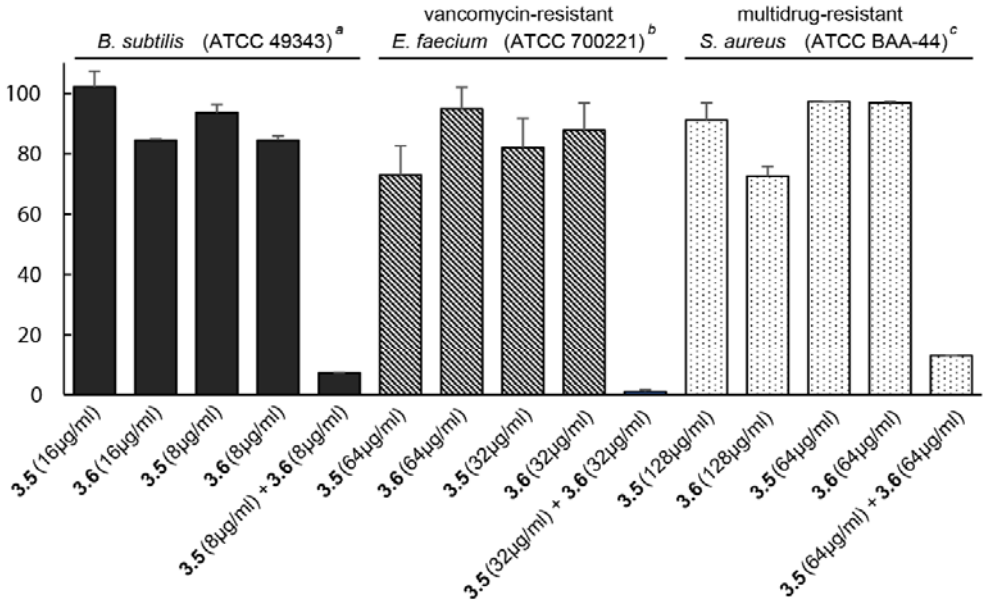

a) 99% growth inhibition with positive control chloramphenicol (125 µg/ml)
b) 99% growth inhibition with positive control nitrofurantoin (125 µg/ml)
c) 100% growth inhibition with positive control vancomycin (125 µg/ml)

Figure 3.6: Synergistic activity of **3.5** and **3.6** against Gram-positive bacteria

3.4 Experimental

General experimental procedures. UV spectra were recorded on a BioRad SmartSpec3000. IR spectra were recorded on a Thermo Scientific Nicolet 6700 FT-IR spectrometer. ECD spectra were recorded on a JASCO J-1000 spectrometer. Optical rotations were recorded on a JASCO P-1010 polarimeter. NMR spectra were acquired on a Bruker Avance III 500 MHz, Bruker Avance III 700 MHz, or a Bruker Avance III 800 MHz spectrometer equipped with a 5 mm TXI probe or 5 mm BBO probe (500 MHz and 700 MHz), DCH cryoprobe (700 MHz), or TCI cryoprobe (800 MHz), with the residual solvent used as an internal standard ($CDCl_3$: 7.26/77.16; MeOD: 3.31/49.03; DMSO: 2.50/39.53). Low resolution ESI-MS and HRTOFMS (ESI^+) mass spectra were recorded on Agilent 1100 series LC with MSD 1946 or Agilent 1260 infinity II LC with 6545 QTOF MS, respectively. Analytical HPLC was performed using an Agilent 1100 HPLC system equipped with a photodiode array detector. The mobile phase consisted of ultra-pure water (A) and MeCN (B) with 0.05% formic acid. A gradient method from 10% A to 100% B in 35 min at a flow rate of 0.8 mL/min was used. The column (Phenomenex Kinetex C_{18}, 5 μm x 150 mm x 4.6 mm) was re-equilibrated before each injection and the column compartment was maintained at 30˚C throughout each run. Semi-preparative HPLC (Phenomenex Kinetex C_{18}, 5 μm x 150 mm x 10 mm) utilized isocratic elution conditions or a gradient system with a flow rate of 4 mL/min on an Agilent 1100 HPLC system operating at room temperature equipped

with a photodiode array detector. Preparative HPLC (Phenomenex Luna C_{18}, 5 μm x 250 mm x 21mm) was conducted at room temperature, using isocratic elution conditions or a gradient system with a flow rate of 20 mL/min utilizing an Agilent 1260 Infinity series HPLC equipped with a DAD detector. All samples were filtered through a 0.45 μm nylon filter or centrifuged at 14,000 rpm for five mins before LCMS and HPLC analysis. Analytical thin layer chromatography (TLC) was performed on pre-coated silica gel 60 F_{254} plates (Eppendorf). TLC plates were visualized by UV (254 and 360 nm), and by spraying with anisaldehyde solution followed by heating at 80 °C. General reagents were from Sigma-Aldrich Corp. and VWR International.

Identification of fungal species. Phylogenetic identification of the fungal strain was achieved by PCR amplification and sequencing of the ITS gene fragments of DNA according to published procedure.[26] ITS1 forward primer and ITS4 reverse primer were used to amplify the complete ITS sequence.[16] The two closest matches for the ITS gene fragment from a nucleotide megaBLAST was *Aspergillus ustus* (strain ATCC 58983) with 100% sequence coverage and 100% identity (GenBank: AY373874.1) and *Aspergillus insuetus* (strain IG 105) with 100% sequence coverage and 100% identity (GenBank:MG973290.1).

The evolutionary history was inferred by using the Maximum Likelihood method based on the Kimura 2-parameter model.[27] The tree with the highest log likelihood (-1305.1674) is shown. The percentage of trees in which the associated taxa clustered

together is shown next to the branches. Initial tree(s) for the heuristic search were obtained automatically by applying Neighbor-Join and BioNJ algorithms to a matrix of pairwise distances estimated using the Maximum Composite Likelihood (MCL) approach, and then selecting the topology with superior log likelihood value. A discrete Gamma distribution was used to model evolutionary rate differences among sites (5 categories (+G, parameter = 0.1468)). The tree is drawn to scale, with branch lengths measured in the number of substitutions per site. The analysis involved 17 nucleotide sequences retrieved from GeneBank[28] or the NCBI BLAST targeted loci partial beta-tubulin sequence from the fungi type and reference material collection.[17] All positions with less than 95% site coverage were eliminated. That is, fewer than 5% alignment gaps, missing data, and ambiguous bases were allowed at any position. There was a total of 416 positions in the final dataset. Evolutionary analyses were conducted in MEGA7.[29]

Extraction and isolation. Fungal cultures were treated with XAD-7 resin (10% w/v) and left overnight after separation of fungal mycelia from culture broth by filtration. XAD-7 resin was collected by filtration, washed with 2 L of DI-water, and then extracted with 2 L of 1:1 acetone:methanol mixture. The extract was concentrated before partitioning between EtOAc and water. The aqueous layer was washed three times with EtOAc. The organic layers were combined, dried and concentrated *in vacuo*. The organic extract of a 7 L culture in 1158 media (malt extract 20 g/L; D-glucose

10g/L; yeast extract 2g/L; NH_4HSO_4 0.5 g/L; pH 6.0) was separated into 7 fractions by normal phase vacuum liquid chromatography (VLC) eluted with a DCM to MeOH gradient (Fraction 1: 99:1 DCM:MeOH; Fraction 2: 30:1 DCM:MeOH; Fraction 3: 15:1 DCM:MeOH; Fraction 4: 9:1 DCM:MeOH; Fraction 5: 3:1 DCM:MeOH; Fraction 6: 1:1 DCM:MeOH; Fraction 7: 0:1 DCM:MeOH). Compounds were isolated directly from these fractions using preparative HPLC with isocratic mobile phases or shallow gradients of mobile phase (20% CH_3CN to 56% CH_3CN over 28 mins). Prior to isolation of **3.4** and **3.5**, 5 µg of butylated hydroxytoluene (BHT) was added to the collection vial to prevent oxidation. HPLC purification yielded ustusal A (**3.1**) - 3.0 mg; ustusolate F (**3.2**) - 2.51 mg; ustusolate G (**3.3**) - 3.4 mg; ustusoic acid A (**3.4**) - 1.7 mg; ustusoic acid B (**3.5**) - 1.5 mg.

Ustusal A (**3.1**)**:** white amorphous solid; $[\alpha]_D^{21}$ +5 (*c* 0.1, MeOH); ECD (*c* 0.1, MeOH) 209 (+0.8), 305 (+0.1); UV (*c* 0.1, MeOH) λ_{max} (log ε) 205 (0.2); ^{13}C NMR (176 MHz, DMSO-d_6) and ^{1}H NMR (500 MHz, DMSO-d_6) see Table 3.1; HRESIMS: *m/z* 275.1615 $[M+Na]^+$ (calcd for $C_{15}H_{24}NaO_3$(+1) 275.162; Δppm = 1.0)

Ustusolate F (**3.2**)**:** white amorphous solid; $[\alpha]_D^{21}$ -75 (*c* 0.1, MeOH); IR (ATR): ν_{max} = 3358, 2923, 2852, 1695, 1653, 1600, 1392, 1355, 1272, 1067; ECD (*c* 0.1, MeOH) 206 (-5.4), 300 (-1.0); UV (MeOH, *c* 0.1) λ_{max} (log ε) 304 (4.0); ^{13}C NMR (176

MHz, MeOH-d_4) and ^{1}H NMR (500 MHz, MeOH-d_4) see Table 3.1; HRESIMS: *m/z* 415.1770 $[M-H]^-$ (calcd for $C_{23}H_{27}O_7$(-1) 415.176; Δppm = 1.9)

Ustusolate G (**3.3**)**:** white amorphous solid; $[\alpha]_D^{22}$ -18 (*c* 0.1, MeOH); ECD (*c* 0.1, MeOH) 213 (-2.4); UV (*c* 0.1, MeOH) λ_{max} (log ε) 216 (3.1); ^{13}C NMR (176 MHz, MeOH-d_6) and ^{1}H NMR (500 MHz, MeOH-d_6) see Table 3.1; HRESIMS: *m/z* 391.1771 $[M-H]^-$ (calcd for $C_{21}H_{27}O$(-1) 319.176; Δppm = 2.2)

Ustusoic acid A (**3.4**)**:** white amorphous solid; $[\alpha]_D^{21}$ -29 (*c* 0.1, MeOH); ECD (*c* 0.1, MeOH) 219 (-2.0), 311 (-0.5); UV (*c* 0.1, MeOH) λ_{max} (log ε) 308 (3.8); ^{13}C NMR (176 MHz, MeOH-d_6) and ^{1}H NMR (500 MHz, MeOH-d_6) see Table 3.1; HRESIMS: *m/z* 403.2136 $[M-H]^-$ (calcd for $C_{23}H_{31}O_6$(-1) 403.213; Δppm = 2.5)

Ustusoic acid B (**3.5**)**:** white amorphous solid; $[\alpha]_D^{21}$ -23 (*c* 0.1, MeOH); ECD (*c* 0.1, MeOH) 234 (-1.3), 306 (-0.4), 338 (0.2); UV (*c* 0.1, MeOH) λ_{max} (log ε) 308 (3.5); ^{13}C NMR (176 MHz, MeOH-d_6) and ^{1}H NMR (500 MHz, MeOH-d_6) see Table 3.1; HRESIMS: *m/z* 401.1978 $[M-H]^-$ (calcd for $C_{23}H_{29}O_6$(-1) 401.197; Δppm = 2.1)

Methylation of ustusolate F. Compound **3.2** (1.85 μmols in 75 μl of DMF) was added to a DMF solution of MeI (25 μl of 0.115 M) and K_2CO_3 (3.5 mg) and the reaction was monitored by TLC. After 24 hr, the reaction was complete and quenched with 1 mL of water. The solution was then extracted 5 times with EtOAc. Organic layers were combined and concentrated under reduced pressure. The methylated

product was then purified by semi-preparative HPLC (60% CH_3CN isocratic). Selected ^{13}C NMR data (176 MHz, $CDCl_3$) δ 166.9 (C, C-8'), 51.9 (H_3, C-9'); Selected ^{1}H NMR data (700 MHz, $CDCl_3$) δ 3.77 (3H, s, H-9'); LRESIMS: *m/z* 453.3 $[M+Na]^+$, 431.0 $[M+H]^+$, 413.2 $[M-18+H]^+$

Computational details. Initial conformational analysis was performed in Spartan[30] using the MMFF force field and random rotor conformational search with 100 conformers. Density functional theory calculations were performed using the Gaussian 09 package.[31] The conformer sets generated were subjected to gas phase QM geometry optimizations and frequency calculations at B3LYP/6-31+G before solvated geometry optimizations at M062X/TZVP with SDM-IEFPCM in methanol. ECD spectra were calculated by the TDDFT methodology at the ωB97X/def2-TZVP utilizing IEFPCM in methanol, CAM-B3LYP/TZVP with IEFPCM in methanol and M062X/def2-TZVP utilizing IEFPCM in methanol. ECD spectra were simulated using SpecDis 1.71.[32] NMR shielding tensors were computed from the gas phase QM geometry optimizations with the GIAO methodology at the mPW1PW91/6-311+G(2d,p) level of theory with IEFPCM in methanol. Shielding tensors were extracted from Gaussian out files and Boltzmann weighted following the published procedure[22] on a Windows 10 operating system. DP4+ probabilities[21] were used for relative stereochemistry analysis directly with unscaled shielding tensors.

Antimicrobial assays. Organic extracts and fractions were tested for inhibitory activity against multidrug-resistant *Staphylococcus aureus* (ATCC BAA-44), vancomycin-resistant *Enterococcus faecium* (ATCC 700221), *Bacillus subtilis* (ATCC 49343), *Pseudomonas aeruginosa* (ATCC 15442), and *Candida albicans* (ATCC 90027), in micro-broth assays performed following established protocols.[33] MIC determination for fractions and pure compounds followed published procedures.[34] For MIC of **3.4** and **3.5**, along with combi-treatments, BHT was added to all wells, included controls, at 2.5 μg/mL. For combi-treatment, **3.5** and **3.6** were added to test wells in a 1:1 μg/mL ratio and the above MIC determination procedure was followed. CDI's were determined according to published procedure.[25] All human pathogens used in the study were acquired from commercially sources like the American Type Culture Collection (ATCC, Manassas, VA) in 2014 and met specification prior to shipping.

Cytotoxicity Assay. Cytotoxic activities of extracts and pure compounds were evaluated against colon (HCT-116) cancer models by measuring the reduction of the tetrazolium salt MTT (3-(4, 5-dimethylthiazolyl-2)-2, 5-diphenyltetrazolium bromide) by metabolically active cells following standard procedures.[35]

3.5 Acknowledgments

This work was supported by OSU start-up funds and by the National Science Foundation under grant CHE 1808717. *Aspergillus ustus* was provided by Joey Spatafora (OSU) – thank you! We acknowledge the support of the Oregon State

University's NMR Facility funded in part by the National Institutes of Health, HEI grant 1S10OD018518, and by the M. J. Murdock Charitable Trust grant no. 2014162. We thank Z. Zhu and P. Mandelare for performing the cytotoxicity and antifungal assays, respectively.

3.6 References

(1) Hutchings, M.; Truman, A.; Wilkinson, B. *Current Opinion in Microbiology* **2019**, *51*, 72.
(2) CDC, Antibiotic Resistance Threats in the United States. Services, U. S. D. o. H. a. H., Ed. CDC: Atlanta, GA, 2019.
(3) (a) Blair, J. M. A.; Webber, M. A.; Baylay, A. J.; Ogbolu, D. O.; Piddock, L. J. V. *Nature Reviews Microbiology* **2015**, *13*, 42. (b) Bush, K.; Courvalin, P.; Dantas, G.; Davies, J.; Eisenstein, B.; Huovinen, P.; Jacoby, G. A.; Kishony, R.; Kreiswirth, B. N.; Kutter, E.; Lerner, S. A.; Levy, S.; Lewis, K.; Lomovskaya, O.; Miller, J. H.; Mobashery, S.; Piddock, L. J. V.; Projan, S.; Thomas, C. M.; Tomasz, A.; Tulkens, P. M.; Walsh, T. R.; Watson, J. D.; Witkowski, J.; Witte, W.; Wright, G.; Yeh, P.; Zgurskaya, H. I. *Nature Reviews Microbiology* **2011**, *9*, 894.
(4) (a) de Niederhäusern, S.; Bondi, M.; Messi, P.; Iseppi, R.; Sabia, C.; Manicardi, G.; Anacarso, I. *Current Microbiology* **2011**, *62*, 1363. (b) Patel, R.; Uhl, J. R.; Kohner, P.; Hopkins, M. K.; Cockerill, F. R., 3rd *Journal of Clinical Microbiology* **1997**, *35*, 703.
(5) O'Neil, J. Report on Antimicrobial Resistance. https://amr-review.org.
(6) (a) Hemaiswarya, S.; Kruthiventi, A. K.; Doble, M. *Phytomedicine* **2008**, *15*, 639. (b) Cheesman, M. J.; Ilanko, A.; Blonk, B.; Cock, I. E. *Pharmacognosy Reviews* **2017**, *11*, 57. (c) Obiang-Obounou, B. W.; Jang, Y. P. *Archives of Pharmacal Research* **2011**, *34*, 1579.
(7) Horak, R. M.; Steyn, P. S.; Vleggaar, R.; Rabie, C. J. *Journal of the Chemical Society, Perkin Transactions 1* **1985**, 363.
(8) Kohno, J.; Hiramatsu, H.; Nishio, M.; Sakurai, M.; Okuda, T.; Komatsubara, S. *Tetrahedron* **1999**, *55*, 11247.
(9) Hayes, M. A.; Wrigley, S. K.; Chetland, I.; Reynolds, E. E.; Ainsworth, A. M.; Renno, D. V.; Latif, M. A.; Cheng, X. M.; Hupe, D. J.; Charlton, P.; Doherty, A. M. *The Journal of Antibiotics* **1996**, *49*, 505.

(10) Zhu, T.; Lu, Z.; Fan, J.; Wang, L.; Zhu, G.; Wang, Y.; Li, X.; Hong, K.; Piyachaturawat, P.; Chairoungdua, A.; Zhu, W. *Journal of Natural Products* **2018**, *81*, 2.
(11) Ayer, W. A.; Pena-Rodriguez, L. M. *Journal of Natural Products* **1987**, *50*, 408.
(12) (a) Lu, Z.; Wang, Y.; Miao, C.; Liu, P.; Hong, K.; Zhu, W. *Journal of Natural Products* **2009**, *72*, 1761. (b) Liu, H.; Edrada-Ebel, R.; Ebel, R.; Wang, Y.; Schulz, B.; Draeger, S.; Müller, W. E. G.; Wray, V.; Lin, W.; Proksch, P. *Journal of Natural Products* **2009**, *72*, 1585.
(13) Shiono, Y.; Hiramatsu, F.; Murayama, T.; Koseki, T.; Funakoshi, T.; Ueda, K.; Yasuda, H. *Zeitschrift für Naturforschung B* **2007**, *62*, 1585.
(14) (a) Barrow, C. J.; Doleman, M. S.; Bobko, M. A.; Cooper, R. *Journal of Medicinal Chemistry* **1994**, *37*, 356. (b) Barrow, C. J.; Sedlock, D. M.; Sun, H. H.; Cooper, R.; Gillum, A. M. *The Journal of Antibiotics* **1994**, *47*, 1182.
(15) (a) Hopmann, C.; Knauf, M. A.; Weithmann, K.-u.; Wink, J. Preparation of stromemycins as stromelysin inhibitors. 2001. (b) Bringmann, G.; Lang, G.; Steffens, S.; Günther, E.; Schaumann, K. *Phytochemistry* **2003**, *63*, 437.
(16) White, T. J.; Bruns, T.; Lee, S.; Taylor, J., Amplification and direct sequencing of fungal ribosomal RNA genes for phylogenetics. In *PCR Protocols*, Innis, M. A.; Gelfand, D. H.; Sninsky, J. J.; White, T. J., Eds. Academic Press: San Diego, 1990; pp 315.
(17) Altschul, S. F.; Gish, W.; Miller, W.; Myers, E. W.; Lipman, D. J. *Journal of Molecular Biology* **1990**, *215*, 403.
(18) (a) Houbraken, J.; Due, M.; Varga, J.; Meijer, M.; Frisvad, J. C.; Samson, R. A. *Studies in Mycology* **2007**, *59*, 107. (b) Samson, R. A.; Varga, J.; Meijer, M.; Frisvad, J. C. *Studies in Mycology* **2011**, *69*, 81.
(19) Malani, A. N.; Kauffman, C. A. *Drugs* **2007**, *67*, 1803.
(20) Coupling constant cannot be measured due to unresolved splitting in 1H NMR spectrum.
(21) Grimblat, N.; Zanardi, M. M.; Sarotti, A. M. *The Journal of Organic Chemistry* **2015**, *80*, 12526.
(22) Willoughby, P. H.; Jansma, M. J.; Hoye, T. R. *Nature Protocols* **2014**, *9*, 643.
(23) Compounds 3 and 5 have been found to be commercially available from Aurora Fine Chemicals LLC. No source has been made available to the authors.
(24) (a) Hall, M. J.; Middleton, R. F.; Westmacott, D. *The Journal of Antimicrobial Chemotherapy* **1983**, *11*, 427. (b) Martinez-Irujo, J. J.; Villahermosa, M. L.; Alberdi, E.; Santiago, E. *Biochemical Pharmacology* **1996**, *51*, 635.
(25) Chen, L.; Ye, H.-L.; Zhang, G.; Yao, W.-M.; Chen, X.-Z.; Zhang, F.-C.; Liang, G. *PLoS One* **2014**, *9*, e85771.
(26) Adpressa, D. A.; Loesgen, S. *Chemistry & Biodiversity* **2016**, *13*, 253.
(27) Kimura, M. *Journal of Molecular Evolution* **1980**, *16*, 111.

(28) Clark, K.; Karsch-Mizrachi, I.; Lipman, D. J.; Ostell, J.; Sayers, E. W. *Nucleic Acids Research* **2016**, *44*, D67.
(29) Kumar, S.; Stecher, G.; Tamura, K. *Molecular Biology and Evolution* **2016**, *33*, 1870.
(30) Hanwell, M. D.; Curtis, D. E.; Lonie, D. C.; Vandermeersch, T.; Zurek, E.; Hutchison, G. R. *Journal of Cheminformatics* **2012**, *4*, 1.
(31) Frisch, M. J.; Trucks, G. W.; Schlegel, H. B.; Scuseria, G. E.; Robb, M. A.; Cheeseman, J. R.; Scalmani, G.; Barone, V.; Mennucci, B.; Petersson, G. A.; Nakatsuji, H.; Caricato, M.; Li, X.; Hratchian, H. P.; Izmaylov, A. F.; Bloino, J.; Zheng, G.; Sonnenberg, J. L.; Hada, M.; Ehara, M.; Toyota, K.; Fukuda, R.; Hasegawa, J.; Ishida, M.; Nakajima, T.; Honda, Y.; Kitao, O.; Nakai, H.; Vreven, T.; Montgomery Jr., J. A.; Peralta, J. E.; Ogliaro, F.; Bearpark, M. J.; Heyd, J.; Brothers, E. N.; Kudin, K. N.; Staroverov, V. N.; Kobayashi, R.; Normand, J.; Raghavachari, K.; Rendell, A. P.; Burant, J. C.; Iyengar, S. S.; Tomasi, J.; Cossi, M.; Rega, N.; Millam, N. J.; Klene, M.; Knox, J. E.; Cross, J. B.; Bakken, V.; Adamo, C.; Jaramillo, J.; Gomperts, R.; Stratmann, R. E.; Yazyev, O.; Austin, A. J.; Cammi, R.; Pomelli, C.; Ochterski, J. W.; Martin, R. L.; Morokuma, K.; Zakrzewski, V. G.; Voth, G. A.; Salvador, P.; Dannenberg, J. J.; Dapprich, S.; Daniels, A. D.; Farkas, Ö.; Foresman, J. B.; Ortiz, J. V.; Cioslowski, J.; Fox, D. J. *Gaussian 09*, Gaussian, Inc.: Wallingford, CT, USA, 2009.
(32) Bruhn, T.; Schaumloffel, A.; Hemberger, Y.; Bringmann, G. *Chirality* **2013**, *25*, 243.
(33) L, N. C. f. C., Approved Standard M02-A11 and M100-S25. NCCLS, Ed. Wayne, PA, USA, 2002.
(34) Wiegand, I.; Hilpert, K.; Hancock, R. E. *Nature Protocols* **2008**, *3*, 163.
(35) Riss, T. L., Moravec, R.A. ,Niles, A.L., Duellman, S., Benink, H.A., Worzella, T.J., Minor, L. , Cell Viability Assays. In *Assay Guidance Manual*, Sittampalam, G. S.; Coussens, N. P.; Nelson, H. E. A., Eds. Eli Lilly & Company, and the National Center for Advancing Translational Sciences (NIH): Bethesda, MD, 2013.

Chapter Four: Polyketides from Marine-derived *Aspergillus porosus*: Challenges and Opportunities for Determining Absolute Configuration

George F. Neuhaus, Donovon A. Adpressa, Torsten Bruhn, and Sandra Loesgen

Journal of Natural Products

1155 16th St. NW, Washington, DC 20036

Published September 26, 2019

82, pp. 2780-2789

doi: 10.1021/acs.jnatprod.9b00416

4.1 Abstract

Fungal natural products have inspired and enabled countless modern therapeutics. During a survey of the secondary metabolites of endophytic fungi, we found that *Aspergillus porosus* produces new polyketides with interesting structural features named porosuphenol A-D (**4.1**, **4.2**, **4.3a**, and **4.3b**). The structural elucidation of these metabolites was performed with 1D and 2D NMR techniques, Mosher ester analysis, *J*-based conformational analysis, and isotope exchange studies. The absolute configuration of these compounds was determined using typical approaches including comparative analysis of experimental NMR and electronic circular dichroism spectra with DFT calculations. However, these efforts were not providing conclusive results for porosuphenol A (**4.1**). To resolve this issue, we applied a strategy in which NMR data guides the conformer search. Herein are presented the structure elucidation of porosuphenols A-D as a case study in the challenges and opportunities for determination of absolute configuration. Lastly, bioassay-guided fractionation of cytotoxic fractions resulted in the additional isolation of pimarane diterpenes, sphaeropsidin A (**4.4**) and aspergiloid E (**4.5**).

4.2 Introduction

Determining the absolute configuration of a molecule is a vital step in reaching a complete understanding of its structure. Even today, with state-of-the-art spectroscopic techniques at our disposal, the continued challenge of this problem is evident by the number of recent revisions to natural product configurational assignments.[1] Natural products in particular, which inspire the majority of clinically approved drugs,[2] often pose difficult obstacles in the determination of absolute configuration due to their numerous asymmetric centers and overall complex chemical structures. This challenge is amplified when working with structures that have substantial conformational freedom. Molecular flexibility can be an obstacle in structure elucidation based on solution NMR experiments as the experimentally observed parameters are averages of multiple conformations at the NMR time scale. Similarly, computational models provide predictions for spectroscopic parameters that can be invaluable for configurational assignment, but models must be developed using correctly identified conformers.[3] Modeling the full conformational space and solvation effects of flexible structures can be prohibitively expensive computationally and may even require more accuracy than current methods can provide. Nonetheless, determining the absolute configuration of natural products is imperative for understanding their biological activity and also for developing drug leads. Herein, we report on four new, linear polyketides, porosuphenols A, B, C, and D (**4.1**, **4.2**, **4.3a**, and **4.3b**) as well as two

known metabolites (**4.4** and **4.5**) from *Aspergillus porosus*. Initial efforts to the absolute configuration of porosuphenol A (**4.1**) were obstructed by the conformational flexibility of the structure and inconclusive modeling results. As an alternative approach to the usually applied Boltzmann weighting, we employed experimentally informed conformational restrictions that were developed for the structure determination using NMR calculations (CASE-3D).[3a]

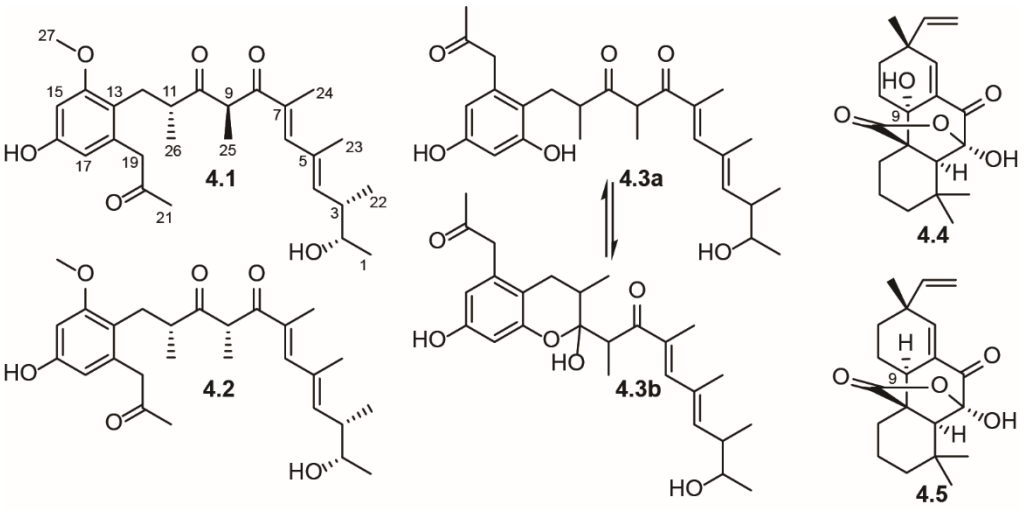

Figure 4.1: Structures of isolated NPs

As part of an ongoing research program to explore the chemical diversity of endophytic fungi, we performed chemical- and bioactivity-guided screening of extracts from a marine-derived endophyte, *Aspergillus porosus*.[4] The organic extract of a malt-based broth culture was found to contain a class of new polyketides (**4.1**-**4.3**), exhibiting a dynamic diene-dione functionality within a flexible carbon chain. The

closest structural relative of these new fungal polyketides can be found in a benzaldehyde intermediate within the azaphilone biosynthetic pathway.[5] The common benzenediol is functionalized with a highly methylated[6] polypropionate-like[7] side chain and a methyl ketone, both containing a fully reduced carbon attached directly to the aromatic ring. This is unlike the common fungal benzenediol lactones[8] and azaphilones,[9] in which carbonyl groups are directly attached to the aromatic ring. Other structurally related compounds are the acyclic tetraprenylquinols found in brown algae,[10] in which the benzenediol core is prenylated to create the acyclic sidechain.

Alongside the structurally interesting porosuphenol polyketides, two known diterpene cytotoxins, sphaeropsidin A and aspergiloid E (**4.4** and **4.5**), were isolated and identified by comparing their spectroscopic data to literature values. Sphaeropsidin A (**4.4**) first isolated from *Aspergillus chevalieri*,[11] is an established phytotoxin[12] that has recently gained interest as a cytotoxic agent,[13] showing selectivity toward melanoma and kidney cancer cell lines with a unique mechanism of action targeting regulatory volume increase.[14] Interestingly, the nearly isostructural aspergiloid E (**4.5**), recently reported by Yan et al.,[15] has no bioactivity associated with it. Our bioactivity testing supports this difference in activity and adds to the established structure-activity-relationship studies.

4.3 Results and discussion

Isolated as an algal endophyte from the marine environment by BioViotica Naturstoffe GmbH, the *Aspergillus porosus* strain (G23N) was provided to us for chemical analysis with a putative identification as a member of the *Aspergillus* family based on preliminary morphological analysis. Upon amplification and sequencing of the complete internal transcribed spacer (ITS) regions 1 and 2, using primers ITS1 and ITS4,[16] we could place the fungus into *Aspergillus* section *Aspergillus* (Figure C.1, Appendix C). The ITS region is highly conserved within this section,[4] which required additional amplification of protein encoding regions, such as the partial β-tubulin (BenA), calmodulin (CaM), or RNA polymerase II second largest subunit (RPB2) genes for identification to the species level.[17] Phylogenetic analyses of the BenA region, amplified with primers Bt2a and Bt2b,[18] identified this strain as *Aspergillus porosus* (Figure C.2, Appendix C), a species recently described by Chen and co-workers.[4]

Compound **4.1** was isolated as a colorless oil (0.65 mg/L). The HRESIMS gave an *m/z* 459.2739 ($[M+H]^+$), providing a molecular formula of $C_{27}H_{38}O_6$ (Δ ppm 0.4; calcd for $C_{27}H_{39}O_6$, 459.2741) with 9 degrees of unsaturation. The UV spectrum of **4.1** (CH_3CN) displayed maximum absorbances at 202 and 286 nm, indicating a conjugated system. Major bands in the IR spectrum of **4.1** include a broad band for a hydroxy group at 3390 cm^{-1}, a sharp strong carbonyl stretch at 1709 cm^{-1}, a strong band at

Table 4.1: ^{1}H and ^{13}C NMR spectroscopic data for compounds **4.1** and **4.2**

	porosuphenol A (**4.1**)		porosuphenol B (**4.2**)	
position	δ_C, type	δ_H (J in Hz)	δ_C, type	δ_H (J in Hz)
1	21.3, CH_3	1.12, d (6.4)	21.4, CH_3	1.09, d (6.3)
2	71.7, CH	3.60, p (6.4)	71.8, CH	3.57, p (6.3)
3	41.3, CH	2.52, dqd (9.8, 6.8, 6.4)	41.4, CH	2.50, dqd (10, 6.8, 6.3)
4	142.3, CH	5.59, d (9.8)	141.5, CH	5.57, d (10)
5	133.0, C		133.0, C	
6	146.1, CH	6.69, s	145.7, CH	6.98, s
7	134.4, C		134.9, C	
8	201.9, C		200.9, C	
9	54.8, CH	3.97, q (6.9)	53.8, CH	4.53, q (6.9)
10	212.1, C		212.3, C	
11	45.9, CH	2.80, dqd (8.7, 6.7, 6.2)	45.8, CH	2.90, dqd (8.3, 7.0, 6.0)
12a	31.5, CH_2	2.56, dd (13.8, 8.7)	29.6, CH_2	2.62, dd (13.9, 6.0)
12b		2.40, dd (13.8, 6.2)		2.45, dd (13.9, 8.3)
13	119.0, C		119.3, C	
14	159.8, C		160.2, C	
15	98.7, CH	6.34, d (2.1)	98.7, CH	6.32, d (2.2)
16	157.2, C		157.0, C	
17	110.4, CH	6.17, d (2.1)	110.3, CH	6.13, d (2.2)
18	136.5, C		136.7, C	
19a	48.6, CH_2	3.62, d (16.9)	48.8, CH_2	3.72, d (16.9)
19b		3.56, d (16.9)		3.57, d (16.9)
20	206.9, C		207.2, C	
21	29.7, CH_3	2.08, s	29.8, CH_3	2.10, s
22	16.2, CH_3	1.03, d (6.8)	16.4, CH_3	1.00, d (6.8)
23	16.8, CH_3	1.88, br s	16.9, CH_3	1.88, br s
24	13.3, CH_3	1.84, br s	13.6, CH_3	1.87, br s
25	13.8, CH_3	1.00, d (6.9)	14.1, CH_3	1.14, d (6.9)
26	17.3, CH_3	0.95, d (6.7)	17.1, CH_3	0.90, d (7.0)
27	56.0, CH_3	3.71, s	56.0, CH_3	3.73, s

1645 cm^{-1} indicative of an unsaturated ketone, and a strong band at 1606 cm^{-1} correlating with a conjugated diene. The ^{13}C NMR spectrum displayed three keto carbon atoms above 200 ppm, ten aromatic or olefinic carbons atoms and thirteen aliphatic carbon atoms (Table 4.1). The ^{1}H NMR spectrum of **4.1** exhibited two

aromatic and two olefinic signals (5.5-7.0 ppm), one methoxy signal (δ_H 3.71 ppm), two sets of diastereotopic methylene signals, four methine multiplets, three methyl singlets, and four methyl doublets.

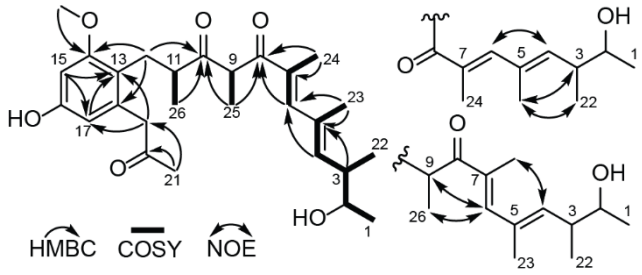

Figure 4.2: Key COSY, HMBC (left), and NOE correlations (right) of **4.1** and **4.2**

Determination of the structure of **4.1** required 2D NMR correlation experiments including COSY, HMBC, and HSQC. Utilizing COSY, four distinct spin systems were constructed and connected with key HMBC correlations (Figure 4.2). The trisubstituted double bond between C-4 (δ_C 142.3 ppm) and C-5 (δ_C 133.0 ppm) was supported by a long-range COSY correlation between H-4 and H-23 (δ_H 5.59 and 1.88 ppm) along with HMBC correlations from H-3 (δ_H 2.52 ppm) and H-23 to C-5. The second trisubstituted double bond (C-6/C-7; δ_C 146.1/134.4 ppm) was placed by a long-range COSY correlation between H-6 and H-24 (δ_H 6.69 and 1.84 ppm), along with a HMBC correlation from H-24 to C-7 (δ_C 134.4 ppm). HMBC correlations between H-4 and H-23 to C-6 (δ_C 146.1 ppm); and from H-6 and H-24 to C-8 (δ_C 201.9 ppm), supported the attachment of the double bonds to the carbonyl group at C-8 and fully described the dieneone moiety. The isolated H-9/H_3-25 spin system could be placed between the 1,3-

diketone moiety due to the deshielded signal of H-9 (δ_H 3.97 ppm) along with HMBC correlations from H-25 (δ_H 1.00 ppm) to C-8 and C-10 (δ_C 201.9 and 212.1 ppm). The final H-11/H-12/H_3-26 spin system could be linked to C-10 by the HMBC correlations from H-26, H-12a, and H-12b to C-10, thus completing the side chain. HMBC correlations from H_3-21 (δ_H 2.08 ppm) to C-20 and C-19 (δ_C 206.9 and 48.6 ppm) confirmed an acetonyl moiety. The benzenediol core consisted of four aromatic carbons (δ_C 119.0, 98.7, 110.4, and 136.5 ppm) and two oxygenated aromatic carbons (δ_C 159.8 and 157.2 ppm). A long-range COSY (J = 2.2 Hz) correlation between H-15 and H-17 (δ_H 6.34 and 6.17 ppm) required that these protons are *meta* to one another. Strong HMBC correlations from H-15 to C-13 and C-17 (δ_C 119.0 and 110.4 ppm) along with correlations from H-17 to C-13 and C-15 (δ_C 119.0 and 98.7) further supported the assignment proposed. The methoxy group (δ_H 3.71 ppm) was placed at C-14 (δ_C 159.8 ppm) due to its HMBC correlation. HMBC correlations from the methylene H-12a/H-12b to C-14 (δ_C 159.8) and C-18 (δ_C 136.5) support the placement of the side chain next to the methoxy group. The acetonyl moiety was located *meta* to the methoxy group due to HMBC correlations from H-19a/H-19b (δ_H 3.62/3.56 ppm) to C-13 and C-17 in **4.1**.

The double bond geometry of **4.1** was established from NOE experiments. The C-4/C-5 double bond was determined as *E* based on three NOE correlations that were observed: H-4/H-6, H-23/H-3, and H-23/H-22 (Figure 4.2). The C-6/C-7 double bond

was also assigned *E* as shown by NOE correlations between H-4/H-24, H-6/H-9, and H-6/H-25 (Figure 4.2).

With four asymmetric carbon centers and a flexible linear sidechain, assigning the absolute configuration of **4.1** proved to be a difficult task. The secondary alcohol was accessible to Mosher ester analysis[19] by separately reacting **4.1** with both *R* and *S* α-methoxy-α-trifluoromethylphenylacetic (MTPA) acid chlorides to give the **4.1***S* and **4.1***R* MTPA esters, respectively. Comparative analysis of the ^{1}H NMR spectra of both MTPA esters assigned unequivocally C-2 as being *S* configured (Figure 4.3 and Figure C.28, Appendix C). With the absolute configuration of the secondary alcohol established, a *J*-based conformational analysis[20] was used to determine the configuration of the vicinal methyl group (C-22). Due to the medium magnitude of the $^{3}J_{(H2\text{-}H3)}$ coupling constant (6.4 Hz), an equilibrium of conformers must be considered.[20] Out of the six possible pairs of conformers (3-*erythro*; 3-*threo*) (Figure C.32, Appendix C), the **A1**/**A2** equilibrium was the only one with the expected coupling constants that matched the $^{2\text{-}3}J_{(C\text{-}H)}$ coupling constants measured from HETLOC[21] spectrum (Figure 4.3). This supported a *threo* relationship between H-2 and H-3, making the absolute configuration 3*S*. To save precious material, the remaining two asymmetric centers were assigned by the loss-free comparative analysis of computed and experimental spectroscopic data, including ^{1}H and ^{13}C chemical shifts, coupling constants, NOE

distances, UV, and electronic circular dichroism (ECD) spectra. A discussion of the computational analysis performed is presented below.

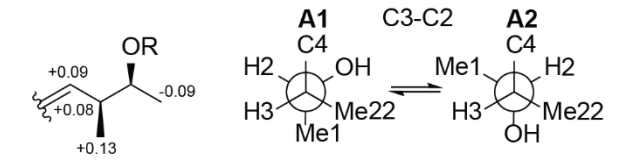

4.1*S* R = (S)-MTPA
4.1*R* R = (R)-MTPA

	4.1(Hz)	**4.2**(Hz)	
$^{3}J_{(H2,H3)}$	6.4	6.3	medium
$^{3}J_{(Me1,H3)}$	2.2	2.5	small
$^{3}J_{(C4,H2)}$	2.7	2.7	small
$^{3}J_{(Me22,H2)}$	4.7	3.4	medium
$^{2}J_{(C2,H3)}$	-4.8	-4.6	medium

Figure 4.3: $\Delta\delta_{S\text{-}R}$ values for MTPA esters of **4.1** (**4.1***S* and **4.1***R*). Experimental $^{3}J_{(H\text{-}H)}$ and $^{2\text{-}3}J_{(C\text{-}H)}$ values of **4.1** and **4.2** leading to assignment of the rotamer equilibrium between A1 and A2.

Compound **4.2** was isolated as a colorless oil and was found to have an identical mass and molecular formula of $C_{27}H_{38}O_6$ ($[M+H]^+$, *m/z* 459.2738; Δ ppm 0.7; calcd for $C_{27}H_{39}O_6$, 459.2741) compared to **4.1**. Similar UV, IR, and NMR data (Table 4.1) indicate that **4.2** is a stereoisomer (Figure 4.2). The double bond geometry was examined with NOE experiments and both double bonds were established as *E*, establishing a diastereomeric relationship between **4.1** and **4.2.**

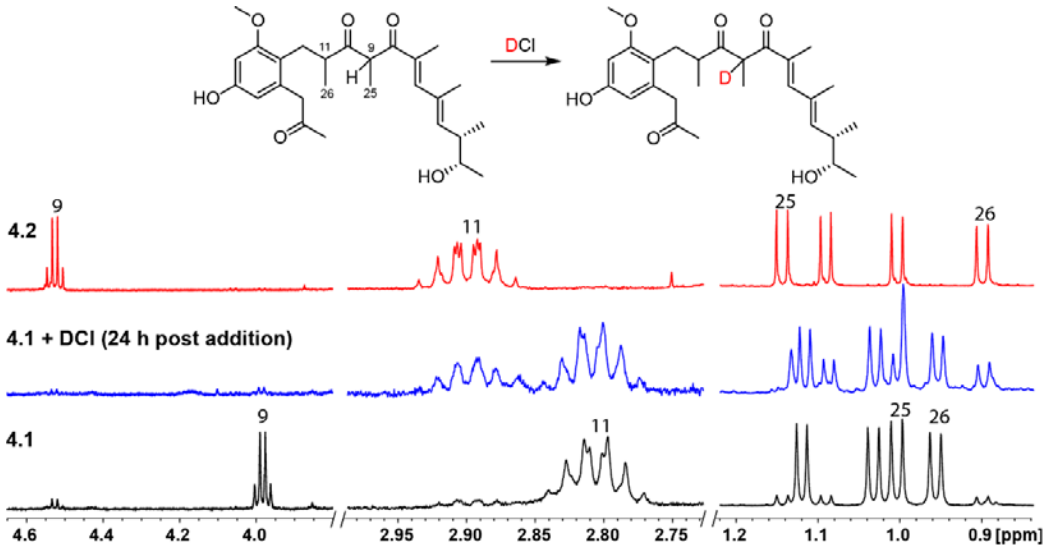

Figure 4.4: Key regions of the ^{1}H NMR spectrum of a deuterium-exchange study using compound **4.1**

Deuterium exchange studies were used to establish the stereochemical relationship between **4.1** and **4.2**. DCl was added to a solution of **4.1** and the mixture was monitored by ^{1}H NMR spectroscopy. Once equilibrated, the ^{1}H NMR spectrum showed a mixture of **4.1** and **4.2** (1.4:1), with the signal corresponding to H-9 clearly diminished as expected from the acidic proton H-9 in a 1,3 diketo system (Figure 4.4). This was used to establish **4.1** and **4.2** as C-9 epimers and supports the absolute configuration as *S* for both C-2 and C-3 of **4.2**. The lower pH in the fungal culture (pH 5.5) could be responsible for production of both diastereomers. This stereochemical relationship was further supported by the Mosher ester analysis of **4.1**, and by the $^{3}J_{(H2\text{-}H3)}$ and $^{2\text{-}3}J_{(C\text{-}H)}$ values of **4.2** being almost identical to those observed in **4.1** (Figure 4.3). The

remaining two asymmetric centers for both **4.1** and **4.2** were assigned by comparison of QM calculated NMR.

To determine the absolute configuration for the porosuphenols, computational methods were used to predict chiroptical properties (ECD) and chemical shift computations of candidate structures.[3c] A standard pipeline was used initially for performing this analysis: (1) a library of conformers was created using automatic sampling tools based on molecular mechanics calculations; (2) density functional theory (DFT) calculations were applied to determine optimized geometries, free energies, and NMR shielding tensors for NMR chemical shift predications; (3) Boltzmann-average of NMR shift data were assembled, and computed chemical shifts and ECD spectra were compared to experimental data.[22]

Table 4.2**:** CMAE for compounds **4.1** and **4.2** compared with NMR isotropic shift values computed at the WP04/aug-cc-pVDZ level with chloroform IEFPCM solvation

	2*S*,3*S*,9*R*,11*R*	2*S*,3*S*,9*S*,11*R*	2*S*,3*S*,9*R*,11*S*	2*S*,3*S*,9*S*,11*S*
CMAE **4.1**:	0.14	**0.10**	0.18	0.19
CMAE **4.2**:	**0.13**	0.16	0.20	0.23

An initial conformational analysis of the four possible configurations (2*S*,3*S*,9*R*,11*R*; 2*S*,3*S*,9*S*,11*R*; 2*S*,3*S*,9*R*,11*S*; 2*S*,3*S*,9*S*,11*S*) was performed using Spartan and the MMFF force field. The subsequent reoptimization of the conformers was done with the hybrid density functional B3LYP with the 6-31+G* basis set.

Conformers within an energy range of 3 kcal/mol were further processed with the hybrid WP04 functional for computation of high accuracy proton chemical shifts.[23] The results from these computations excluded the configurations 2*S*,3*S*,9*R*,11*S* and 2*S*,3*S*,9*S*,11*S* for **4.1** and **4.2** (Table 4.2), with 2*S*,3*S*,9*S*,11*R* providing a corrected mean absolute error (CMAE) of 0.10 for **4.1** and 2*S*,3*S*,9*R*,11*R* providing a CMAE of 0.13 for **4.2**. This result agreed with the deuterium-exchange study that established **4.1** and **4.2** as C-9 epimers.

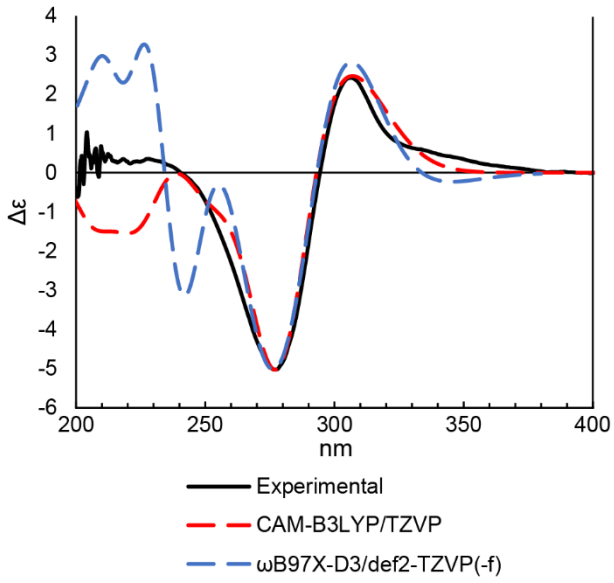

Figure 4.5: Experimental ECD spectra of **4.2** in acetonitrile with computed 2*S*,3*S*,9*R*,11*R* diastereomer. Red dotted line: CAM-B3LYP/TZVP (shift: 6 nm; σ = 0.25 eV; Δ_{ESI} = 0.9059), blue dotted line: ωB97X-D3/def2-TZVP(-f) (shift: 20 nm; σ = 0.3 eV; Δ_{ESI} = 0.8165)

Since it is desirable and good practice to support assignments with multiple lines of evidence,[3c] next ECD spectra were computed for each possible configuration of **4.1** and **4.2**. TDDFT calculations of ECD spectra of the 2*S*,3*S*,9*R*,11*R*-configured diastereomer at the CAM-B3LYP/TZVP level with integral equation formalism PCM (IEFPCM) in acetonitrile provided a good match for the experimental spectra of **4.2** with a Δ_{ESI} = 0.9059 (Figure 4.5), providing further support for this as the correct configuration. In addition, wB97X-D3/def2-TZVP(-f) gave a similar curve, showing that the functionals used were well-suited for the ECD calculations.

Interestingly, none of the computed ECD spectra of any tested configurations (2*S*,3*S*,9*R*,11*R*; 2*S*,3*S*,9*S*,11*R*; 2*S*,3*S*,9*R*,11*S*; or 2*S*,3*S*,9*S*,11*S*) produced a good fit with the experimental ECD spectra for **4.1**. However, with confidence gained in the computational assignment of ECD and NMR shifts for **4.2** and the knowledge from the deuterium-exchange experiments that **4.1** had to be the C9 epimer of **4.2**, the conformational analysis for **4.1** were revisited and the dispersion-corrected B3LYP-D3 method was used to re-evaluate the conformational ensemble. At the same time, the automatic sampling process in Spartan was revisited and indeed additional conformations were found of the C-9 enantiomer, which were not originally included. This highlights the need to thoroughly review the conformational space, rather than use automatic tools as black box approaches.

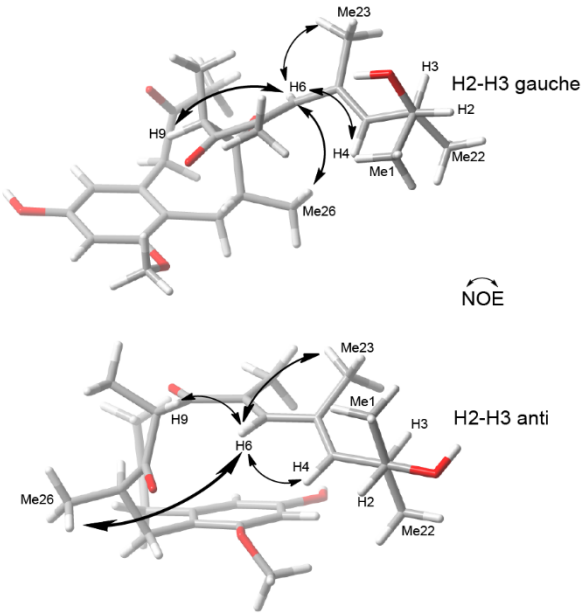

Figure 4.6: The two best 2*S*,3*S*,9*S*,11*R* conformers for **4.1** resulting from Stereofitter analysis with NOE and coupling constant constraints

Closer analysis of the low energy conformers comprising the Boltzmann distributions based on the DFT energies for **4.1** revealed that none of the significantly populated conformers exhibited an *anti*-configuration between H-2 and H-3 (Figure 4.3 and 4.6). To yield the averaged 6.4 Hz $^{3}J_{(H2\text{-}H3)}$ coupling constant observed experimentally for compound **4.1**, an approximate 3:2 ratio of *anti*:*gauche* conformers must be present. Even single point energy calculations using implicit solvent effects (CPCM, PCM) with and without dispersion at a number of levels of theory (M06-2X, B3LYP-D3, B3LYP) and coupled-cluster calculations using DLPNO-CCSDT/def2-

TZVP[24] (Table C.1, Appendix C) failed to produce a conformer ensemble that reflected the experimentally observed spectra for **4.1**.

Table 4.3: NOE distances and coupling constants used as constraints in Stereofitter, alongside computed averages for each conformer ensemble and χ^2 values for each ensemble

	expt.	2*S*,3*S*,9*R*,11*R*	2*S*,3*S*,9*S*,11*R*	2*S*,3*S*,9*R*,11*S*	2*S*,3*S*,9*S*,11*S*
$NOE_{H6,H9}$ (Å)	2.1	2.3	2.2	1.9	2.0
$NOE_{H6,H4}$ (Å)	2.6	2.7	2.6	2.9	2.6
$NOE_{H6,Me23}$ (Å)	3.0	2.8	3.0	2.9	2.9
$NOE_{H6,Me26}$ (Å)	3.5	3.8	3.9	3.3	3.8
$^3J_{H2,H3}$ (Hz)	6.4	6.3	6.1	6.5	6.1
$^3J_{Me1,H3}$ (Hz)	2.2	1.7	2.1	3.6	2.4
$^3J_{Me22,H2}$ (Hz)	4.7	3.5	4.1	3.8	3.3
χ^2		5.7	**4.4**	5.5	4.6

Based on these results, it appeared that conformational flexibility and an accumulation of small effects prevented efforts to construct an accurate conformer ensemble for compound **4.1** by computational methods. Approximations for dispersion and solvent effects significantly changed the energy of single conformers and yielded very different conformer ensembles. In the presented study, dispersion slightly overestimated hydrogen bonds, but the DLPNO-CCSDT results more or less confirmed the energetic order found with the DFT-D3 method. Similarly, addition of implicit solvent effects significantly changed the energetic order of conformers even with the coupled-cluster method, but did not produce an ensemble consistent with NMR data. It is possible that ab initio construction of an accurate conformer ensemble for **4.1** may

require consideration of explicit solvent effects, which would be prohibitively intensive computationally.

As an alternative, it was examined as to whether the conformer search could be guided by the experimental NMR data. Stereofitter (Mestrelab)[3a] was used to sample conformers based on experimental $^{3}J_{(C\text{-}H)}$ coupling constants and NOE-derived distances of **4.1** to more accurately model the conformation of the side chain. From the HETLOC spectra recorded in the *J*-based conformational analysis, $^{3}J_{(H2\text{-}H3)}$, $^{3}J_{(Me1\text{-}H3)}$, and $^{3}J_{(Me22\text{-}H2)}$ were used as constraints for the terminal end of the side chain. In addition to this, NOE distances between H-6/H-9, H-6/H-4, H-6/Me-26, and H-6/Me-23 were obtained using the Peak Amplitude Normalization for Improved Cross-relaxation (PANIC) approach.[25] Briefly, fully relaxed 1D PFGSE NOE spectra[26] with zero-quantum suppression[27] were recorded with varying mixing times. PANIC plots (integral ratio of NOE peak to inverted peak plotted against mixing time, Figure C.29, Appendix C) were then used to obtain the cross-relaxation rate constants, from which accurate NOE distances were obtained.[28] Combining these NOE distances to the above-mentioned coupling constants provided experimental evidence for the conformation of the side chain. Next, these NOE derived distances, $^{3}J_{HH}$, and $^{3}J_{CH}$ couplings (Table 4.3) were used as constraints to generate conformer ensembles. In each instance, Stereofitter provided combinations of two conformers (Figure 4.6, Table C.2, Appendix C) that best fit the NOE distances and *J* values. Of the four configurations, 2*S*,3*S*,9*S*,11*R*

provided the best χ^2 values for *J* and NOE distance values (Table 4.3) for **4.1**. Computation of ECD spectra for this ensemble at the ωB97XD/def2-TZVP level with conductor-like PCM (CPCM) in acetonitrile provided a good match for the experimental spectra, with a Δ_{ESI} = 0.9221 (Figure 4.7). This established the absolute configuration of **4.1** as 2*S*,3*S*,9*S*,11*R*, which was in full agreement with our NMR data and deuterium-exchange results obtained.

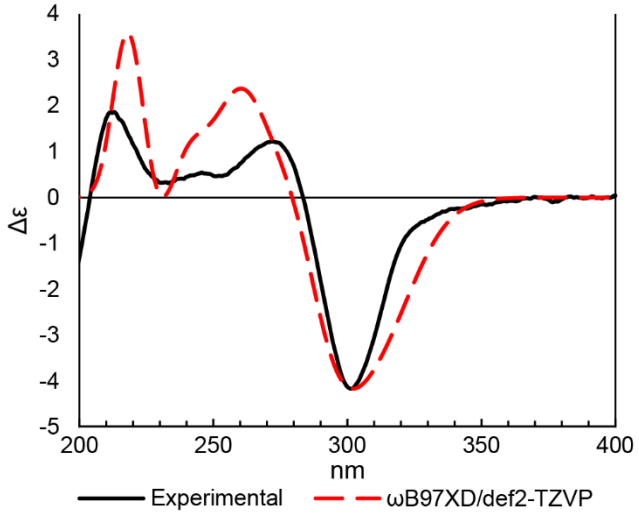

Figure 4.7: Experimental ECD spectra of **4.1** in acetonitrile with computed spectra of 2*S*,3*S*,9*S*,11*R* diastereomer. Red dotted line: ωB97XD/def2-TZVP (shift: -1 nm; σ = 0.22 eV; Δ_{ESI} = 0.9221)

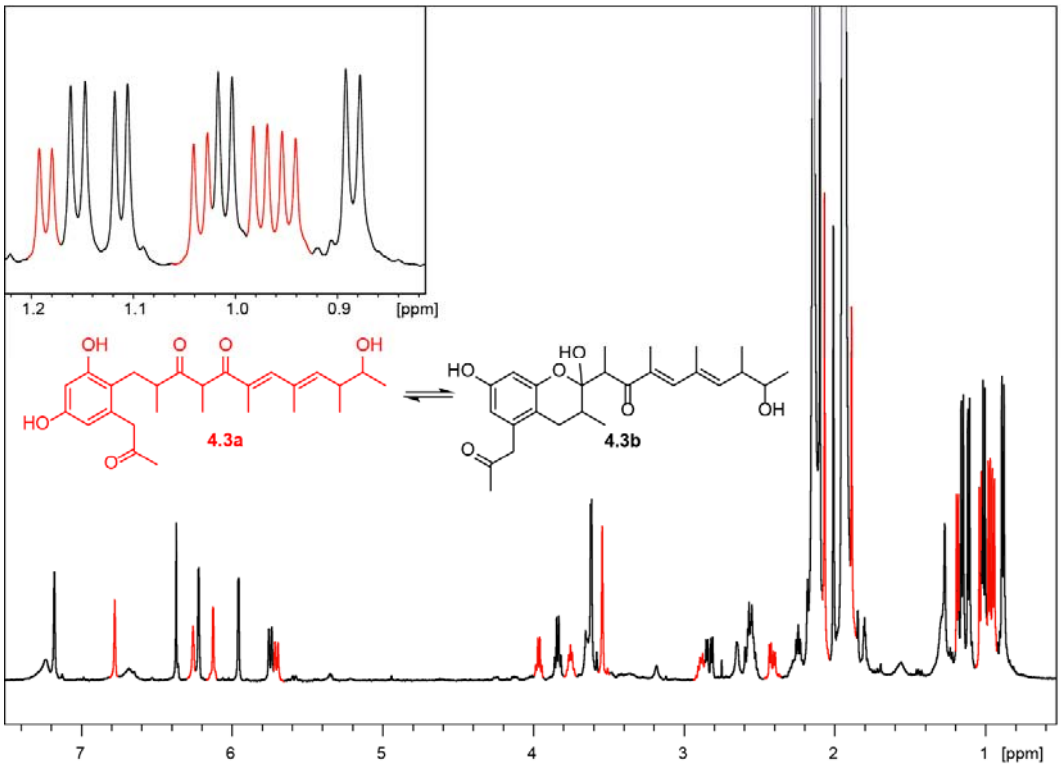

Figure 4.8: ^{1}H NMR spectrum of **4.3a** and **4.3b** in d_3-acetonitrile

Further chemical analysis efforts resulted in the isolation of compound **4.3**, a colorless oil with *m/z* 445.2572 ([M+H]$^{+}$) in HRESIMS. This was 14 mass units less than **4.1** and corresponded to a molecular formula of $C_{26}H_{36}O_6$ (Δ ppm = 2.8; calcd for $C_{26}H_{37}O_6$, 445.2580). The UV spectrum of **4.3** (acetonitrile) was only slightly shifted from that of **4.1**, with maxima at 210 and 289 nm, implying a similar structure. When a ^{1}H NMR spectrum was recorded in d_3-acetonitrile, **4.3** proved to be a mixture of two compounds (Figure 4.8) in a 1:1.35 ratio. After recording the 2D NMR spectra,

including COSY, HMBC and HSQC, the minor component, **4.3a** (porosuphenol C), could be determined as the 14-desmethyl analogue of **4.1** (Figure 4.9). With nearly identical correlations, the distinguishing feature of **4.3b** (porosuphenol D) was a ring closure, as evident by HMBC correlations from H-12a/H-12b, H-25, and H-26 to C-10 with a chemical shift of δC 102.7 in **4.3b** but δC 212.4 in **4.3a** (Table 4.4). This is a result of a nucleophilic attack by the phenol on C-14 to the C-10 carbonyl group in **4.3a**, generating the hemiketal **4.3b**. While both isomers are easily separated via preparative HPLC, the hemiketal formation/opening occurred within minutes, always resulting in a mixture of **4.3a** and **4.3b**. Due to rapid epimerization alongside the ketone-hemiketal equilibrium, attempts to assign the configuration of compound **4.3** were unsuccessful.

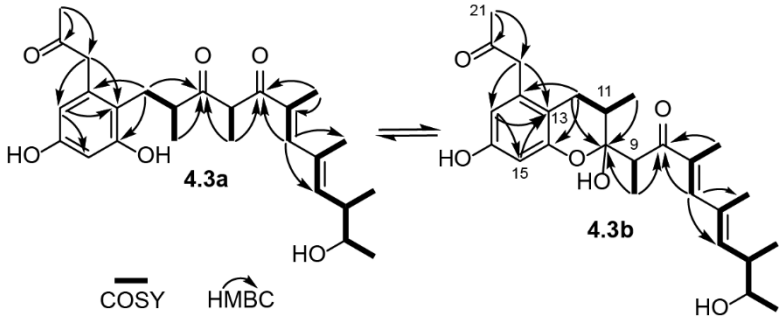

Figure 4.9: Key COSY and HMBC correlations of **4.3a** and **4.3b**

Table 4.4: ^{1}H and ^{13}C NMR spectroscopic data for compounds **4.3a** and **4.3b**

	porosuphenol C (**4.3a**)		porosuphenol D (**4.3b**)	
position	δ_C, type	δ_H (J in Hz)	δ_C, type	δ_H (J in Hz)
1	21.7, CH_3	1.19, d (6.3)	21.1, CH_3	1.11, d (6.3)
2	72.4, CH	3.75, dq (6.3, 5.7)	71.4, CH	3.65, m[a]
3	40.9, CH	2.55, dqd (9.9, 6.7, 5.7)	41.0, CH	2.55, m[a]
4	143.6, CH	5.71, d (9.9)	142.0, CH	5.75, d (9.9)
5	-[a]		-[a]	
6	146.8, CH	6.78, s	146.8, CH	7.18, s
7	134.2, C		135.3, C	
8	202.1, C		210.8, C	
9	54.5, CH	3.96, q (6.8)	41.5, CH	3.84 q (7.1)
10	212.4, C		102.7, C	
11	45.6, CH	2.89, dqd (9.2, 6.6, 5.7)	31.1, CH	2.24, m
12a	31.7, CH_2	2.42, dd (13.6, 5.7)	26.6, CH_2	2.83, dd (15.8, 5.9)
12b		2.57, dd (13.6, 9.2)		2.16, m[a]
13	117.2, C		112.4, C	
14	157.0, C		154.0, C	
15	102.3, CH	6.26, s	102.9, CH	5.96, br s
16	-[a]		-[a]	
17	110.3, CH	6.13, s	111.3, CH	6.22, br s
18	137.1, C		137.0, C	
19a	48.6, CH_2	3.54, s	48.3, CH_2	3.64, d (16.7)
19b				3.60, d (16.7)
20	207.0, C		206.8, C	
21	29.6, CH_3	2.07, s	29.5, CH_3	2.10, s
22	17.2, CH_3	1.03, d (6.7)	16.8, CH_3	1.01, d (6.8)
23	16.5, CH_3	1.94, s[b]	16.6, CH_3	1.93, s[b]
24	13.0, CH_3	1.89, s	13.4, CH_3	2.01, s
25	13.6, CH_3	0.98, d (6.8)	14.0, CH_3	1.15, d (7.1)
26	17.0, CH_3	0.95, d (6.6)	14.9, CH_3	0.88, d (7.0)

[a] Overlapped peaks

[b] Under residual solvent peak

Table 4.5: Bioactivity of sphaeropsidin A (**4.4**) and aspergiloid E (**4.5**)

	IC_{50} (μM)	
	sphaeropsidin A **4.4**	aspergiloid E **4.5**
S. aureus (ATCC 25923)	32.6 ± 1.3	71.6 ± 5.2
S. aureus (ATCC BAA-41)	35.3 ± 1.5	77.8 ± 5.4
P. aeruginosa (ATCC 15442)	>100	>100
HCT-116 (ATCC CCL-247)	4.9 ± 0.4	32.7 ± 2.3

[a] Positive controls: *S. aureus* ATCC 25923, *P. aeruginosa* ATCC 15442: 100% growth inhibition with 0.125 mg/ml kanamycin; *S. aureus* ATCC BAA-41: 100% growth inhibition with 0.125 mg/ml vancomycin. HCT-116 ATCC CCL-247: 82.8% cell growth inhibition with 200 μM etoposide.

All compounds isolated from *Aspergillus porosus* were tested for biological activity in antibacterial (*S. aureus,* ATCC 25923; *S. aureus,* ATCC BAA-41) and cytotoxicity assays (colon carcinoma HCT-116, ATCC CCL-247). Interestingly, only sphaeropsidin A (**4.4**) showed significant activity (Table 4.5), despite the nearly identical structure to aspergiloid E (**4.5**), as previously reported.[15] The only structural difference between these two diterpenoids is a hydroxy group at C-9 in **4.4**, compared to a methine in **4.5**. Although both structures contain a reactive Michael acceptor and a labile hemiketal, the inactivity of **4.5** might indicate that these shared functional groups are not the sole cause of bioactivity even if these functional groups may be considered PAINS.[29] It was also observed that **4.5** is less stable than **4.4**, when left in MeOD, **4.5** will form a mixture of methanol adducts, while **4.4** remains stable. The

porosuphenols A, B and C/D (**4.1**, **4.2**, **4.3a**, and **4.3b**) were inactive in antibacterial and cell viability assays and no activity was observed for antifungal, antimalaria,[30] antitubercular,[31] antioxidant, and metal chelating activity (> 50 μM).

Concluding Remarks: The present study presents a survey of the chemical structures and bioactivity of the algal endophyte *A. porosus*. This strain produces a diversity of secondary metabolites, consistent with previous studies that have found marine fungi are under-explored compared to terrestrial fungi and that marine plant-associated fungi are an especially rich source for metabolites. Four new metabolites named porosuphenol A-D (**4.1**, **4.2**, **4.3a**, and **4.3b**), and two known diterpenes (**4.4** and **4.5**) were isolated and their structures derived from extensive MS and NMR experiments. To establish the absolute configuration of these flexible polyketides, Mosher ester analysis was used combined with a *J*-based conformational analysis, DFT-based computations of spectroscopic and chiroptical data in comparison with experimental data. Initially, using the hybrid WP04 functional to compute ^{1}H NMR chemical shifts provided results that agreed with a deuterium-exchange study in that **4.1** and **4.2** are C-9 epimers. However, while computed ECD spectra provided a good fit for **4.2** as 2*S*,3*S*,9*R*,11*R*, none of the other configurations were a good fit for compound **4.1**. Further investigation revealed that the construction of the conformer ensemble was highly sensitive to a number of small effects. A refined conformational search guided by experimental NMR parameters was required to determine the absolute

configuration of **4.1** as 2*S*,3*S*,9*S*,11*R*, with best fit for all experimental parameters including $^{3}J_{(H\text{-}H)}$ and $^{3}J_{(C\text{-}H)}$ coupling constants, NOE distances, ^{1}H NMR chemical shifts, as well as ECD spectra. An unusual case of structures for which standard DFT-based conformational sampling failed for one specific configuration has been presented, most probably due to explicit solvent effects, and a solution using Stereofitter with implemented experimentally derived parameters was applied to yield the correct conformers for **4.1**. The structure of **4.3a**/**4.3b** was derived from MS and NMR experiments to be a 14-desmethyl derivative, however, due to rapid equilibrium between **4.3a** and **4.3b**, the linear and ring-closed isomers, the absolute configuration was not determined.

4.4 Experimental

General experimental procedures. Optical rotations were recorded on a JASCO P-1010 polarimeter. UV spectra were recorded on a BioRad SmartSpec3000. IR spectra were recorded on a Thermo Scientific Nicolet 6700 FT-IR spectrometer. ECD spectra were recorded on a JASCO J-1000 spectrometer. NMR spectra were acquired on a Bruker Avance III 500 MHz, Bruker Avance III 700 MHz, or a Bruker Avance III 800 MHz spectrometer equipped with a 5 mm TXI probe or 5 mm BBO probe (500 MHz and 700 MHz), TCI cryoprobe (700 MHz), or TXI cryoprobe (800 MHz), with the residual solvent used as an internal standard ($CDCl_3$: 7.26/77.16; CD_3CN: 1.94/118.26). Low-resolution ESIMS and HRTOFMS (ESI^+) mass spectra were

recorded on Agilent 1100 series LC with MSD 1946 and Agilent 1200 series LC with 6230 TOF MS, respectively. A Teledyne Isco CombiFlash Companion system was used for adaptive gradient, automated flash chromatography. Analytical HPLC was performed using an Agilent 1100 HPLC system equipped with a photodiode array detector. The mobile phase consisted of ultra-pure water (A) and CH_3CN (B) with 0.05% formic acid in each solvent. A gradient method from 10% A to 100% B in 35 min at a flow rate of 0.8 mL/min was used. The column (Phenomenex Kinetex C_{18}, 5 µm x 150 mm x 4.6 mm) was re-equilibrated before each injection and the column compartment was maintained at 30˚C throughout each run. Semi-preparative HPLC (Phenomenex Kinetex C_{18}, 5 µm x 150 mm x 10 mm) utilized isocratic elution conditions or a gradient system with a flow rate of 4 mL/min on an Agilent 1100 HPLC system operating at room temperature equipped with a photodiode array detector. Preparative HPLC (Phenomenex Luna C_{18}, 5 µm x 250 mm x 21mm) was conducted at room temperature, using isocratic elution conditions or a gradient system with a flow rate of 20 mL/min utilizing an Agilent 1260 Infinity series HPLC equipped with a DAD detector. All samples were filtered through a 0.45 µm nylon filter or centrifuged at 14,000 rpm for five min before LCMS and HPLC analysis. Analytical thin-layer chromatography (TLC) was performed on pre-coated silica gel 60 F_{254} plates (Eppendorf). TLC plates were visualized by UV (254 and 360 nm), and by spraying

with anisaldehyde solution followed by heating at 80 °C. General reagents were from Sigma-Aldrich and VWR International.

Identification of fungal species. The endophytic fungus *Aspergillus* sp., strain G23, was obtained from Bioviotica. Phylogenetic identification of the fungal strain was achieved by PCR amplification and sequencing of both the ITS and partial beta-tubulin encoding genes of DNA, according to a published procedure.[32] ITS1 forward primer and ITS4 reverse primer were used to amplify the complete ITS sequence[16] while Bt2a forward primer and Bt2b reverse primer were used to amplify the partial beta-tubulin encoding gene.[18] The closest match for the beta-tubulin gene fragment from a nucleotide megaBLAST was *Aspergillus porosus* (strain CBS 1417700) with 96% sequence coverage and 100% identity (GenBank:LT671130.1). The beta-tubulin gene fragment was required to further distinguish within *Aspergillus* section *Aspergillus*; see the phylogenetic trees below.[4]

The phylogeny was inferred by using the Maximum Likelihood method (Tamura 3-parameter model[33] for ITS and Kimura 2-parameter model[34] for partial beta tubulin gene fragment). The trees with the highest log likelihood (ITS = -862.4657; beta tubulin = -1353.3207) are shown (Figure C.1 and C.2, Appendix C). Initial tree(s) for the heuristic search were obtained automatically by applying Neighbor-Join and BioNJ algorithms to a matrix of pairwise distances estimated using the Maximum Composite Likelihood (MCL) approach, and then selecting the topology with superior log

likelihood value. The trees are drawn to scale, with branch lengths measured in the number of substitutions per site. The analysis involved 26 nucleotide sequences for ITS and nine for beta tubulin, all retrieved from GeneBank[35] or the NCBI BLAST targeted loci sequences from the fungi type and reference material collection.[36] All positions with less than 95% site coverage were eliminated. Accordingly, fewer than 5% alignment gaps, missing data, and ambiguous bases were allowed at any position. There was a total of 458 positions in the final dataset for the ITS region and 295 for the beta tubulin. Phylogenetic analyses were conducted in MEGA7.[37]

Extraction and isolation. All fungal cultures were extracted with 10 L EtOAc with shaking/stirring overnight after separation of fungal mycelia from culture broth by filtration. The organic layer was separated and washed with 10 L H_2O before evaporation to dryness in vacuo. The culture broth was then treated with XAD-7 resin and left overnight. XAD-7 resin was separated by filtration, washed with 2 L of DI-water, and then extracted with 2 L of 1:1 acetone-methanol mixture. The organic extract was concentrated before partitioning between EtOAc and water. In turn, the aqueous layer was washed three times with EtOAc. The organic layers were combined, dried and concentrated in vacuo. The organic extract of a 10 L culture in 1158 medium (malt extract 20 g/L; D-glucose 10g/L; yeast extract 2g/L; NH_4HSO_4 0.5 g/L; pH 6.0) was separated into seven fractions by normal phase vacuum-liquid chromatography (VLC) eluted with a CH_2Cl_2 to MeOH gradient. Altogether, 6.5 mg of porosuphenol A (**4.1**),

5.0 mg of porosuphenol B (**4.2**), and a combined 3.0 mg of porosuphenol C and D (**4.3a** and **4.3b**) were isolated from Fraction 5.

Porosuphenol A (**4.1**): colorless oil; $[\alpha]_D^{21}$ -130.8 (*c* 0.1, CH_3CN); IR (ATR): ν_{max} 3390, 2970, 2932, 1709, 1645, 1606, 1457, 1358, 1307, 1276, 1198, 1149, 1086, 1022, 833; ECD (*c* 0.1, CH_3CN) 194.3 (-2.3), 215.4 (+1.7), 234.4 (+0.3), 245.3 (+0.5), 255.1 (+0.6), 274.6 (+1.2), 299.9 (-4.7); UV (*c* 0.1, CH_3CN) λ_{max} (log ε) 204 (4.2), 285 (3.8) nm; ^{13}C NMR (176 MHz, CH_3CN-d_3) and ^1H NMR (700 MHz, CH_3CN-d_3) see table 4.1; HRESIMS *m/z* 459.2739 $[M+H]^+$ (calcd for $C_{27}H_{39}O_6$(+1) 459.274; Δppm = 0.4).

Porosuphenol B (**4.2**): colorless oil; $[\alpha]_D^{21}$ -35.8 (*c* 0.1, CH_3CN); IR (ATR): ν_{max} 3362, 2969, 2931, 1708, 1646, 1606, 1457, 1357, 1308, 1277, 1198, 1149, 1087, 1022, 832; ECD (*c* 0.1, CH_3CN) 192.6 (-1.9), 204.5 (+0.8), 221.2 (+0.2), 230.5 (+0.3), 277.5 (-5.0), 306.2 (+2.4); UV (*c* 0.1, CH_3CN) λ_{max} (log ε) 203 (4.2), 285 (3.8) nm; ^{13}C NMR (176 MHz, CH_3CN-d_3) and ^1H NMR (700 MHz, CH_3CN-d_3) see table 4.1; HRESIMS: *m/z* 459.2738 $[M+H]^+$ (calcd for $C_{27}H_{39}O_6$(+1) 459.274; Δppm = 0.7).

Porosuphenol C (**4.3a**): colorless oil; $[\alpha]_D^{21}$ -39.8 (*c* 0.1, CH_3CN); IR (ATR): ν_{max} 3343, 2971, 2931, 1700, 1620, 1456, 1355, 1329, 1232, 1144, 1126, 1053. 1027, 1004, 939, 921; UV (30% CH_3CN:H_2O) λ_{max} 210, 288 nm[38]; ^{13}C NMR (176 MHz, CH_3CN-d_3) and ^1H NMR (700 MHz, CH_3CN-d_3) see table 4.4; HRESIMS: *m/z* 467.2392 $[M+Na]^+$ (calcd for $C_{26}H_{36}O_6Na$(+1) 467.24; Δppm = 2.8).

Porosuphenol D (**4.3b**): colorless oil; $[\alpha]_D^{21}$ -39.8 (*c* 0.1, CH_3CN); IR (ATR): ν_{max} 3343, 2971, 2931, 1700, 1620, 1456, 1355, 1329, 1232, 1144, 1126, 1053. 1027, 1004, 939, 921; UV (30% CH_3CN:H_2O) λ_{max} 210, 288 nm; ^{13}C NMR (176 MHz, CH_3CN-d_3) and ^1H NMR (700 MHz, CH_3CN-d_3) see table 4.4; HRESIMS: *m/z* 467.2392 $[M+Na]^+$ (calcd for $C_{26}H_{36}O_6Na$(+1) 467.24; Δppm = 2.8).

Preparation of (*R*)- and (*S*)-MTPA ester derivatives of porosuphenol A (4.1). Compound **4.1** (0.88 mg, 1.91x10 μmol) was dissolved in 100 μL of dry acetonitrile. To this, pyridine (3.0 μL, 37.4 μmol) dissolved in 100 μL of dry acetonitrile was added, followed by (*S*)-(+)-α-methoxy-α-(trifluoromethyl)phenylacetyl (MTPA) chloride, dissolved in 100 μL of dry acetonitrile. The reaction was monitored by TLC. After 24 h, the reaction was quenched with H_2O and extracted with ethyl acetate. The organic layers were combined, dried with $MgSO_4$, and concentrated to dryness under reduced pressure. The desired product, the (*R*)-MTPA (**4.1***R*) ester of porosuphenol A, was purified by HPLC and its structure determined using 1 and 2-dimensional NMR techniques. Selected ^1H NMR data of **4.1***R* (800 MHz, CH_3CN-d_3): δ 5.43 (1H, d, *J* = 9.8 Hz, H-4), 5.08 (1H, p, *J* = 6.4 Hz, H-2), 2.80 (1H, dqd, *J* = 9.8, 6.8, 6.4 Hz, H-3), 1.36 (3H, d, *J* = 6.4 Hz, H-1), 0.95 (3H, d, *J* = 6.8 Hz, H-22). In an analogous manner, **4.1** (0.88 mg, 1.91x10 μmol) was converted with (*R*)-(+)-α-methoxy-α-(trifluoromethyl)phenylacetyl (MTPA) chloride to yield (*S*)-MTPA (**4.1***S*) ester of porosuphenol A. Key ^1H NMR shifts of **4.1***S* (800 MHz, CH_3CN-d_3): δ 5.53 (1H, d, *J*

= 9.6 Hz, H-4), 5.10 (1H, p, *J* = 6.4 Hz, H-2), 2.89 (1H, dqd, *J* = 9.8, 6.8, 6.4 Hz, H-3), 1.28 (3H, d, *J* = 6.4 Hz, H-1), 1.09 (3H, d, *J* = 6.8 Hz, H-22).

Deuterium-exchange study. To an NMR tube containing a solution of **4.1** (1 mg, 3.6 mM) in CH_3CN-d_3, DCl (3 μL of 2% w/w in D_2O) was added. The NMR tube was inverted to mix the sample and then monitored by ^1H NMR spectroscopy for 24 h.

Accurate NOE distances. A sample of **4.1** was dissolved in CH_3CN-d_3 (2.5 mg, 9.1 mM) and several 1D PFGSE NOE spectra with zero-quantum suppression,[26] using the Bruker pulse program selnogpzs.2, with 5 sec D1 to insure complete relaxation (T_1 was measured as 1 sec using the inversion-recovery method). For each distance to be determined, seven NOE experiments with varying mixing times were recorded (400, 350, 300, 250, 200, 150, and 50 ms). From the resulting spectra, the integral ratio of the NOE peak to the inverted peak was plotted against the mixing time.[25] The slope of this line was calculated using a linear fit. H-11 and H-26 were used as the calibration distance, setting it to 2.679 Å. As an internal check, the correlation between H-9 and H-25 was found to be 2.71 Å. This was in good agreement with the predicted value of 2.65 Å. Additionally, the distance measurement from H-6 to H-9 of 2.10 Å was in excellent agreement with the measurement from H-9 to H-6 of 2.09 Å.

Computational details. Initial conformational analysis was performed in Spartan[39] using the MMFF molecular mechanics force field and random rotor conformational search with 100 conformers. Density functional theory calculations were performed

using the Gaussian 09 package[40] or ORCA 4.0.1.[41] ECD spectra were calculated by the TDDFT methodology at the ωB97XD/def2-TZVP (UV shift of -1 nm and a σ value of 0.22 eV) utilizing CPCM in acetonitrile (compound **4.1**), CAM-B3LYP/TZVP with IEFPCM in acetonitrile (UV shift of 6 nm and a σ value of 0.25 eV) or ωB97X-D3/def2-TZVP(-f) (UV shift of 20 nm and a σ value of 0.3 eV) utilizing CPCM in acetonitrile (compound **4.2**). ECD spectra were simulated using SpecDis 1.71.[42] High-accuracy ^{1}H NMR shifts were computed at the WP04/aug-cc-pVDZ level utilizing PCM in chloroform according to Wiitala et al.[23] For Stereofitter analysis, the original conformer populations, as well as newly generated conformers from the enantiomeric form 2*R*,3*R*,9*R*,11*S* which were then reflected back to 2*S*,3*S*,9*S*,11*R* increasing the number of low energy 2,3-*anti* conformers present in the 2*S*,3*S*,9*S*,11*R* conformer pool. These conformer sets were subjected to QM geometry optimizations and frequency calculations at M06-2X/6-31+G*. All 2,3-*gauche* conformers below 5 kcal and all 2,3-*anti* conformers for each possible configuration, 2*S*,3*S*,9*R*,11*R*; 2*S*,3*S*,9*S*,11*R*; 2*S*,3*S*,9*R*,11*S*; and 2*S*,3*S*,9*S*,11*S* not exhibiting imaginary frequencies were analyzed with Stereofitter (Mestrelab)[3a] utilizing NOE-derived distance and coupling constant constraints from Table 4.3. Single-point energies for all conformers found in the 2*S*,3*S*,9*S*,11*R* Stereofitter solutions were computed at the *DLPNO-CCSD(T)* level,[24] with a def2-TZVP triple zeta basis set using Resolution of Identity approximation for

Coulomb integrals and COSX numerical integration for Hartree Fock exchange, both with and without CPCM solvation (acetonitrile).

Antimicrobial assays. Extracts and fractions were tested for inhibitory activity against *Staphylococcus aureus* (ATCC 25923), methicillin-resistant *Staphylococcus aureus* (ATCC BAA-41), multidrug-resistant *Staphylococcus aureus* (ATCC BAA-44), *Pseudomonas aeruginosa* (ATCC 15442), *Candida albicans* (ATCC 90027), *Candida krusei* (ATCC 34135), and *Mycobacterium smegmatis* (ATCC 14468) in micro-broth assays performed following an established protocol.[43] Fractions and pure compounds were tested at a concentration of 125 μg/mL. All human pathogens used in the study were acquired from the American Type Culture Collection (ATCC, Manassas, VA, USA).

Cytotoxicity assay. Cytotoxic activities of extracts and pure compounds were evaluated against colon (HCT-116) cancer models by measuring the reduction of the tetrazolium salt MTT (3-(4, 5-dimethylthiazolyl-2)-2, 5-diphenyltetrazolium bromide) by metabolically active cells following standard procedures.[44]

Antioxidant assay. Antioxidant activity was tested using the DPPH radical scavenging assay.[45] Compounds were tested at 50 and 100 μM in MeOH. DPPH final concentration was 0.05 mM. 25 μM Vitamin C was used as positive control. Absorbance at 517 nm was monitored every 10 mins for 30 mins, then every 30 mins

for 4 hrs. The percent of unreacted DPPH was quantified using a calibration curve at 517 nm.

Metal-chelating activity assay: Fe chelating activity was tested with competition assays using $FeCl_2$ and ferrozine,[46] which absorbs 562 nm light when complexed with ferrous ions. Test compounds were dissolved in DMSO and added to 96 well plates. Then, $FeCl_2$ in H_2O was added to the test compounds followed by the addition of ferrozine in H_2O. After 10 mins of incubation, the plates were read at 562 nm. Fungal metabolites were tested at 50 and 100 μM. $FeCl_2$ and ferrozine were at a finial concentration of 40 and 50 μM respectively. 50 μM EDTA was used as a positive control.

4.5 Acknowledgments

This work was supported by OSU start-up funds and by the National Science Foundation under grant CHE 1808717. We wish to thank Bioviotica (Prof. Dr. Axel Zeeck and Hans-Peter Kroll) for providing *Aspergillus porosus*. We also thank Drs. Oliver Schlörke and Jens Bitzer who isolated the strain and Barbara Schulz for initial strain identification. In addition, we thank Dr. Luiz Bermudez (Oregon State University) and Dr. Michael Riscoe (Oregon Health and Science University) for antitubercular and antimalaria screening respectively. We acknowledge the support of the Oregon State University's NMR Facility funded in part by the National Institutes of Health, HEI Grant 1S10OD018518, and by the M. J. Murdock Charitable Trust

grant #2014162. We thank Zoe Zhu and Dr. Birte Plitzko for performing the cytotoxicity assay, Prof. Jeff Stone (Oregon State University) for assistance with fungal taxonomy, and Profs. Phil Proteau and James Strother (Oregon State University) for fruitful discussions.

4.6 References

(1) (a) Chhetri, B. K.; Lavoie, S.; Sweeney-Jones, A. M.; Kubanek, J. *Natural Product Reports* **2018**, *35*, 514. (b) Chhetri, B. K.; Lavoie, S.; Sweeney-Jones, A. M.; Kubanek, J. *Natural Product Reports* **2018**, *35*, 1015.
(2) Newman, D. J.; Cragg, G. M. *Journal of Natural Products* **2016**, *79*, 629.
(3) (a) Navarro-Vázquez, A.; Gil, R. R.; Blinov, K. *Journal of Natural Products* **2018**, *81*, 203. (b) Stefano, S.; Patrizia, S.; Marcin, G.; Gennaro, P. *Current Medicinal Chemistry* **2018**, *25*, 287. (c) Pescitelli, G.; Bruhn, T. *Chirality* **2016**, *28*, 466. (d) Grimblat, N.; Sarotti, A. M. *Chemistry – A European Journal* **2016**, *22*, 12246. (e) Lodewyk, M. W.; Siebert, M. R.; Tantillo, D. J. *Chemical Reviews* **2012**, *112*, 1839.
(4) Chen, A. J.; Hubka, V.; Frisvad, J. C.; Visagie, C. M.; Houbraken, J.; Meijer, M.; Varga, J.; Demirel, R.; Jurjević, Ž.; Kubátová, A.; Sklenář, F.; Zhou, Y. G.; Samson, R. A. *Studies in Mycology* **2017**, *88*, 37.
(5) (a) Keiichi, M.; Harumi, T.; Junji, I.; Haruo, T. *The Journal of Antibiotics* **1998**, *51*, 1004. (b) Chiang, Y.-M.; Szewczyk, E.; Davidson, A. D.; Keller, N.; Oakley, B. R.; Wang, C. C. C. *Journal of the American Chemical Society* **2009**, *131*, 2965.
(6) Stierle, D. B.; Stierle, A. A.; Ganser, B. K. *Journal of Natural Products* **1999**, *62*, 1147.
(7) (a) Norte, M.; Cataldo, F.; González, A. G. *Tetrahedron Letters* **1988**, *29*, 2879. (b) Calter, M. A.; Liao, W. *Journal of the American Chemical Society* **2002**, *124*, 13127. (c) Cutignano, A.; Calado, G.; Gaspar, H.; Cimino, G.; Fontana, A. *Tetrahedron Letters* **2011**, *52*, 4595.
(8) Shen, W.; Mao, H.; Huang, Q.; Dong, J. *European Journal of Medicinal Chemistry* **2015**, *97*, 747.
(9) Gao, J.-M.; Yang, S.-X.; Qin, J.-C. *Chemical Reviews* **2013**, *113*, 4755.
(10) Amico, V.; Cunsolo, F.; Piattelli, M.; Ruberto, G. *Phytochemistry* **1985**, *24*, 2663.

(11) Ellestad, G. A.; Kunstmann, M. P.; Mirando, P.; Morton, G. O. *Journal of the American Chemical Society* **1972**, *94*, 6206.
(12) (a) Evidente, A.; Sparapano, L.; Motta, A.; Giordano, F.; Fierro, O.; Frisullo, S. *Phytochemistry* **1996**, *42*, 1541. (b) Sparapano, L.; Bruno, G.; Fierro, O.; Evidente, A. *Phytochemistry* **2004**, *65*, 189.
(13) Lallemand, B.; Masi, M.; Maddau, L.; De Lorenzi, M.; Dam, R.; Cimmino, A.; Moreno y Banuls, L.; Andolfi, A.; Kiss, R.; Mathieu, V.; Evidente, A. *Phytochemistry Letters* **2012**, *5*, 770.
(14) Mathieu, V.; Chantôme, A.; Lefranc, F.; Cimmino, A.; Miklos, W.; Paulitschke, V.; Mohr, T.; Maddau, L.; Kornienko, A.; Berger, W.; Vandier, C.; Evidente, A.; Delpire, E.; Kiss, R. *Cellular and Molecular Life Sciences* **2015**, *72*, 3731.
(15) Yan, T.; Guo, Z. K.; Jiang, R.; Wei, W.; Wang, T.; Guo, Y.; Song, Y. C.; Jiao, R. H.; Tan, R. X.; Ge, H. M. *Planta Medica* **2013**, *79*, 348.
(16) White, T. J.; Bruns, T.; Lee, S.; Taylor, J., Amplification and direct sequencing of fungal ribosomal RNA genes for phylogenetics. In *PCR Protocols*, Innis, M. A.; Gelfand, D. H.; Sninsky, J. J.; White, T. J., Eds. Academic Press: San Diego, 1990; pp 315.
(17) Raja, H. A.; Miller, A. N.; Pearce, C. J.; Oberlies, N. H. *Journal of Natural Products* **2017**, *80*, 756.
(18) Glass, N. L.; Donaldson, G. C. *Applied and Environmental Microbiology* **1995**, *61*, 1323.
(19) (a) Seco, J. M.; Quiñoá, E.; Riguera, R. *Chemical Reviews* **2004**, *104*, 17. (b) Hoye, T. R.; Jeffrey, C. S.; Shao, F. *Nature Protocols* **2007**, *2*, 2451.
(20) Matsumori, N.; Kaneno, D.; Murata, M.; Nakamura, H.; Tachibana, K. *The Journal of Organic Chemistry* **1999**, *64*, 866.
(21) (a) Kurz, M.; Schmieder, P.; Kessler, H. *Angewandte Chemie International Edition* **1991**, *30*, 1329. (b) Uhrín, D.; Batta, G.; Hruby, V. J.; Barlow, P. N.; Kövér, K. E. *Journal of Magnetic Resonance* **1998**, *130*, 155.
(22) Willoughby, P. H.; Jansma, M. J.; Hoye, T. R. *Nature Protocols* **2014**, *9*, 643.
(23) Wiitala, K. W.; Hoye, T. R.; Cramer, C. J. *Journal of Chemical Theory and Computation* **2006**, *2*, 1085.
(24) (a) Riplinger, C.; Neese, F. *The Journal of Chemical Physics* **2013**, *138*, 034106. (b) Riplinger, C.; Sandhoefer, B.; Hansen, A.; Neese, F. *The Journal of Chemical Physics* **2013**, *139*, 134101.
(25) Hu, H.; Krishnamurthy, K. *Journal of Magnetic Resonance* **2006**, *182*, 173.
(26) Stott, K.; Keeler, J.; Van, Q. N.; Shaka, A. J. *Journal of Magnetic Resonance* **1997**, *125*, 302.
(27) Thrippleton, M. J.; Keeler, J. *Angewandte Chemie International Edition* **2003**, *42*, 3938.

(28) Kolmer, A.; Edwards, L. J.; Kuprov, I.; Thiele, C. M. *Journal of Magnetic Resonance* **2015**, *261*, 101.
(29) (a) Baell, J. B.; Holloway, G. A. *Journal of Medicinal Chemistry* **2010**, *53*, 2719. (b) Baell, J. B. *Journal of Natural Products* **2016**, *79*, 616.
(30) Smilkstein, M.; Sriwilaijaroen, N.; Kelly, J. X.; Wilairat, P.; Riscoe, M. *Antimicrobial Agents and Chemotherapy* **2004**, *48*, 1803.
(31) (a) Bermudez, L. E.; Meek, L. *Tuberculosis Research and Treatment* **2014**, *2014*, 530815. (b) Bermudez, L. E.; Kolonoski, P.; Wu, M.; Aralar, P. A.; Inderlied, C. B.; Young, L. S. *Antimicrobial Agents and Chemotherapy* **1999**, *43*, 1870.
(32) Adpressa, D. A.; Loesgen, S. *Chemistry & Biodiversity* **2016**, *13*, 253.
(33) Tamura, K. *Molecular Biology and Evolution* **1992**, *9*, 678.
(34) Kimura, M. *Journal of Molecular Evolution* **1980**, *16*, 111.
(35) Clark, K.; Karsch-Mizrachi, I.; Lipman, D. J.; Ostell, J.; Sayers, E. W. *Nucleic Acids Research* **2016**, *44*, D67.
(36) Altschul, S. F.; Gish, W.; Miller, W.; Myers, E. W.; Lipman, D. J. *Journal of Molecular Biology* **1990**, *215*, 403.
(37) Kumar, S.; Stecher, G.; Tamura, K. *Molecular Biology and Evolution* **2016**, *33*, 1870.
(38) UV absorbance spectra of 3a and 3b from LCMS analysis. No concentration available.
(39) Hanwell, M. D.; Curtis, D. E.; Lonie, D. C.; Vandermeersch, T.; Zurek, E.; Hutchison, G. R. *Journal of Cheminformatics* **2012**, *4*, 1.
(40) Frisch, M. J.; Trucks, G. W.; Schlegel, H. B.; Scuseria, G. E.; Robb, M. A.; Cheeseman, J. R.; Scalmani, G.; Barone, V.; Mennucci, B.; Petersson, G. A.; Nakatsuji, H.; Caricato, M.; Li, X.; Hratchian, H. P.; Izmaylov, A. F.; Bloino, J.; Zheng, G.; Sonnenberg, J. L.; Hada, M.; Ehara, M.; Toyota, K.; Fukuda, R.; Hasegawa, J.; Ishida, M.; Nakajima, T.; Honda, Y.; Kitao, O.; Nakai, H.; Vreven, T.; Montgomery Jr., J. A.; Peralta, J. E.; Ogliaro, F.; Bearpark, M. J.; Heyd, J.; Brothers, E. N.; Kudin, K. N.; Staroverov, V. N.; Kobayashi, R.; Normand, J.; Raghavachari, K.; Rendell, A. P.; Burant, J. C.; Iyengar, S. S.; Tomasi, J.; Cossi, M.; Rega, N.; Millam, N. J.; Klene, M.; Knox, J. E.; Cross, J. B.; Bakken, V.; Adamo, C.; Jaramillo, J.; Gomperts, R.; Stratmann, R. E.; Yazyev, O.; Austin, A. J.; Cammi, R.; Pomelli, C.; Ochterski, J. W.; Martin, R. L.; Morokuma, K.; Zakrzewski, V. G.; Voth, G. A.; Salvador, P.; Dannenberg, J. J.; Dapprich, S.; Daniels, A. D.; Farkas, Ö.; Foresman, J. B.; Ortiz, J. V.; Cioslowski, J.; Fox, D. J. *Gaussian 09*, Gaussian, Inc.: Wallingford, CT, USA, 2009.
(41) Neese, F. *Wiley Interdisciplinary Reviews: Computational Molecular Science* **2018**, *8*, e1327.

(42) Bruhn, T.; Schaumloffel, A.; Hemberger, Y.; Bringmann, G. *Chirality* **2013**, *25*, 243.
(43) L., N. C. f. C., Approved Standard M02-A11 and M100-S25. Approved Standard M02-A11 and M100-S25. NCCLS: Wayne, PA, USA, 2002.
(44) Riss, T. L., Moravec, R.A. ,Niles, A.L., Duellman, S., Benink, H.A., Worzella, T.J., Minor, L. , Cell Viability Assays. In *Assay Guidance Manual*, Sittampalam, G. S.; Coussens, N. P.; Nelson, H. E. A., Eds. Eli Lilly & Company, and the National Center for Advancing Translational Sciences (NIH): Bethesda, MD, 2013.
(45) (a) Brand-Williams, W.; Cuvelier, M. E.; Berset, C. *LWT - Food Science and Technology* **1995**, *28*, 25. (b) Sharma, O. P.; Bhat, T. K. *Food Chemistry* **2009**, *113*, 1202.
(46) Stookey, L. L. *Analytical Chemistry* **1970**, *42*, 779.

Chapter Five: General Conclusion

George F. Neuhaus

5.1 General conclusion

Natural products (NPs) have inspired generations of chemists and influenced drug discovery. In times of fast genome sequencing and high-throughput screening for bioactivities and novel chemical entities, the question arises if we have exhausted the pool of unique NPs. In agreement with the conclusions of Pye et al,[1] this thesis provides support that the natural world still has much to offer. While the number of known NPs is ever-increasing, the rate at which new molecular architectures are discovered has remained constant over the past decade.[1-2] The exploration of unusual and understudied sources combined with continuously evolving discovery methods will allow this trend to continue.[3] We are just beginning to explore the biological function(s) of many NPs which will inform and guide future screening methods and translational applications. The chapters of this thesis highlight the identification and study of new and known fungal NPs, from structure elucidation and bioactivity survey to their function in fungal development. Recently developed techniques, including computational calculations to access the absolute configuration of new fungal metabolites, and mass spectrometry-based metabolomics to quickly assess metabolite identification and abundance, were employed in the study of *Aspergillus* derived NPs.

Fungi have proven to be a great source for NP discovery,[4] the genus *Aspergillus* being one of them.[5] Starting with the discovery of the aflatoxins[6] and lovastatin,[7] *Aspergillus* species continue to provide novel NPs today.[8] However the ecological

function of most fungal NPs is not well understood,[9] and recently more studies are focusing on the 'when and why' fungi produce NPs.[9-10] Chapter two of this thesis utilizes LCMS-based metabolomics in combination with RNA sequencing to explore the chemical function and regulation of NPs in *A. nidulans* conidia. It was found that the genetic regulatory networks that control conidiation also control which NPs are present in spores. Here, we used metabolomic analysis[11] and rapid compound identification[12] to gain a better understanding of secondary metabolite function.

Chapter three and four of this thesis describe the discovery of nine new NPs from two different *Aspergillus* species, *Aspergillus ustus* and the recently described *Aspergillus porosus*. Determining the molecular structure of a new NP is a non-trivial task that has helped push the limits of synthetic chemistry,[13] spectroscopy,[14] spectrometry,[15] and chromatography.[16] Even today, corrections to proposed structures[17] are inevitable occurrences, with the establishment of the absolute configuration remaining a formidable task. Chapter three highlights the discovery of five new drimane sesquiterpenes from *A. ustus*. Structure elucidation of these compounds utilized state-of-the-art 1D and 2D NMR techniques, chemical modification, and computational methods to support their absolute structure. In chapter four, the determination of the absolute configuration of molecules with high degrees of freedom, here linear polyketides, was achieved. This task required a battery of techniques, including mass spectrometry, NMR spectroscopy, Mosher ester analysis,

J-based conformational analysis, isotope exchange studies, and extensive computational techniques. In the end, use of experimental parameters to guide the conformational search was successful to correctly model ECD spectra and confirm the absolute configuration of porosuphenol A. The ability to collect numerous orthogonal experimental parameters and then to corroborate them with computational modelling will greatly enhance future structure elucidation efforts.

In today's world, the threat from microbial infection has reemerged due to antibiotic resistance. It is predicted that by 2050, antimicrobial resistance will cause 10 million deaths worldwide.[18] In times of the current COVID pandemic, bacterial infections are very likely to occur as secondary infections and are believed to be responsible for almost half of the death toll during viral pandemics.[19] The need for new ways to combat infections is higher than ever including the need for antiviral drugs as opposed to vaccines. Chapter three describes the bioactivity guided isolation of several new drimane sesquiterpenes from *Aspergillus ustus*. Interestingly, while the fungal extract and fraction exhibited moderate antibiotic activity, the three isolated active compounds showed only weak activity against drug resistant *Staphylococcus aureus.* It was found that the activity of the new metabolite ustusoic acid B (**3.5**) was enhanced when tested with equal amounts of stromemycin (**3.6**), a known metabolite isolated from the same culture. For the treatment of various pathogens,[20] viruses,[21] and cancer, [22] despite some controversy in the field,[23] combination therapy of multiple drugs has been successful.[24]

The work presented here provides evidence that fungal extracts can contain inherent synergism which has the potential to increase the effectiveness of antibiotic treatments.[25]

In summary, the work within demonstrates that the exploration of fungal NPs is flourishing as we continue to discover new molecular structures and new biological roles NPs play. Focusing on *Aspergillus* species, a powerhouse in NP production, we studied the connection of metabolite expression and fungal development. Advanced techniques in computational structure elucidation and metabolomics were employed to discovery and identify structures of new and known fungal NPs. In total, 9 new *Aspergillus* derived NPs were discovered while 10 known metabolites were identified by isolation and structure elucidation by NMR. Additionally, 11 others were established by mass spectrometry-based metabolomics. In agreement with Pye et al, there is much to gain in the area of natural products sciences and fungi will continue to surprise us with their complex chemical structures and chemical ecology.

5.2 References

(1) Pye, C. R.; Bertin, M. J.; Lokey, R. S.; Gerwick, W. H.; Linington, R. G. *Proceedings of the National Academy of Sciences* **2017**, *114*, 5601.
(2) Newman, D. J.; Cragg, G. M. *Journal of Natural Products* **2020**, *83*, 770.
(3) (a) Hautbergue, T.; Jamin, E. L.; Debrauwer, L.; Puel, O.; Oswald, I. P. *Natural Product Reports* **2018**, *35*, 147. (b) Hutchings, M.; Truman, A.; Wilkinson, B. *Current Opinion in Microbiology* **2019**, *51*, 72. (c) Harvey, A. L.; Edrada-Ebel, R.; Quinn, R. J. *Nature Reviews Drug Discovery* **2015**, *14*, 111.
(4) Schueffler, A.; Anke, T. *Natural Product Reports* **2014**, *31*, 1425.
(5) (a) Frisvad, J. C.; Larsen, T. O. *Applied Microbiology and Biotechnology* **2015**, *99*, 7859. (b) Vadlapudi, V.; Borah, N.; Yellusani, K. R.; Gade, S.; Reddy, P.;

Rajamanikyam, M.; Vempati, L. N. S.; Gubbala, S. P.; Chopra, P.; Upadhyayula, S. M.; Amanchy, R. *Scientific Reports* **2017**, *7*, 7325.
(6) Rushing, B. R.; Selim, M. I. *Food and Chemical Toxicology* **2019**, *124*, 81.
(7) Tobert, J. A. *Nature Reviews Drug Discovery* **2003**, *2*, 517.
(8) (a) Romsdahl, J.; Wang, C. C. C. *MedChemComm* **2019**, *10*, 840. (b) Sanchez, J. F.; Somoza, A. D.; Keller, N. P.; Wang, C. C. C. *Natural Product Reports* **2012**, *29*, 351. (c) Inglis, D. O.; Binkley, J.; Skrzypek, M. S.; Arnaud, M. B.; Cerqueira, G. C.; Shah, P.; Wymore, F.; Wortman, J. R.; Sherlock, G. *BMC Microbiology* **2013**, *13*, 91. (d) Jiao, W.-H.; Xu, Q.-H.; Ge, G.-B.; Shang, R.-Y.; Zhu, H.-R.; Liu, H.-Y.; Cui, J.; Sun, F.; Lin, H.-W. *Organic Letters* **2020**, *22*, 1825. (e) Wu, Z.; Zhang, X.; Chen, C.; Zhou, P.; Zhang, M.; Gu, L.; Luo, Z.; Wang, J.; Tong, Q.; Zhu, H.; Zhang, Y. *Organic Letters* **2020**, *22*, 2162. (f) Wen, H.; Yang, X.; Liu, Q.; Li, S.; Li, Q.; Zang, Y.; Chen, C.; Wang, J.; Zhu, H.; Zhang, Y. *Journal of Natural Products* **2020**, *83*, 99.
(9) (a) Spiteller, P. *Chemistry – A European Journal* **2008**, *14*, 9100. (b) Spiteller, P. *Natural Product Reports* **2015**, *32*, 971.
(10) (a) Kusari, S.; Hertweck, C.; Spiteller, M. *Chemistry & Biology* **2012**, *19*, 792. (b) Keller, N. P. *Nature Reviews Microbiology* **2019**, *17*, 167. (c) Raffa, N.; Keller, N. P. *PLOS Pathogens* **2019**, *15*, e1007606.
(11) (a) Kuhlisch, C.; Pohnert, G. *Natural Product Reports* **2015**, *32*, 937. (b) Kluger, B.; Lehner, S.; Schuhmacher, R., Metabolomics and Secondary Metabolite Profiling of Filamentous Fungi. In *Biosynthesis and Molecular Genetics of Fungal Secondary Metabolites, Volume 2*, Zeilinger, S.; Martín, J.-F.; García-Estrada, C., Eds. Springer New York: New York, NY, 2015; pp 81. (c) Macel, M.; Van Dam, N. M.; Keurentjes, J. J. B. *Molecular Ecology Resources* **2010**, *10*, 583.
(12) Gaudêncio, S. P.; Pereira, F. *Natural Product Reports* **2015**, *32*, 779.
(13) (a) Hoffmann, R. W., *Classical Methods in Structure Elucidation of Natural Products*. Wiley: 2018. (b) Nicolaou, K. C.; Vourloumis, D.; Winssinger, N.; Baran, P. S. *Angewandte Chemie International Edition* **2000**, *39*, 44. (c) Baran, P. S. *Journal of the American Chemical Society* **2018**, *140*, 4751.
(14) (a) Halabalaki, M.; Vougogiannopoulou, K.; Mikros, E.; Skaltsounis, A. L. *Current Opinion in Biotechnology* **2014**, *25*, 1. (b) Buevich, A. V.; Williamson, R. T.; Martin, G. E. *Journal of Natural Products* **2014**, *77*, 1942. (c) Reynolds, W. F., Chapter 29 - Natural Product Structure Elucidation by NMR Spectroscopy. In *Pharmacognosy*, Badal, S.; Delgoda, R., Eds. Academic Press: Boston, 2017; pp 567. (d) Breton, R. C.; Reynolds, W. F. *Natural Product Reports* **2013**, *30*, 501.
(15) (a) Bouslimani, A.; Sanchez, L. M.; Garg, N.; Dorrestein, P. C. *Natural Product Reports* **2014**, *31*, 718. (b) Allard, P.-M.; Péresse, T.; Bisson, J.; Gindro, K.;

Marcourt, L.; Pham, V. C.; Roussi, F.; Litaudon, M.; Wolfender, J.-L. *Analytical Chemistry* **2016**, *88*, 3317.
(16) (a) Andrade-Eiroa, A.; Canle, M.; Leroy-Cancellieri, V.; Cerdà, V. *TrAC Trends in Analytical Chemistry* **2016**, *80*, 641. (b) Cacciola, F.; Donato, P.; Mondello, L.; Dugo, P., Chapter 8 - Recent Advances in Comprehensive Two-Dimensional Liquid Chromatography for the Analysis of Natural Products A2 - Holčapek, Michal. In *Handbook of Advanced Chromatography/Mass Spectrometry Techniques*, Byrdwell, W. C., Ed. AOCS Press: 2017; pp 287. (c) De Vos, J.; Broeckhoven, K.; Eeltink, S. *Analytical Chemistry* **2016**, *88*, 262.
(17) (a) Chhetri, B. K.; Lavoie, S.; Sweeney-Jones, A. M.; Kubanek, J. *Natural Product Reports* **2018**, *35*, 514. (b) Maier, M. E. *Natural Product Reports* **2009**, *26*, 1105. (c) Nicolaou, K. C.; Snyder, S. A. *Angewandte Chemie International Edition* **2005**, *44*, 1012. (d) Suyama, T. L.; Gerwick, W. H.; McPhail, K. L. *Bioorganic & Medicinal Chemistry* **2011**, *19*, 6675. (e) Usami, Y. *Marine Drugs* **2009**, *7*, 314.
(18) O'Neil, J. Report on Antimicrobial Resistance. https://amr-review.org.
(19) (a) Gerberding, J. L. Antibiotic resistance: the hidden threat lurking behind Covid-19. https://www.statnews.com/2020/03/23/antibiotic-resistance-hidden-threat-lurking-behind-covid-19/. (b) Schacht, O. COVID-19 Patients Need to Be Tested for Bacteria and Fungi, Not Just the Coronavirus. https://blogs.scientificamerican.com/observations/covid-19-patients-need-to-be-tested-for-bacteria-and-fungi-not-just-the-coronavirus/. (c) Morris, D. E.; Cleary, D. W.; Clarke, S. C. *Frontiers in Microbiology* **2017**, *8*.
(20) Worthington, R. J.; Melander, C. *Trends in Biotechnology* **2013**, *31*, 177.
(21) Melville, K.; Rodriguez, T.; Dobrovolny, H. M. *Frontiers in Pharmacology* **2018**, *9*.
(22) Bayat, M., R.; Homayouni, T. S.; Baluch, N.; Morgatskaya, E.; Kumar, S.; Das, B.; Yeger, H. *Oncotarget* **2017**, *8*, 38022.
(23) (a) Pena-Miller, R.; Laehnemann, D.; Jansen, G.; Fuentes-Hernandez, A.; Rosenstiel, P.; Schulenburg, H.; Beardmore, R. *PLOS Biology* **2013**, *11*, e1001540. (b) Doern, C. D. *Journal of Clinical Microbiology* **2014**, *52*, 4124.
(24) Xu, X.; Xu, L.; Yuan, G.; Wang, Y.; Qu, Y.; Zhou, M. *Scientific Reports* **2018**, *8*, 7237.
(25) (a) Ayaz, M.; Ullah, F.; Sadiq, A.; Ullah, F.; Ovais, M.; Ahmed, J.; Devkota, H. P. *Chemico-Biological Interactions* **2019**, *308*, 294. (b) Cheesman, M. J.; Ilanko, A.; Blonk, B.; Cock, I. E. *Pharmacognosy Reviews* **2017**, *11*, 57. (c) Alanjary, M.; Medema, M. H. *The Journal of Biological Chemistry* **2018**, *293*, 19996. (d) Hemaiswarya, S.; Kruthiventi, A. K.; Doble, M. *Phytomedicine* **2008**, *15*, 639.

Appendices Section

Appendix A: Supporting Information for Chapter Two

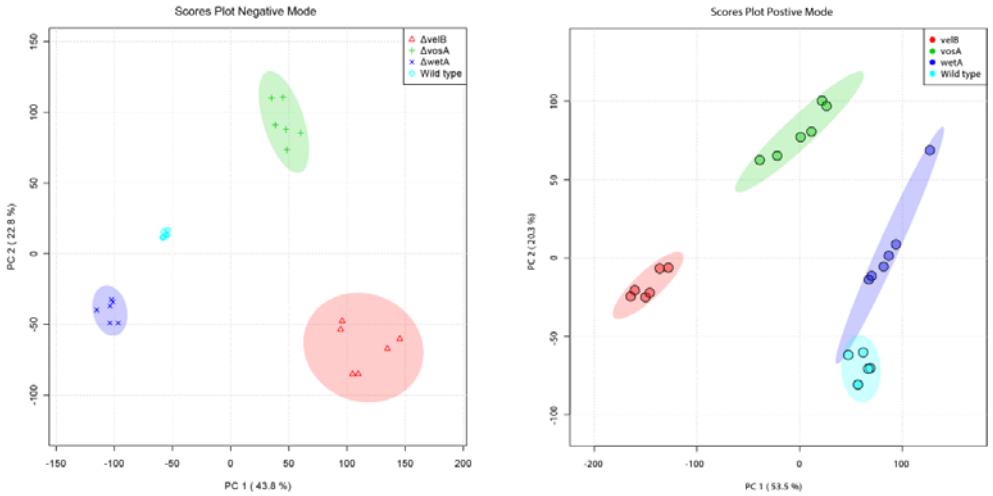

Figure A.1: Principal component analysis 2D scores plots for both negative mode (left) and postive mode (right)

Strain name	Relevant genotype	References
FGSC4	*A. nidulans* wildtype, *veA*$^{+}$	FGSC[a]
THS15	*pyrG89*; *pyroA4*; Δ*vosA*::Afu*pyrG* $^{+}$; *veA*$^{+}$	(1)
THS16	*pyrG89*; *pyroA4*; Δ*velB*::Afu*pyrG* $^{+}$; *veA*$^{+}$	(1)
THS20.1	*pyrG89*; *pyroA*::*velB*(p)::*velB*::FLAG$_{3x}$::*pyroA*[b]; Δ*velB*::*AfupyrG* $^{+}$; *veA*$^{+}$	(1)
THS28.1	*pyrG89*; *pyroA*::*vosA*(p)::*vosA*::FLAG$_{3x}$::*pyroA*[b]; Δ*vosA*::*AfupyrG* $^{+}$; *veA*$^{+}$	(1)
TMY4	*pyrG89*; *pyroA4*; Δ*wetA*::Afu*pyrG* $^{+}$; *veA*$^{+}$	(2)

[a] Fungal Genetic Stock Center

[b] The 3/4 *pyroA* marker causes the targeted integration at the *pyroA* locus.

(1) Park, H. S.; Ni, M.; Jeong, K. C.; Kim, Y. H.; Yu, J. H. *PLoS One* **2012**, *7*, e45935.

(2) Wu, M. Y.; Mead, M. E.; Lee, M. K.; Ostrem Loss, E. M.; Kim, S. C.; Rokas, A.; Yu, J. H. *mBio* **2018**, *9*.

Table A.1: *Aspergillus* strains used in this study

OLIGONUCLEOTIDES		
NAME	**SEQUENCE (5'→3')**	**PURPOSE**
OMY-43	tagcgcattgttgcttaggg	5' flanking of *AniwetA*
OMY-44	gccgttaccgacggatactc	3' flanking of *AniwetA*
OMY-45	gtaatagactcagtggaccgggc	5' nested of *AniwetA*
OMY-46	ctcctcctagaacccattatggc	3' nested of *AniwetA*
OMY-47	gtgaagagcattgtttgaggcaggaagaggctgccagaagacctg	5' *AniwetA* with *AfupyrG* tail
OMY-48	agtgcctcctctcagacagaataggaggaagcttagatctgtggc	3' *AniwetA* with *AfupyrG* tail
OMY-25	gaccactcgttcaacaacgatg	5' *AniwetA*
OMY-26	cgtactgcattaagtgcgg	3' *AniwetA*
OMY-53	ccgaattcttgaagtattgattatgtaattatgc	5' *AniwetA* with *Eco*RI
OMY-54	tagcggccgcgcagaggacagcctctaggg	3' *AniwetA* with *Not*I
OJH-84	gctgaagtcatgatacaggccaaa	5' *AfupyrG* marker
OJH-85	atcgtcgggaggtattgtcgtcac	3' *AfupyrG* marker
OMY-242	ccgctggttcaggtcttctg	5' *AniwetA* upstream WRE (100 bp)
OMY-243	catcttgccagcgggtga	3' *AniwetA* upstream WRE (100 bp)
OMY-268	aagcctagtgtacgcttacaagg	5' AN8643 upstream WRE (100 bp)
OMY-269	ctgcatccgccaatcatgg	3' AN8643 upstream WRE (100 bp)
OMY-270	ctgcggatctcgtttccgtc	5' AN0663 upstream WRE (100 bp)
OMY-271	ctgccctctctacaccaccaatc	3' AN0663 upstream WRE (100 bp)

OMY-272	cgaatttgcggggatagg	5’ AN1918 upstream WRE (100 bp)
OMY-273	gcaagtcttgtgggaatgtactcag	3’ AN1918 upstream WRE (100 bp)
OMY-260	gccctgggagtagagaccag	5’ *AniwetA* upstream WRE (200 bp)
OMY-261	tcggtactcgatgtgtccat	3’ *AniwetA* upstream WRE (200 bp)
OMY-262	gacacccgaactctcttcgag	5’ *AfuwetA* upstream WRE (200 bp)
OMY-263	tgagtccatgtcgacgtactg	3’ *AfuwetA* upstream WRE (200 bp)
OMY-264	gatccgcagttcccttcgac	5’ *AflwetA* upstream WRE (200 bp)
OMY-265	gacgtactgactgaataaatcatcg	3’ *AflwetA* upstream WRE (200 bp)

Table A.2: Oligonucleotides used in this study

Appendix B: Supporting Information for Chapter Three

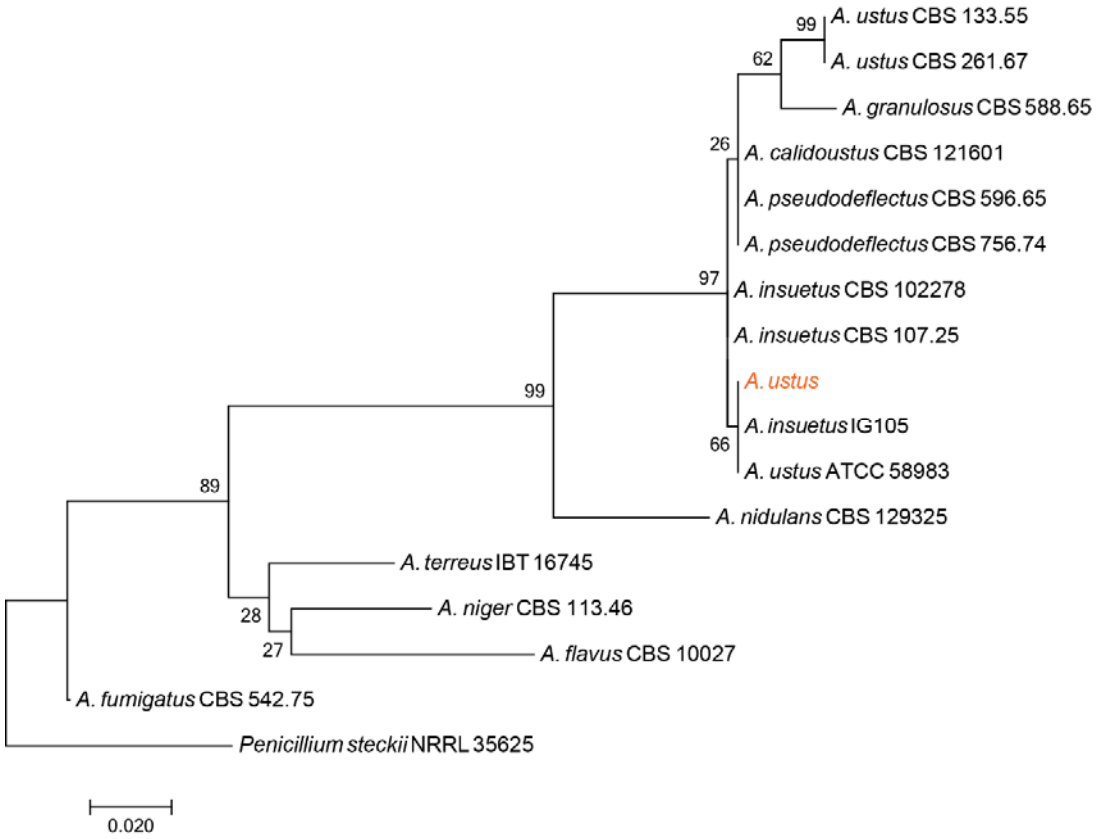

Figure B.1: Phylogenetic tree based off ITS gene fragment

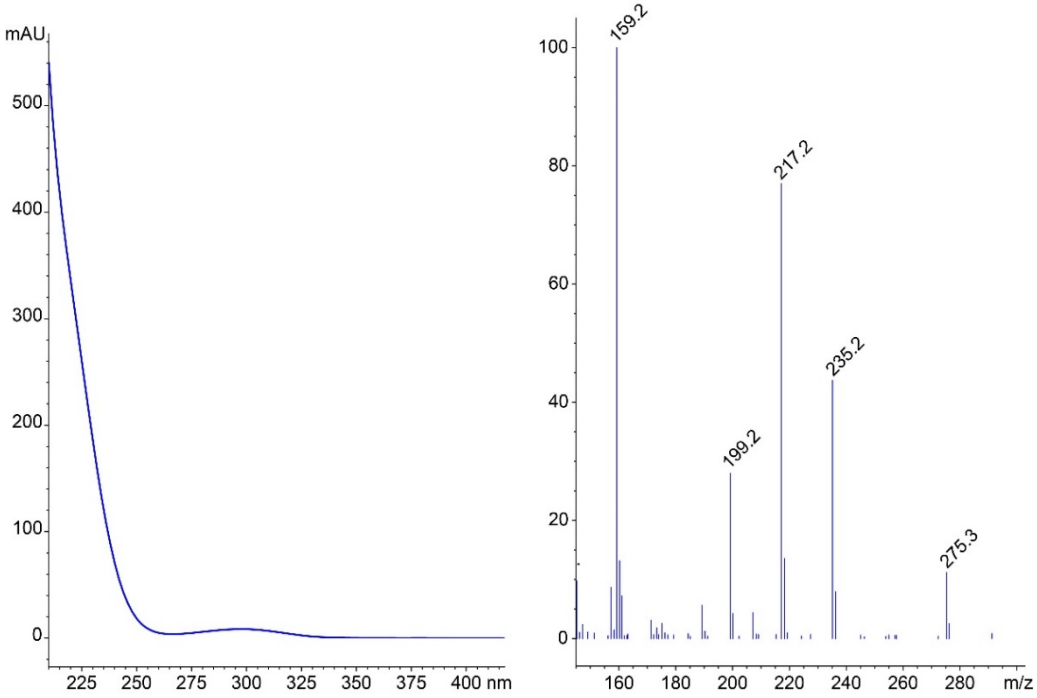

Figure B.2: UV and ESI positive mode low-resolution mass spectrum of **3.1**

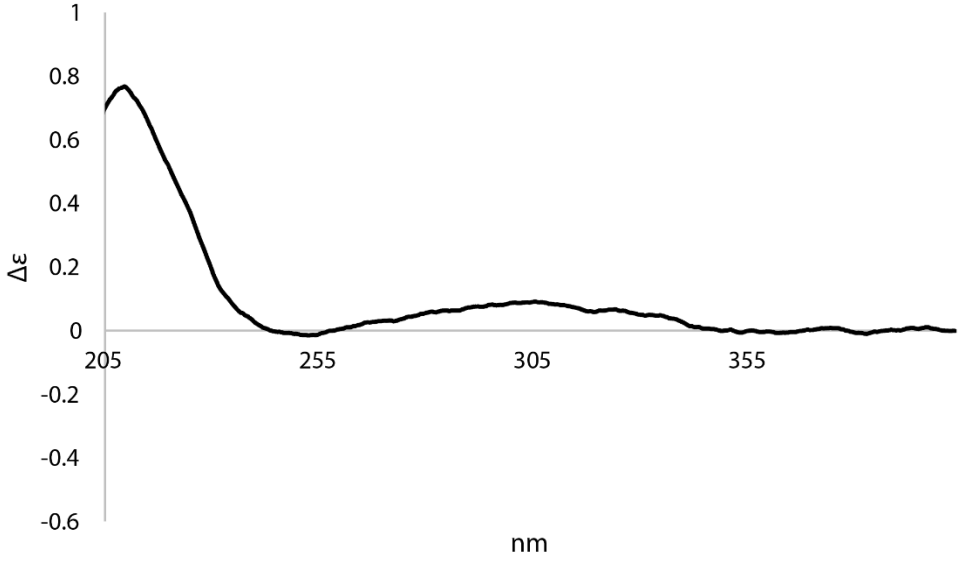

Figure B.3: ECD spectrum of **3.1**

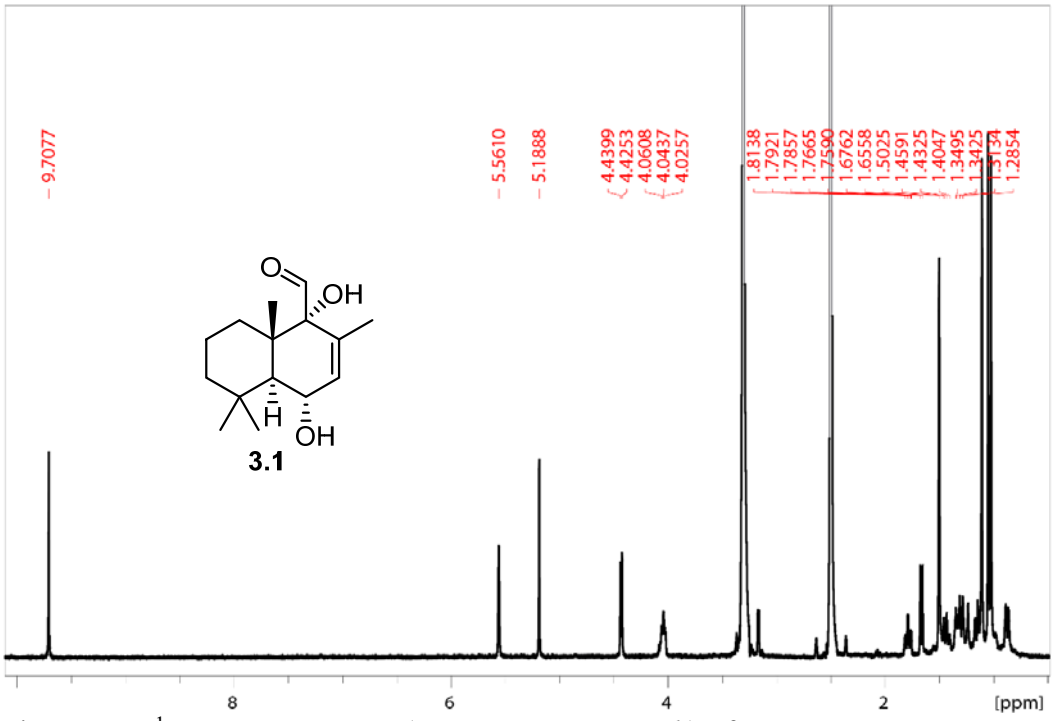

Figure B.4: ^{1}H NMR spectrum (500 MHz, DMSO-d_6) of **3.1**

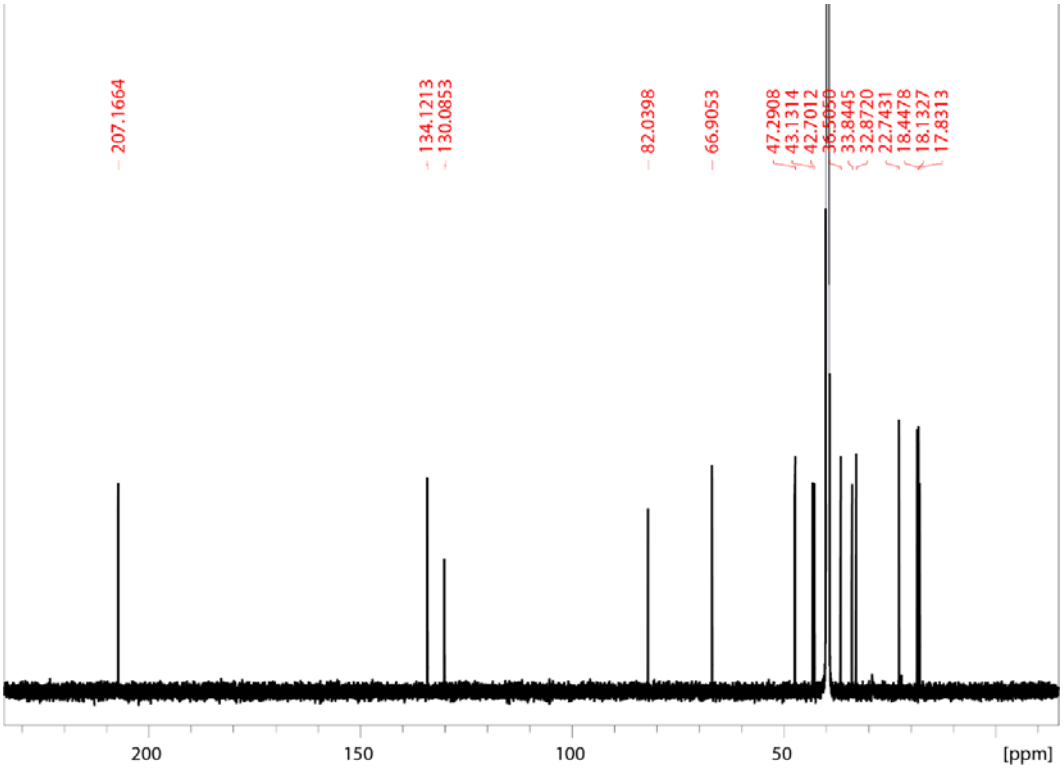

Figure B.5: ^{13}C NMR spectrum (176 MHz, DMSO-d_6) of **3.1**

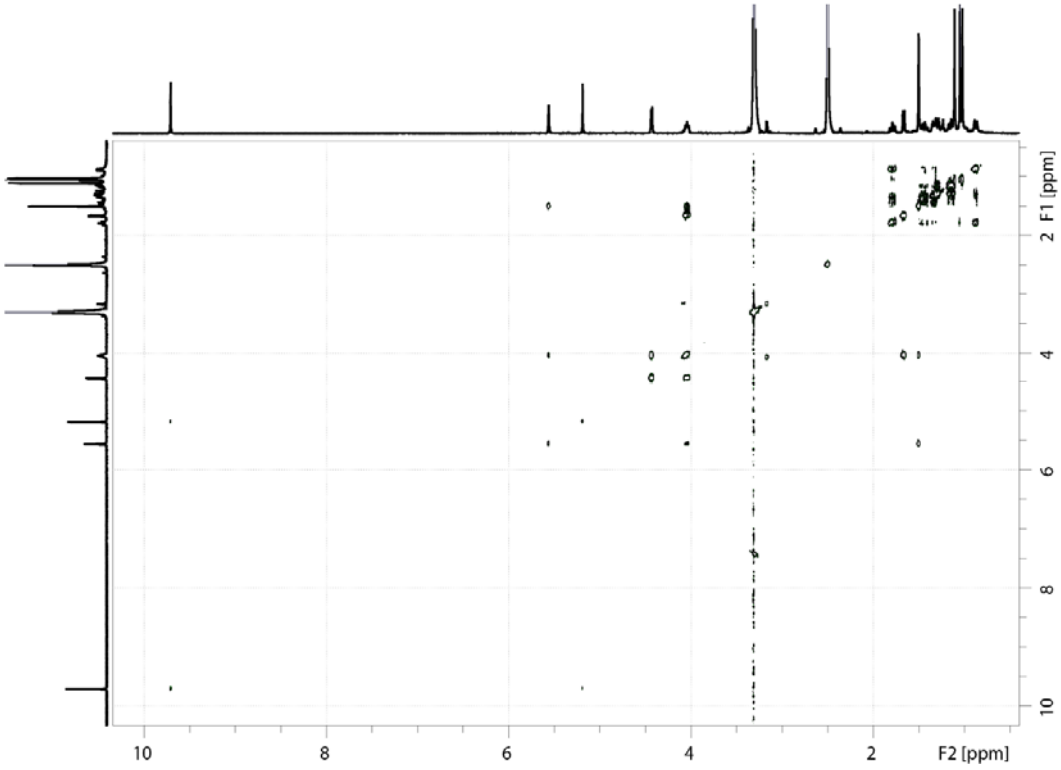

Figure B.6: COSY NMR spectrum (500 MHz, CD_3CN) of **3.1**

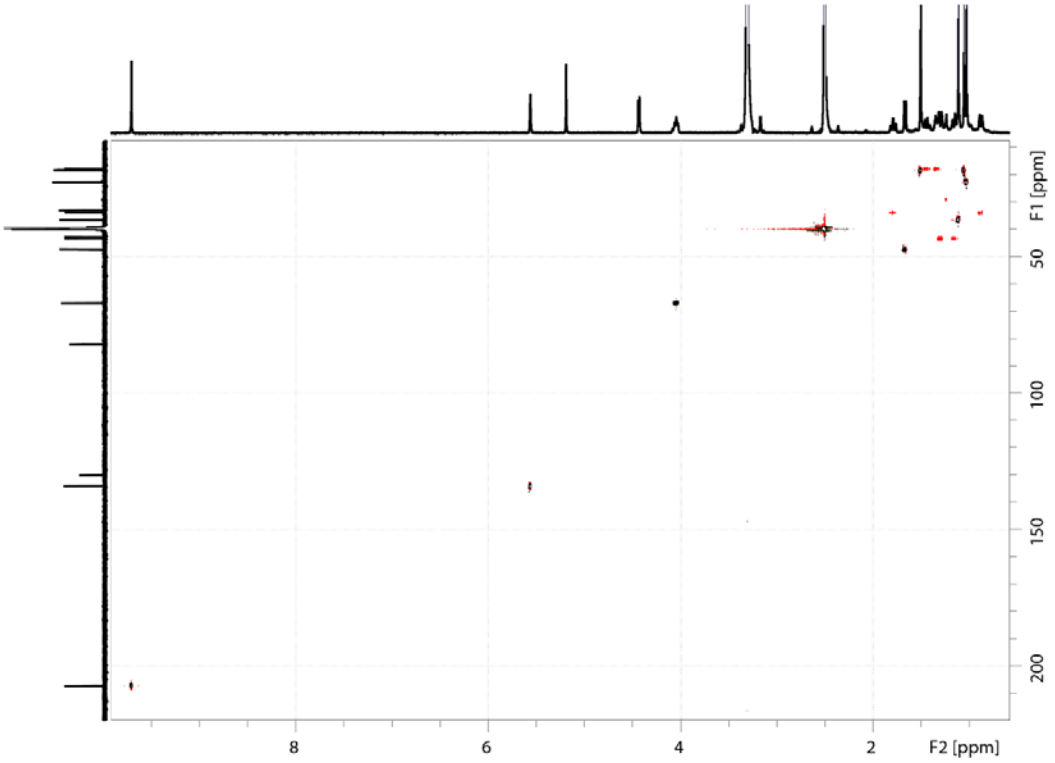

Figure B.7: HSQC-DEPT NMR spectrum (500 MHz, DMSO-d_6) of **3.1**

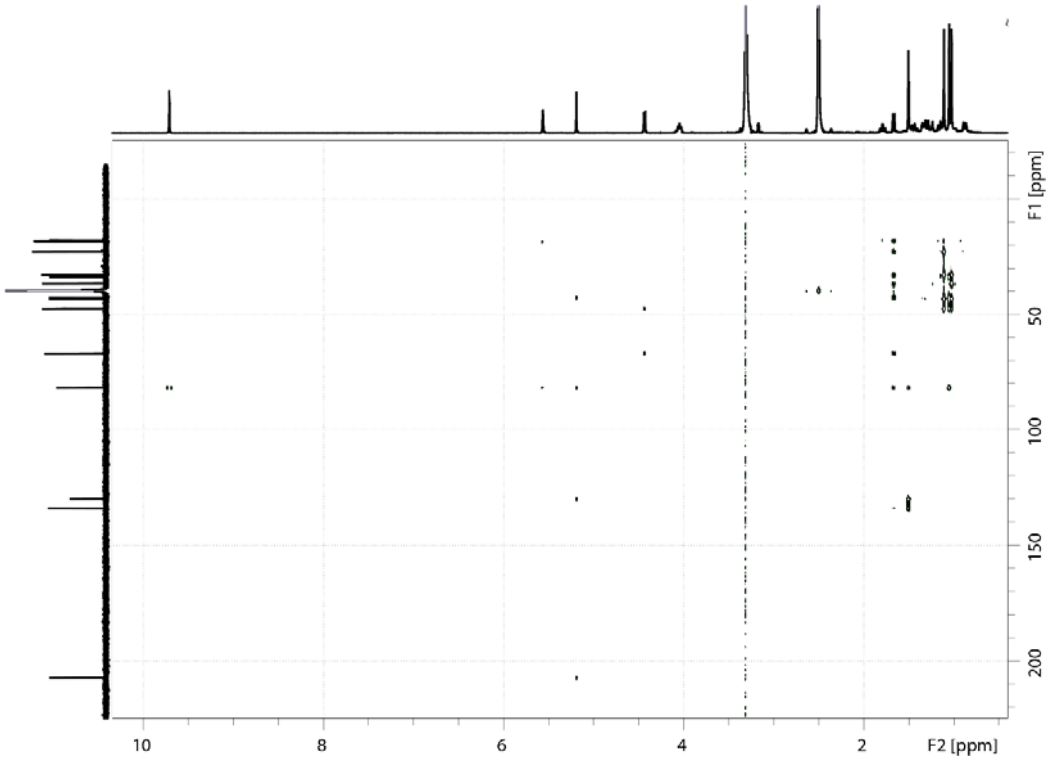

Figure B.8: HMBC NMR spectrum (500 MHz, DMSO-d_6) of **3.1**

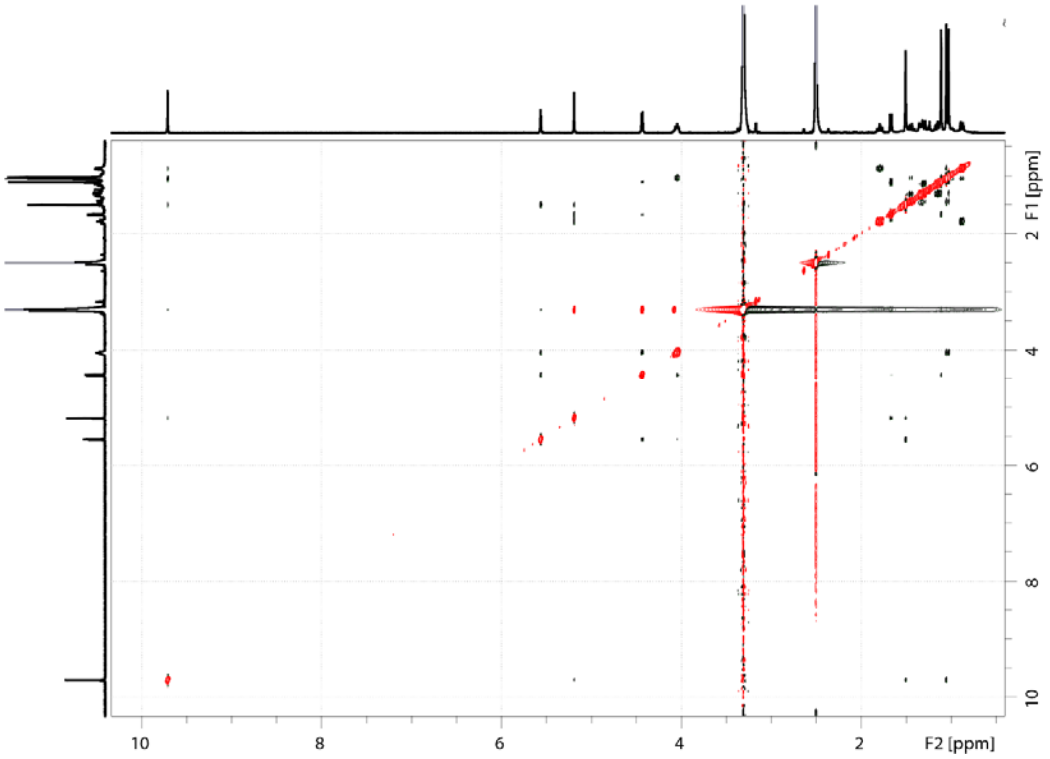

Figure B.9: NOESY NMR spectrum (500 MHz, DMSO-d_6) of **3.1**

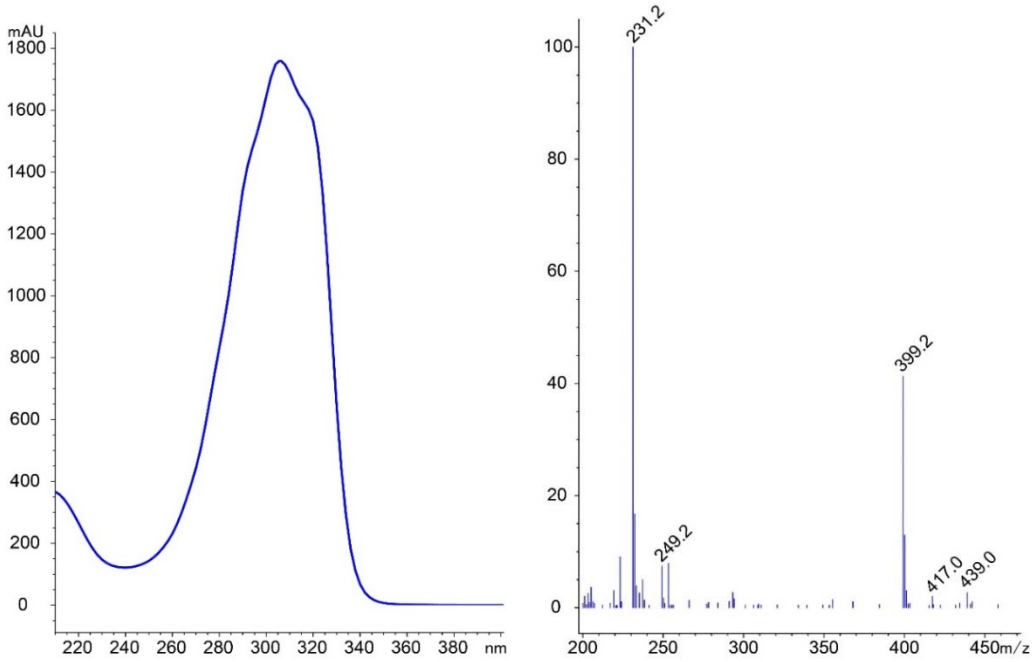

Figure B.10: UV and ESI positive mode low-resolution mass spectrum of **3.2**

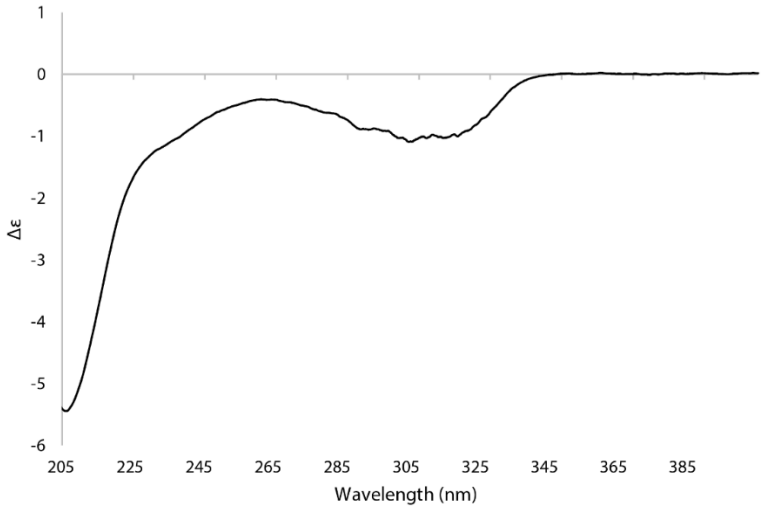

Figure B.11: ECD spectrum of **3.2**

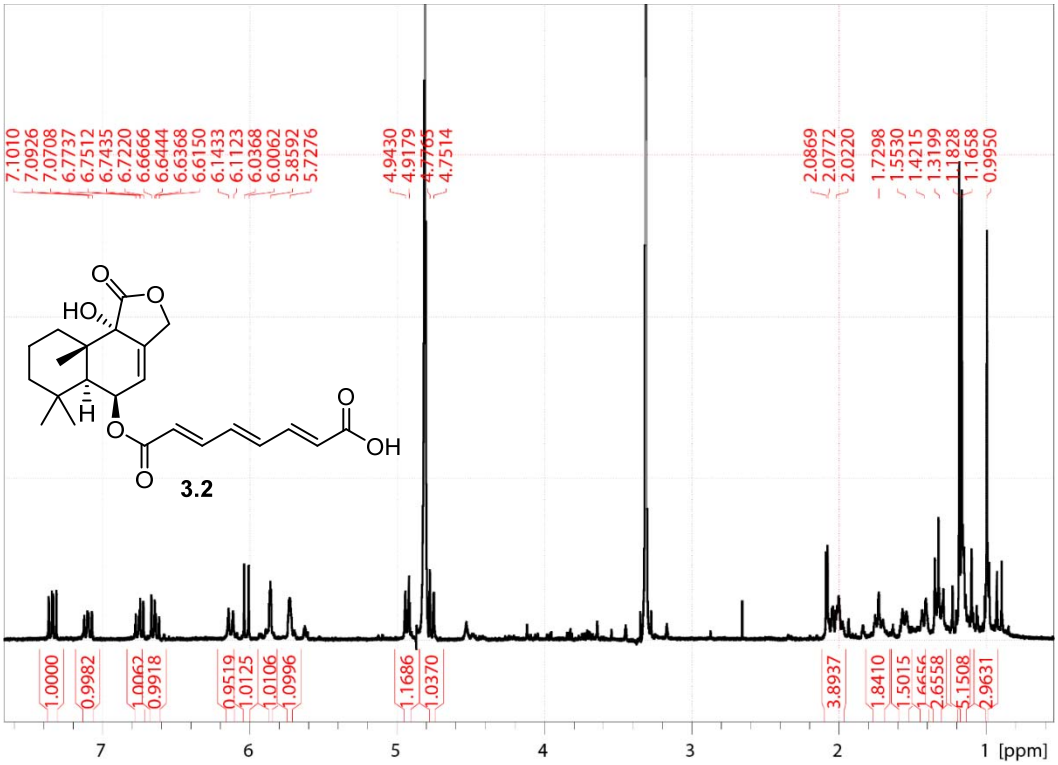

Figure B.12: ^{1}H NMR spectrum (500 MHz, MeOH-d_4) of **3.2**

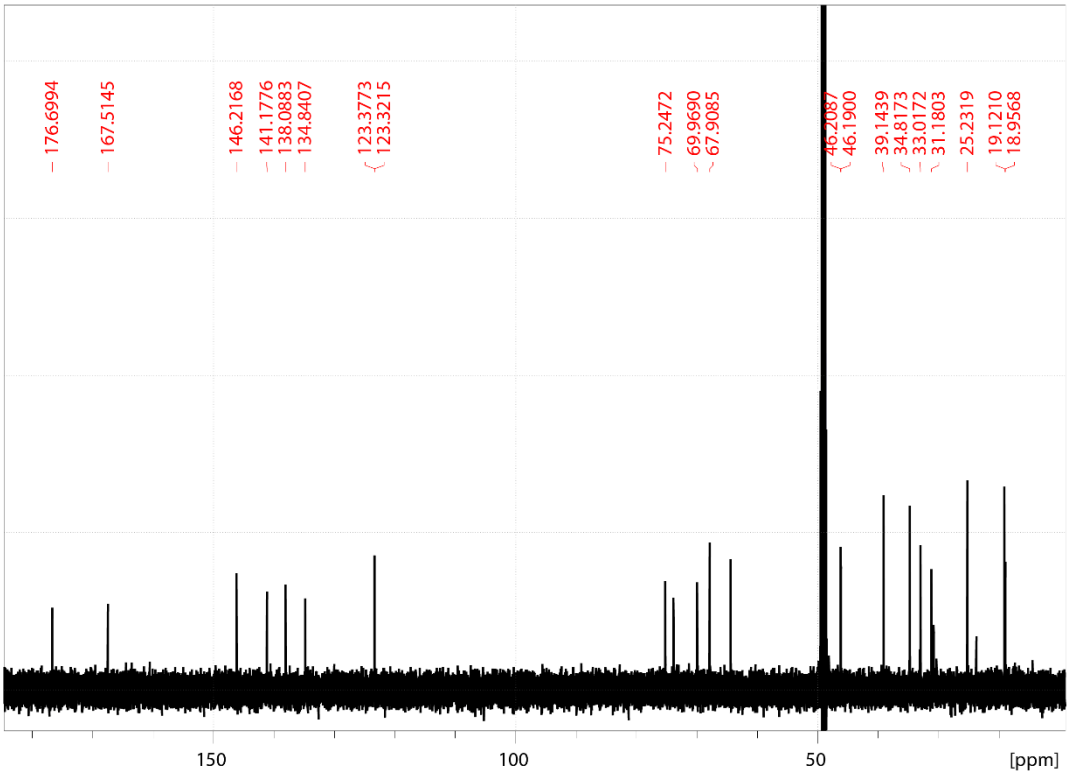

Figure B.13: ^{13}C NMR spectrum (176 MHz, MeOH-d_4) of **3.2**. Carbons C-6', C-7', and C-8' are not present in the ^{13}C spectrum and were derived from the 2D NMR data.

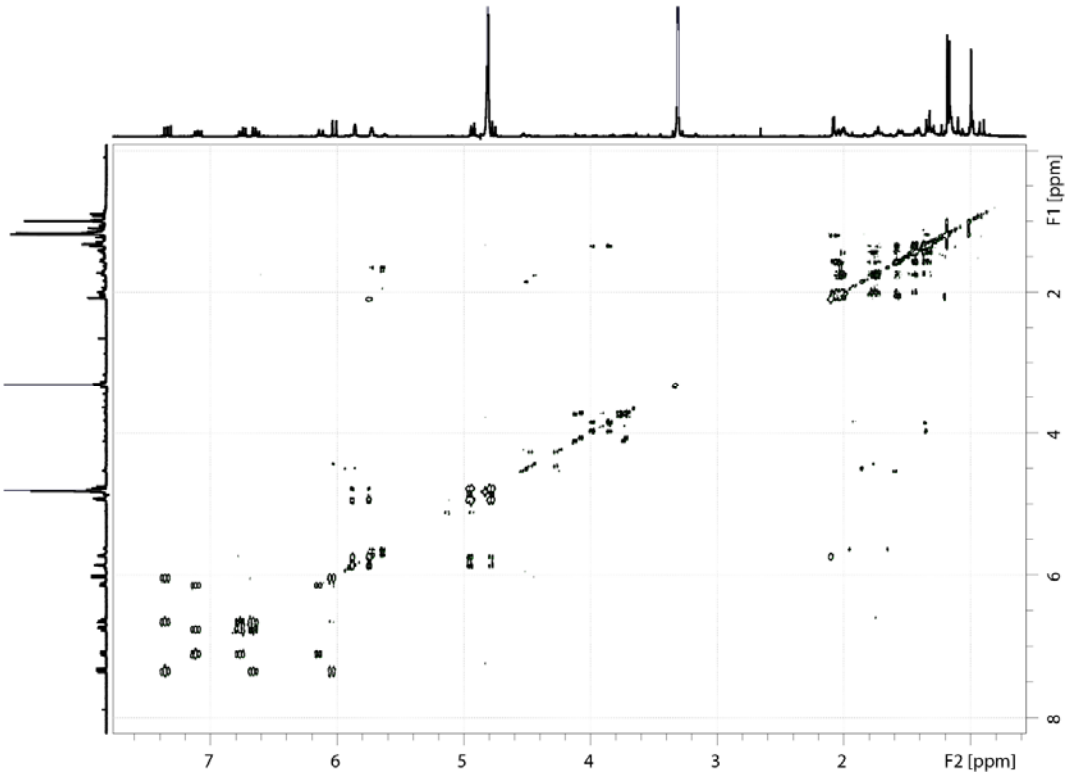

Figure B.14: COSY NMR spectrum (500 MHz, MeOH-d_4) of **3.2**

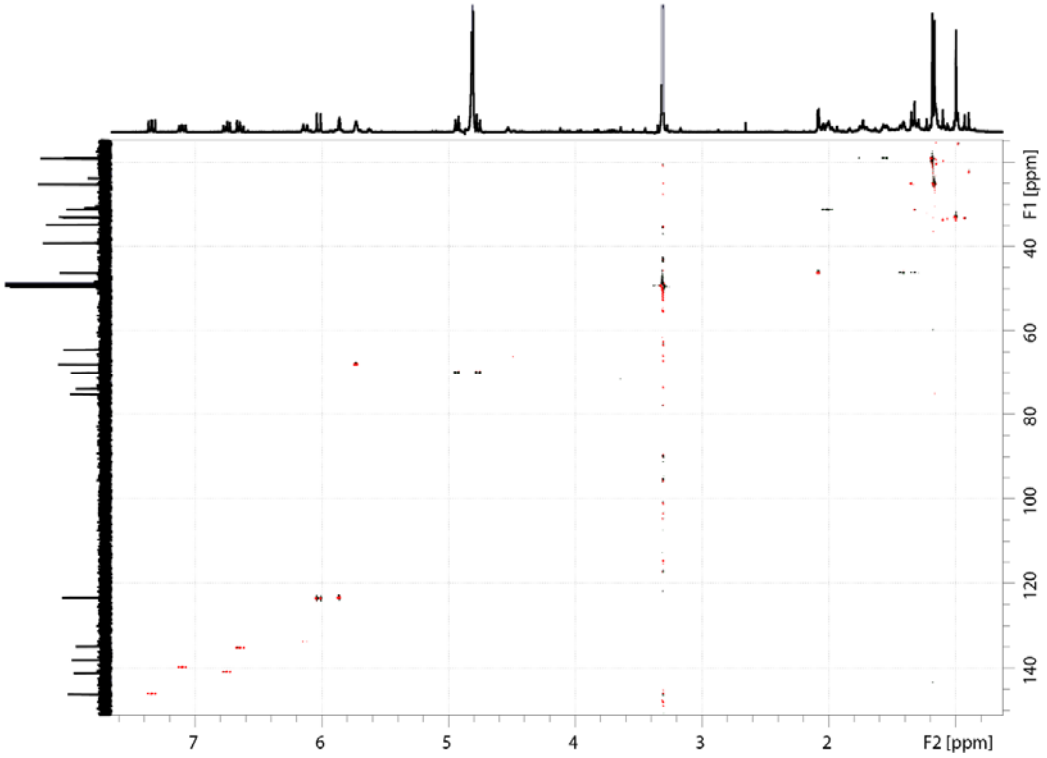

Figure B.15: HSQC-DEPT NMR spectrum (500 MHz, MeOH-d_4) of **3.2**

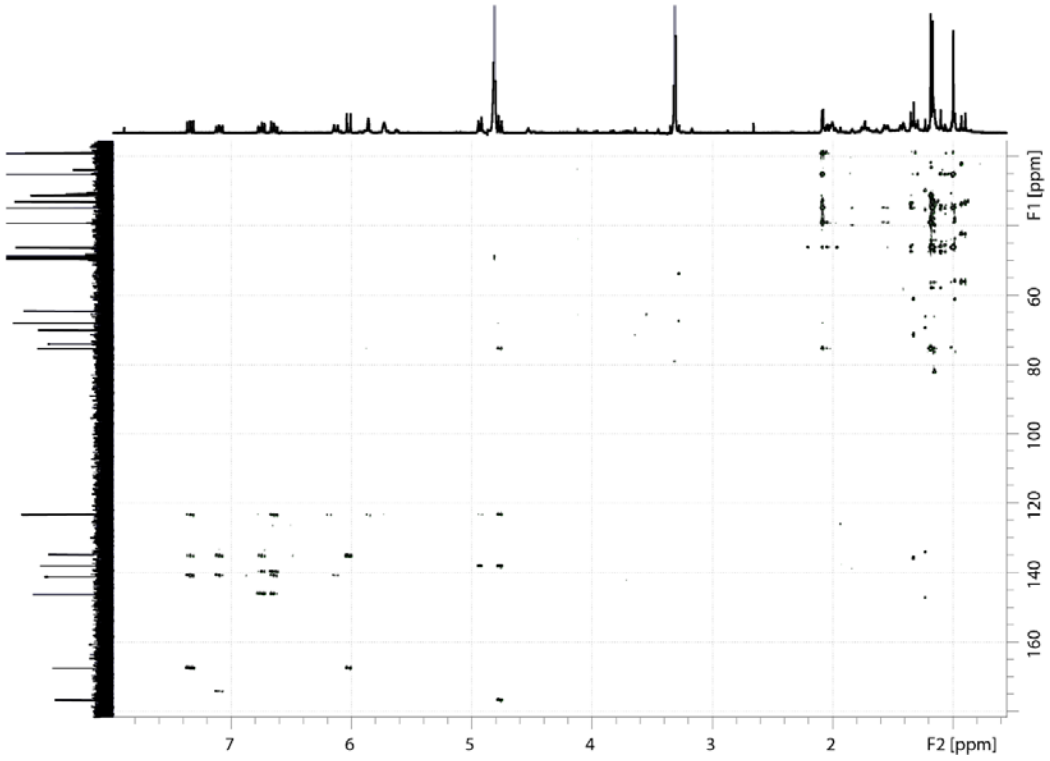

Figure B.16: HMBC NMR spectrum (500 MHz, MeOH-d_4) of **3.2**

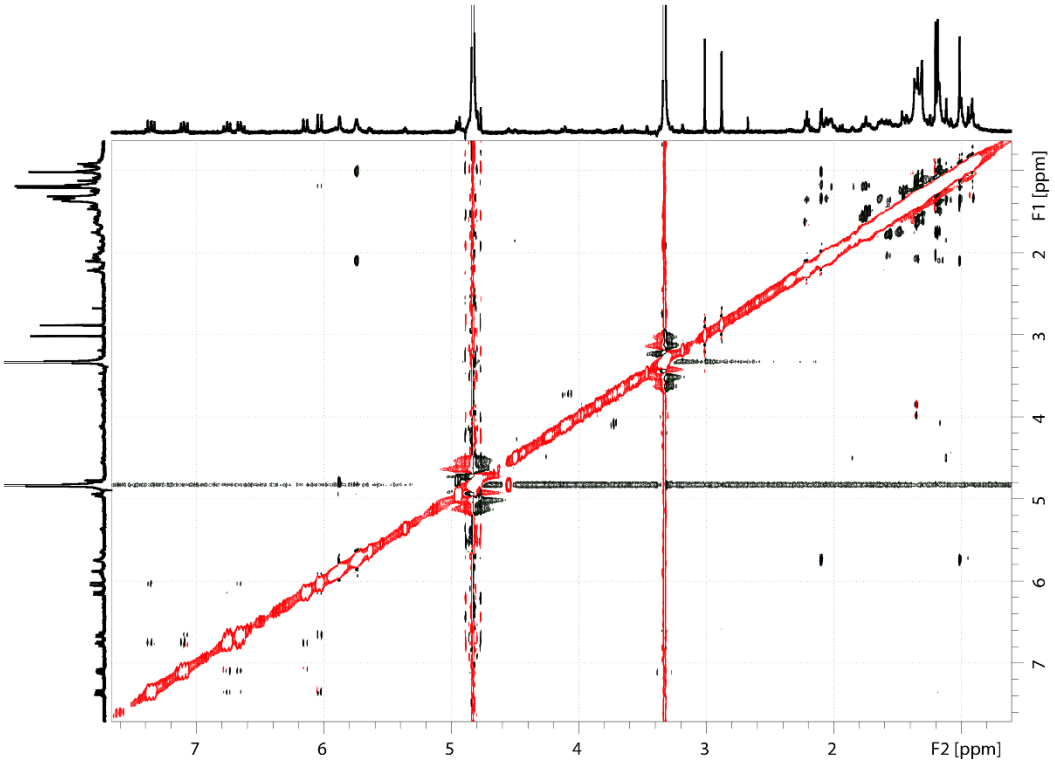

Figure B.17: NOESY NMR spectrum (500 MHz, MeOH-*d*$_4$) of **3.2**

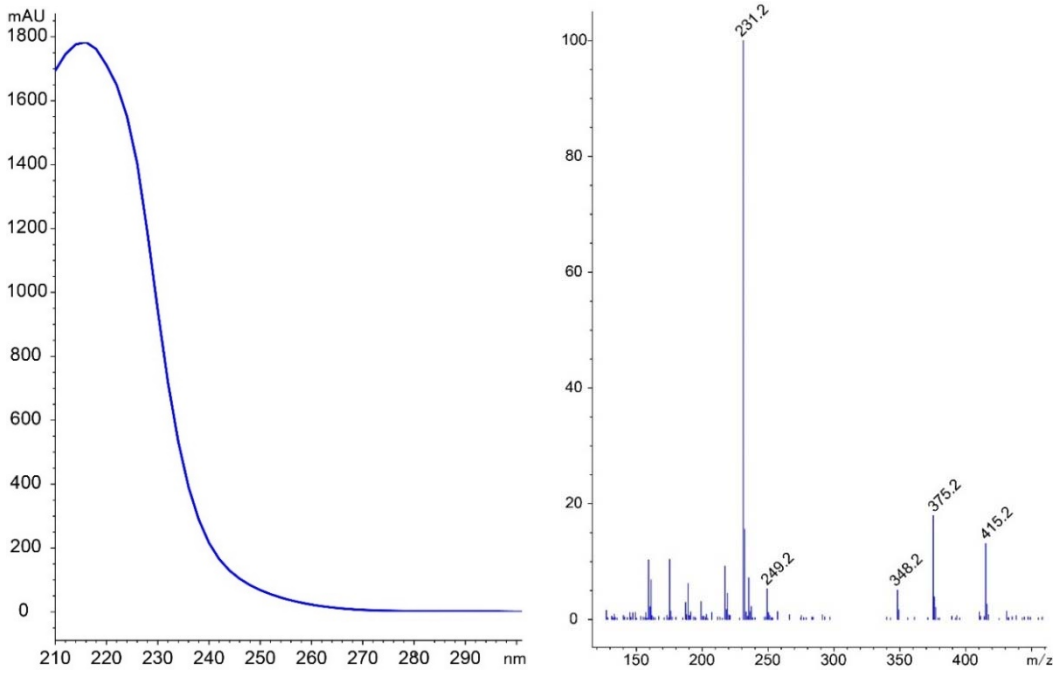

Figure B.18: UV and ESI positive mode low-resolution mass spectrum of **3.3**

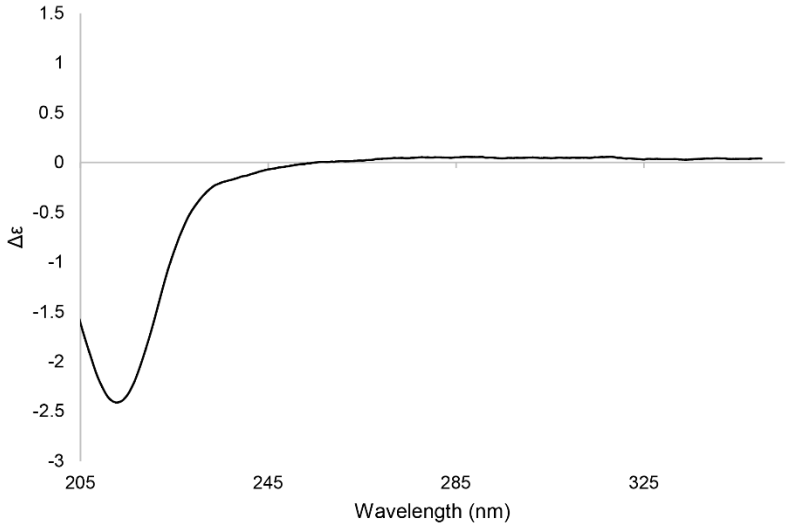

Figure B.19: ECD spectrum of **3.3**

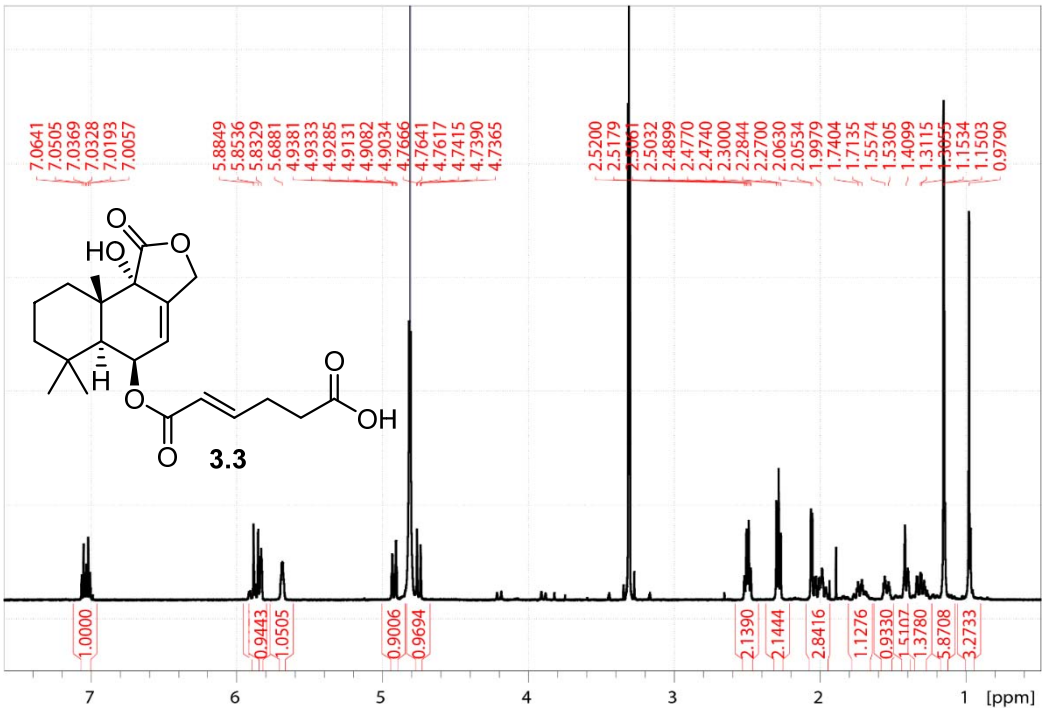

Figure B.20: ^{1}H NMR spectrum (500 MHz, MeOH-d_4) of **3.3**

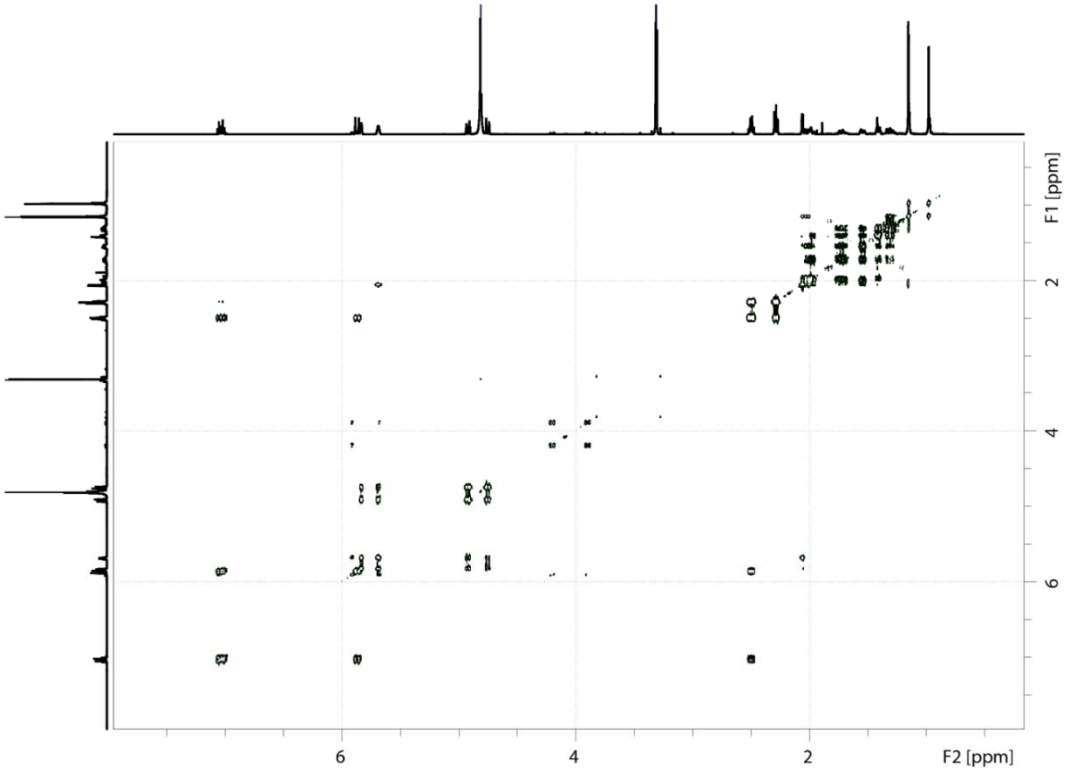

Figure B.21: COSY NMR spectrum (500 MHz, MeOH-d_4) of **3.3**

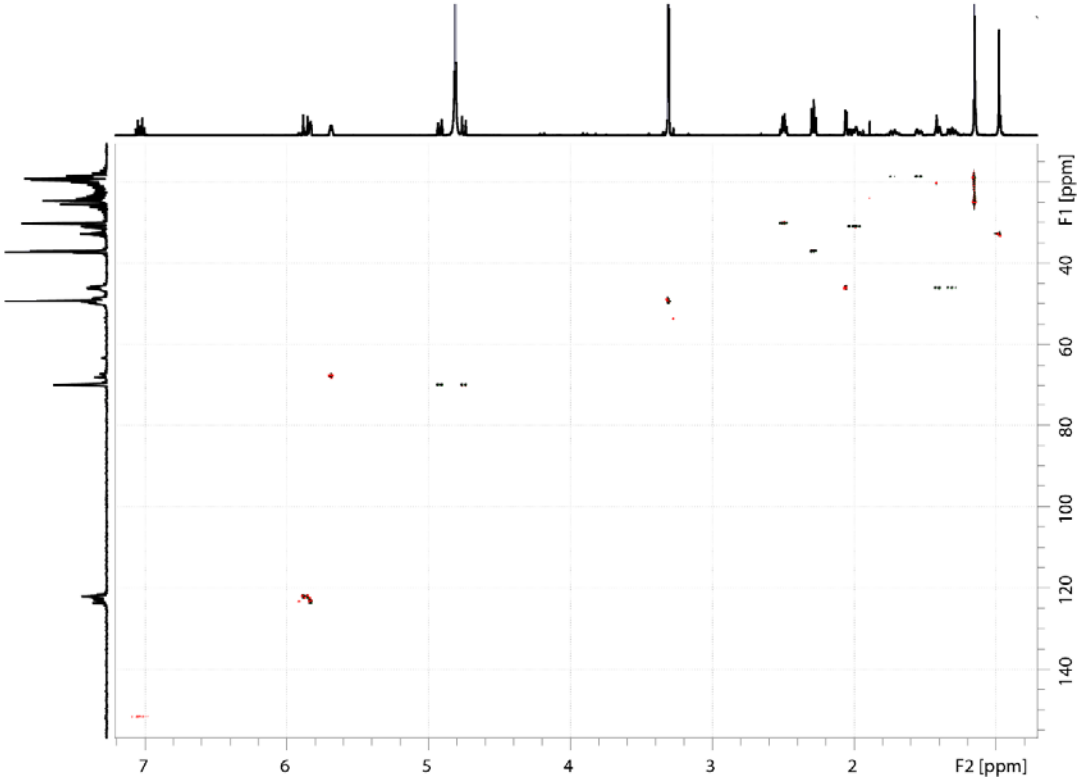

Figure B.22: HSQC-DEPT NMR spectrum (500 MHz, MeOH-d_4) of **3.3**

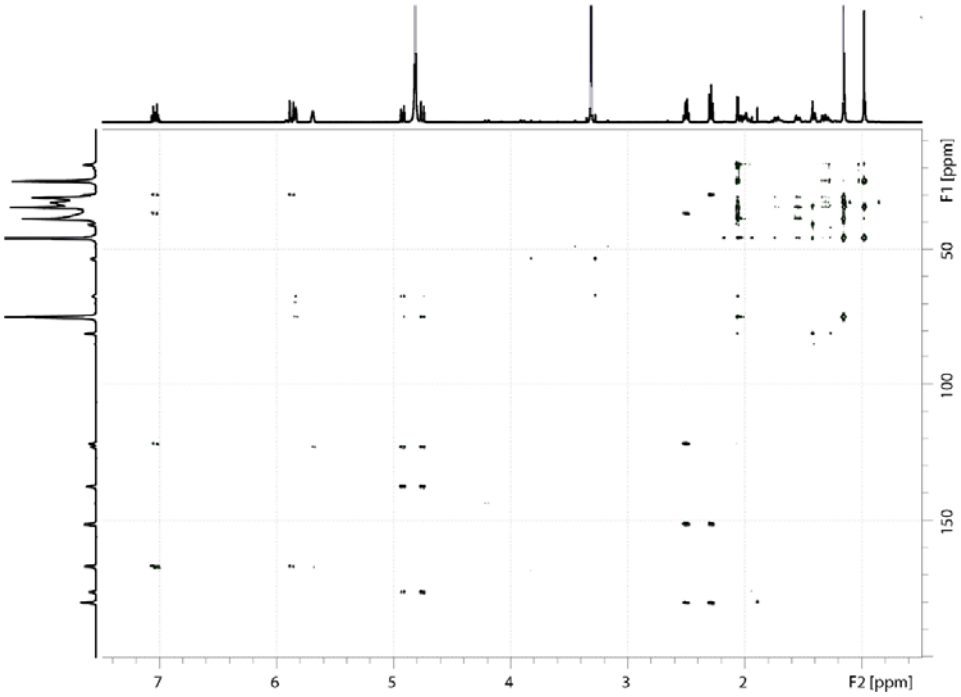

Figure B.23: HMBC NMR spectrum (500 MHz, MeOH-d_4) of **3.3**

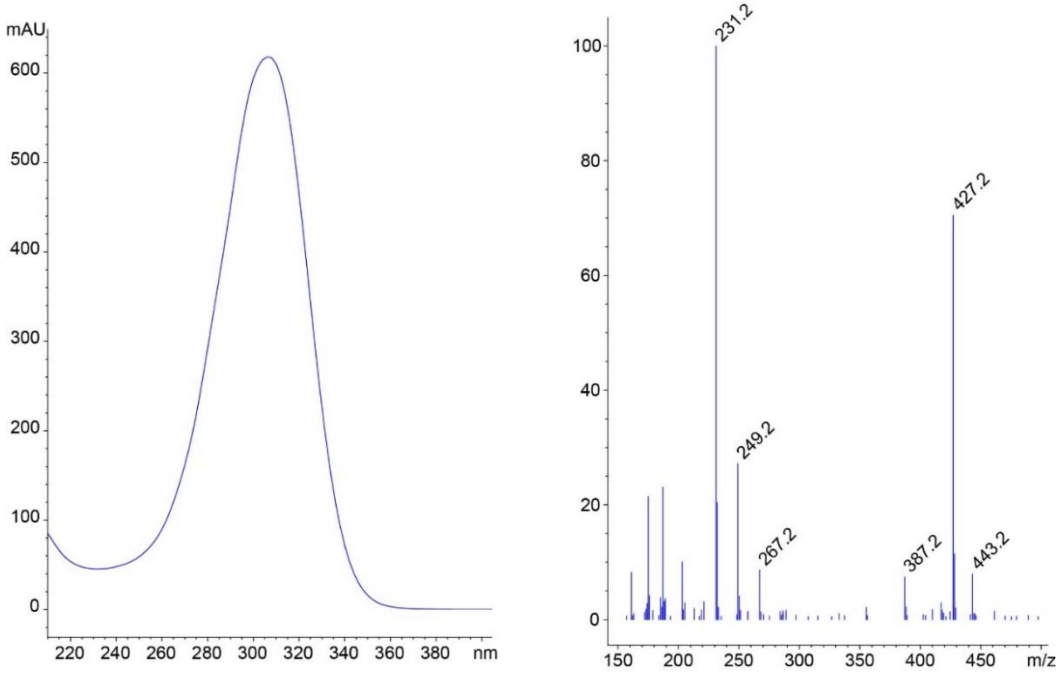

Figure B.24: UV and ESI positive mode low-resolution mass spectrum of **3.4**

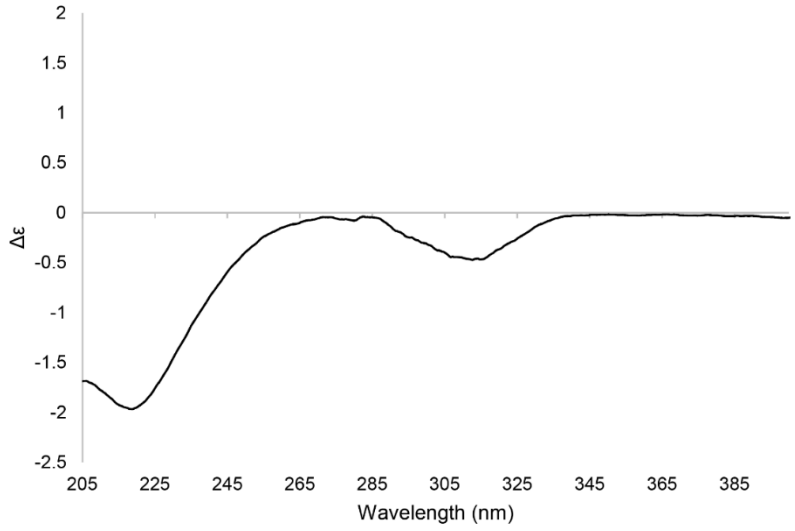

Figure B.25: ECD spectrum of **3.4**

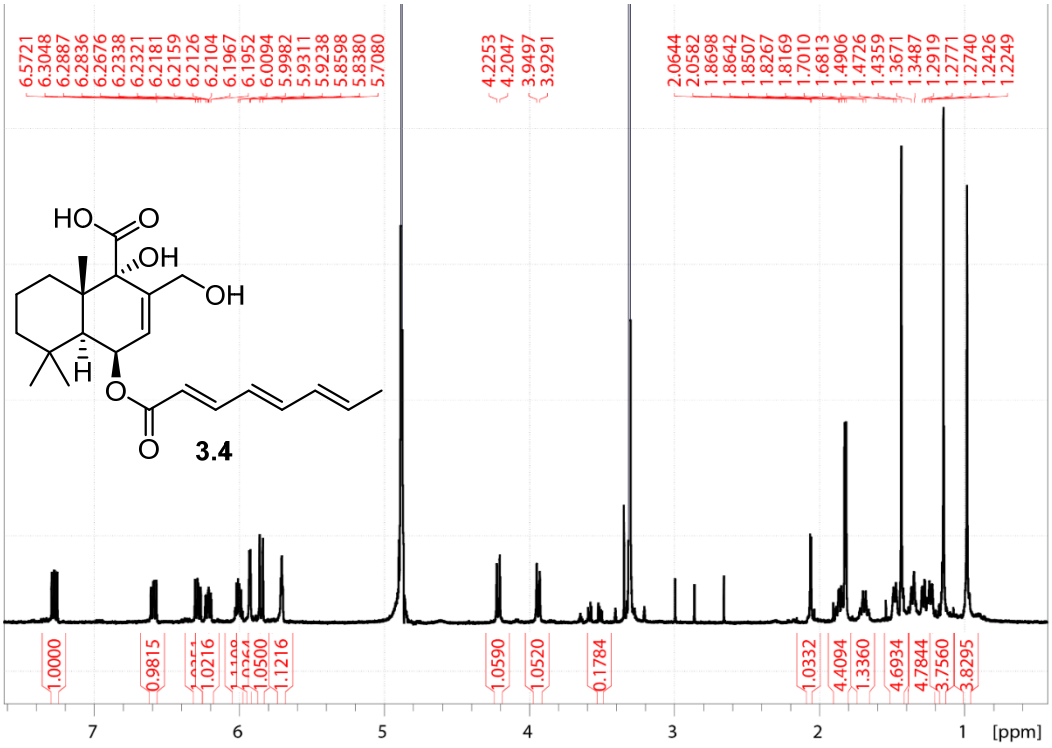

Figure B.26: ^{1}H NMR spectrum (700 MHz, MeOH-d_4) of **3.4**

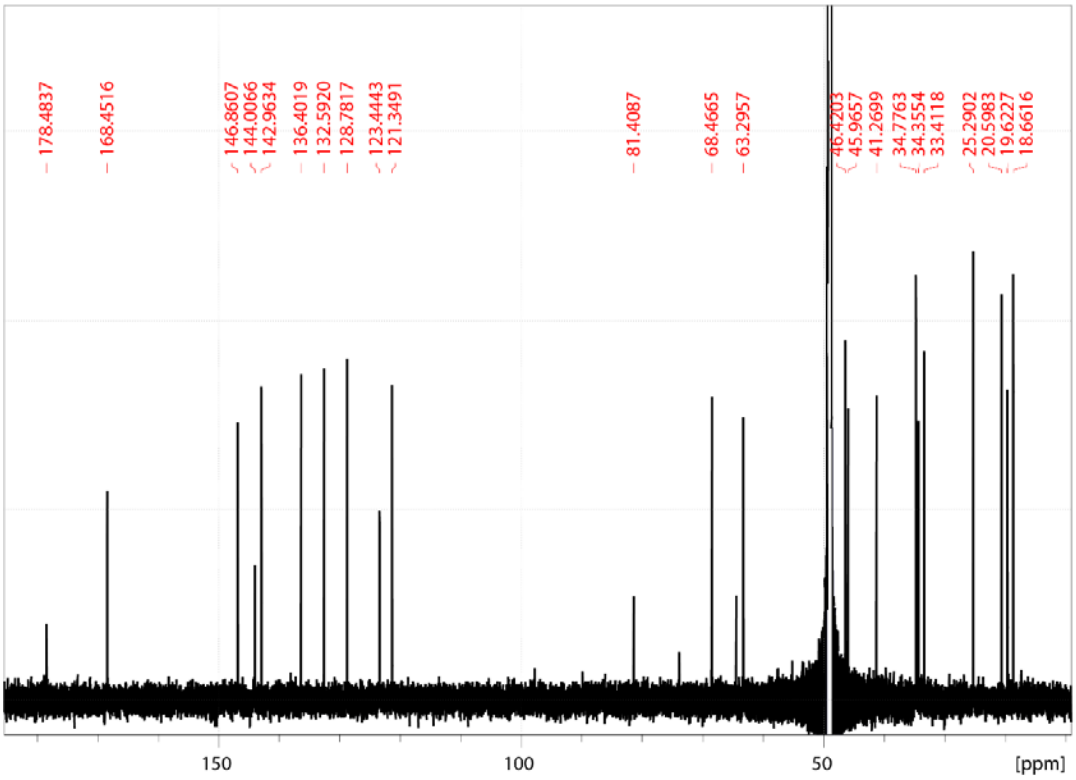

Figure B.27: ^{13}C NMR spectrum (176 MHz, MeOH-d_4) of **3.4**

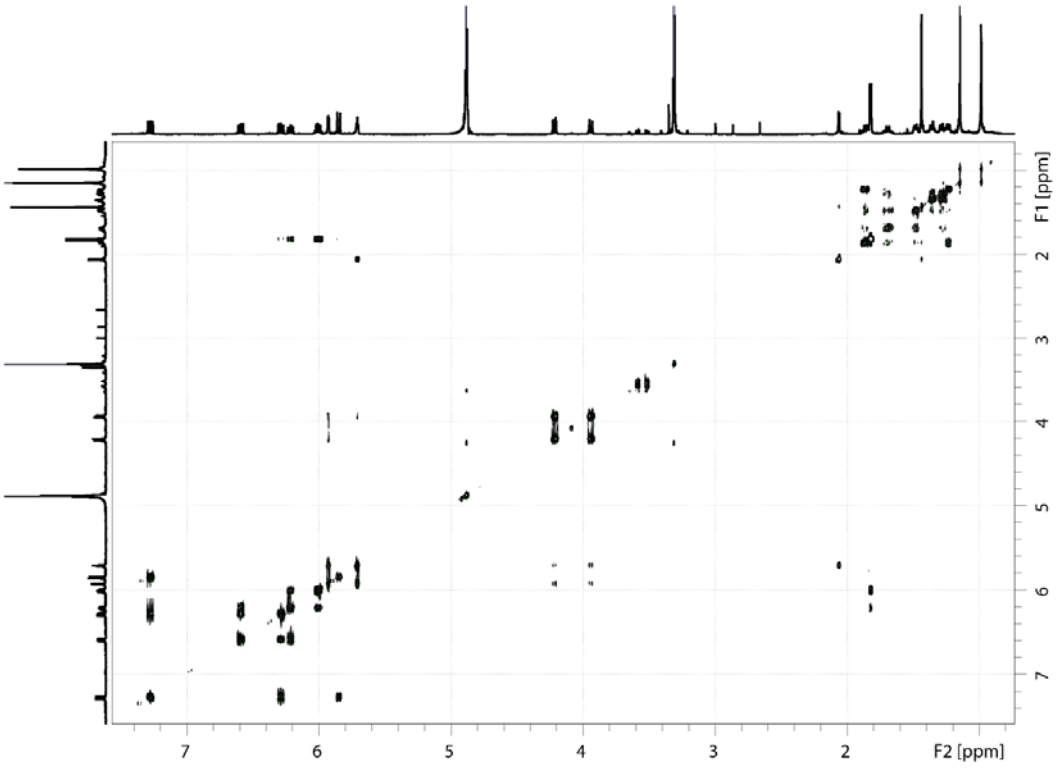

Figure B.28: COSY NMR spectrum (700 MHz, MeOH-d_4) of **3.4**

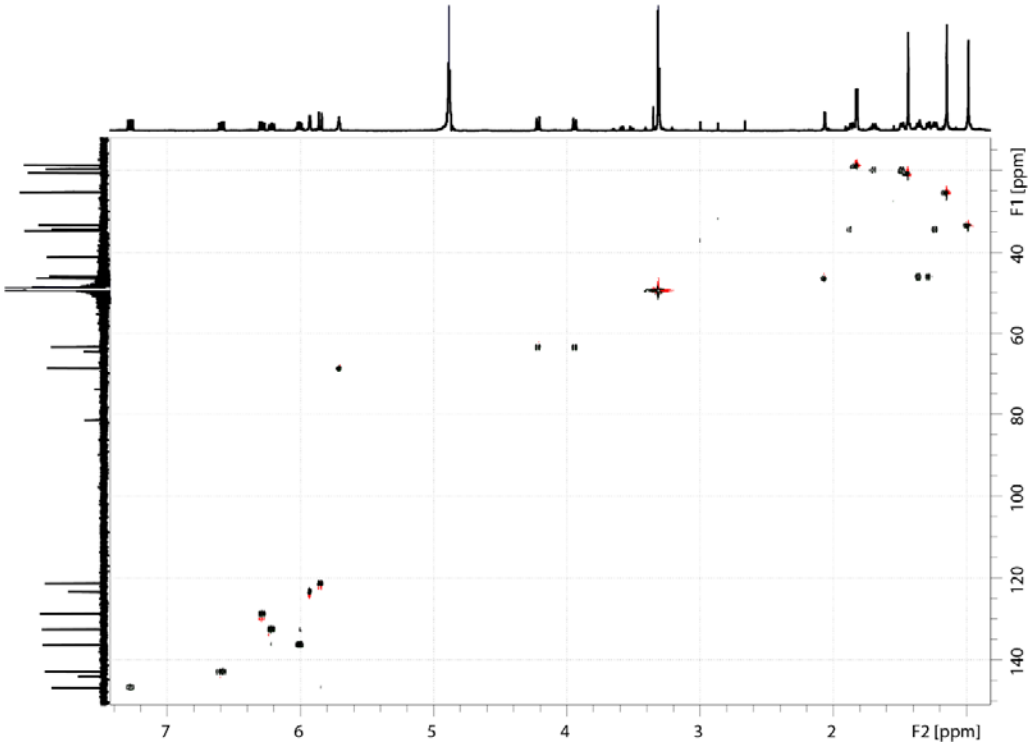

Figure B.29: HSQC NMR spectrum (700 MHz, MeOH-d_4) of **3.4**

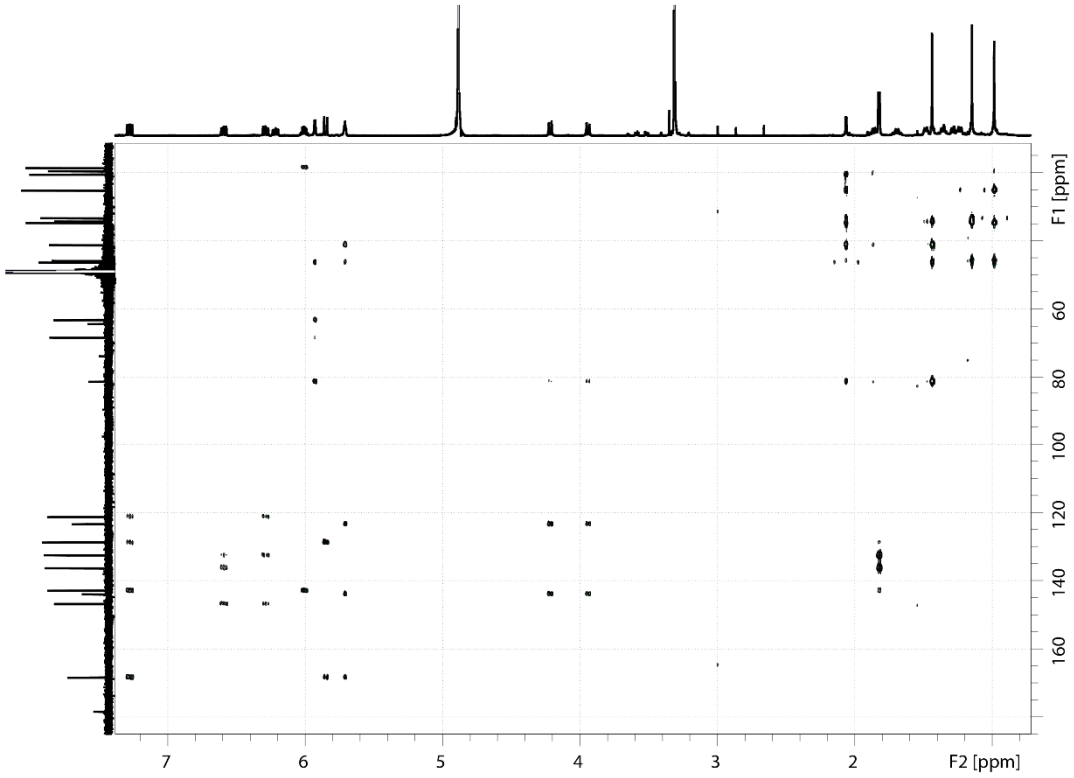

Figure B.30: HMBC NMR spectrum (700 MHz, MeOH-d_4) of **3.4**

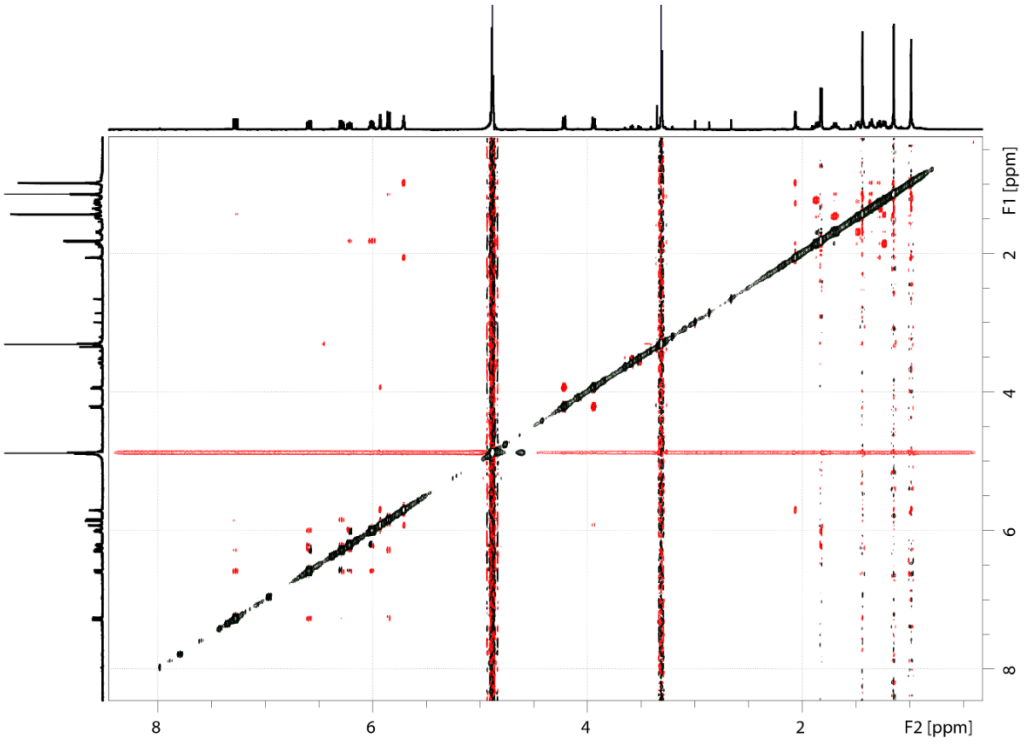

Figure B.31: NOESY NMR spectrum (700 MHz, MeOH-d_4) of **3.4**

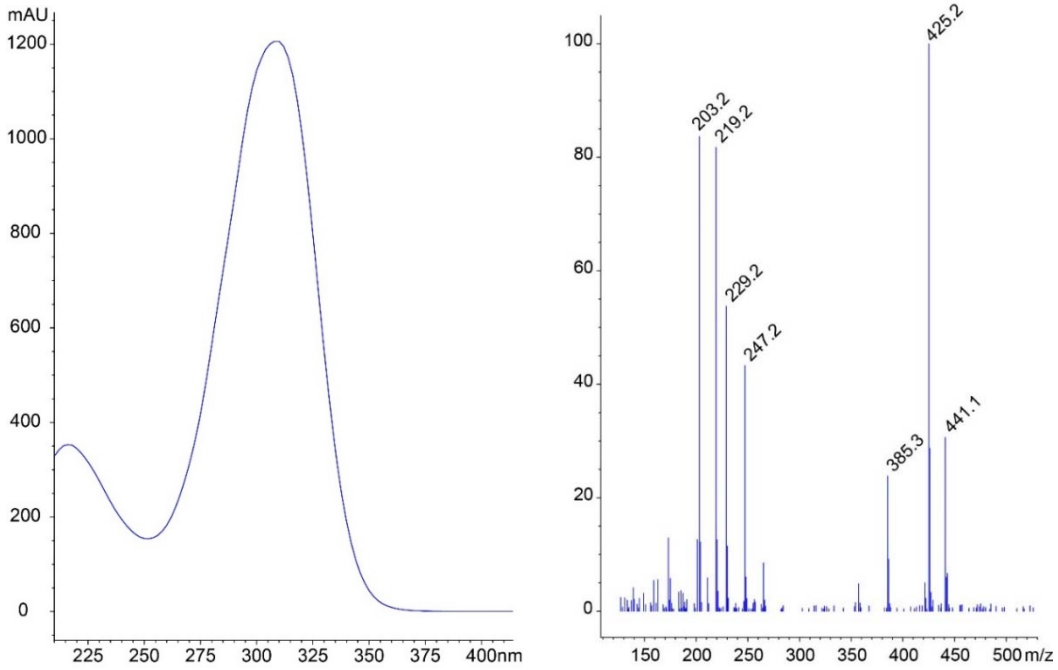

Figure B.32: UV and ESI positive mode low-resolution mass spectrum of **3.5**

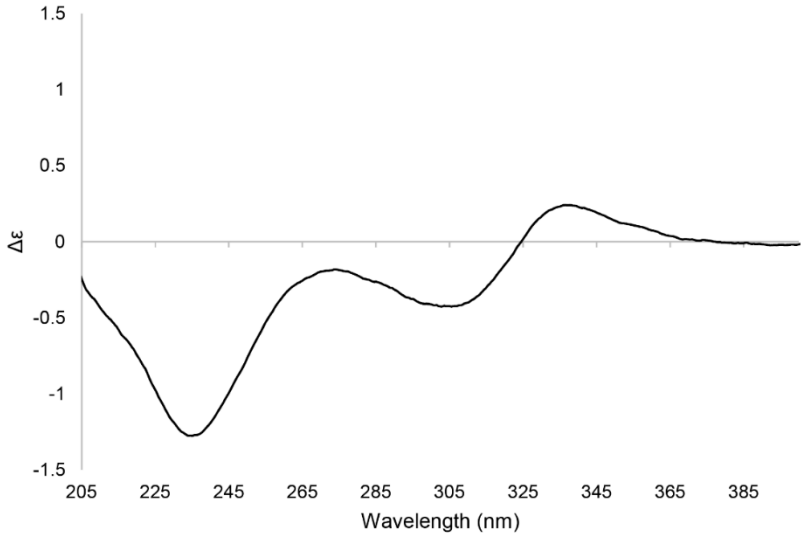

Figure B.33: ECD spectrum of **3.5**

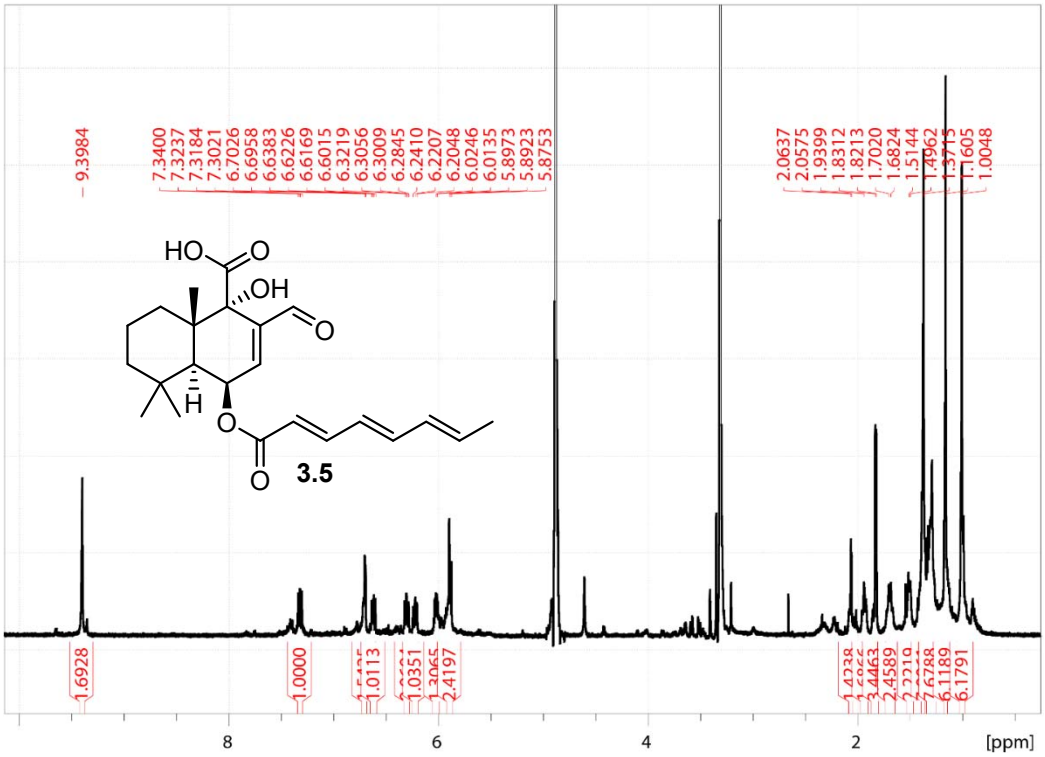

Figure B.34: ^{1}H NMR spectrum (700 MHz, MeOH-d_4) of **3.5**

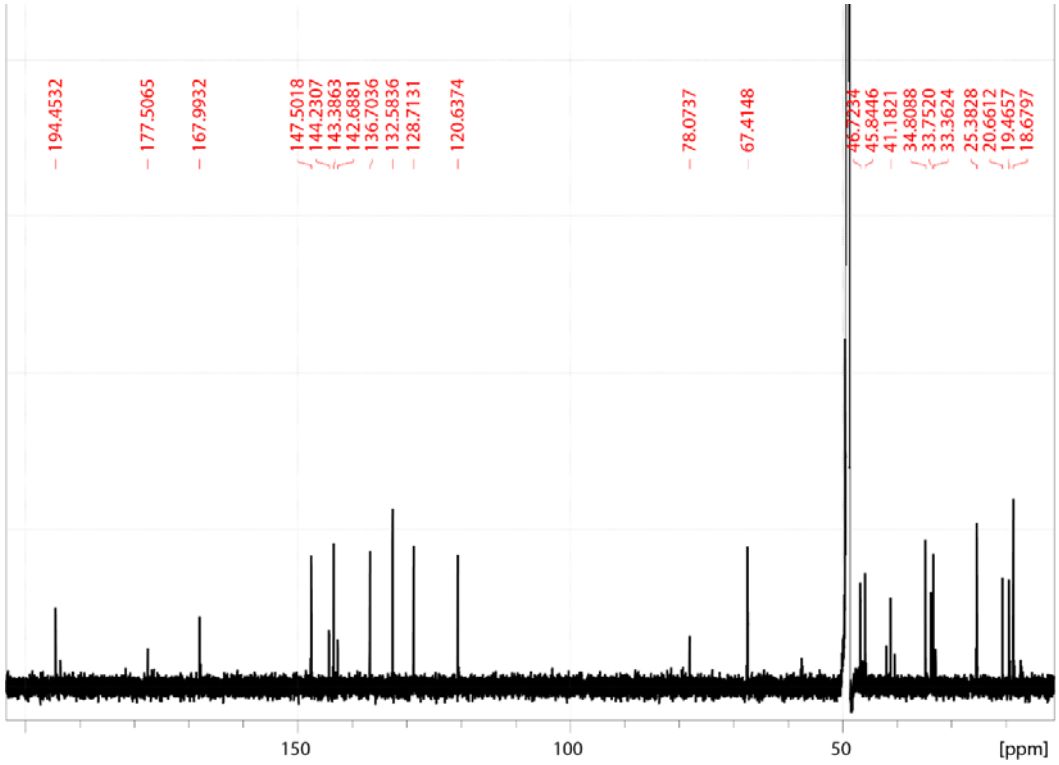

Figure B.35: ^{13}C NMR spectrum (176 MHz, MeOH-d_4) of **3.5**

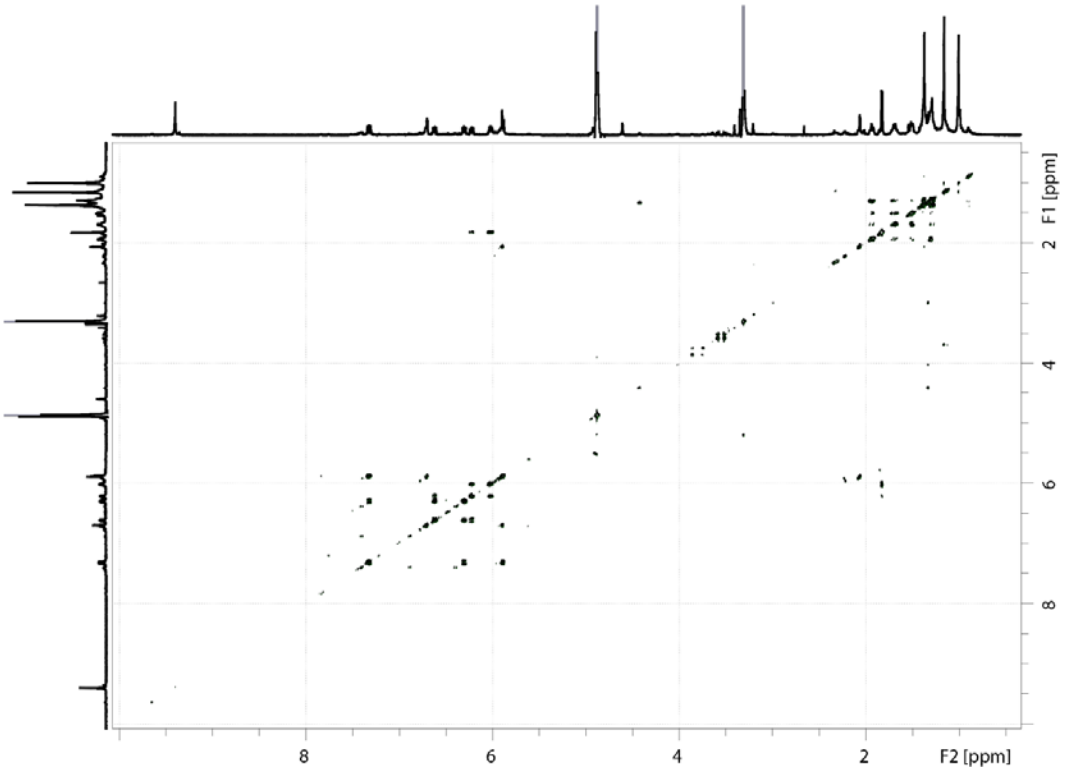

Figure B.36: COSY NMR spectrum (700 MHz, MeOH-d_4) of **3.5**

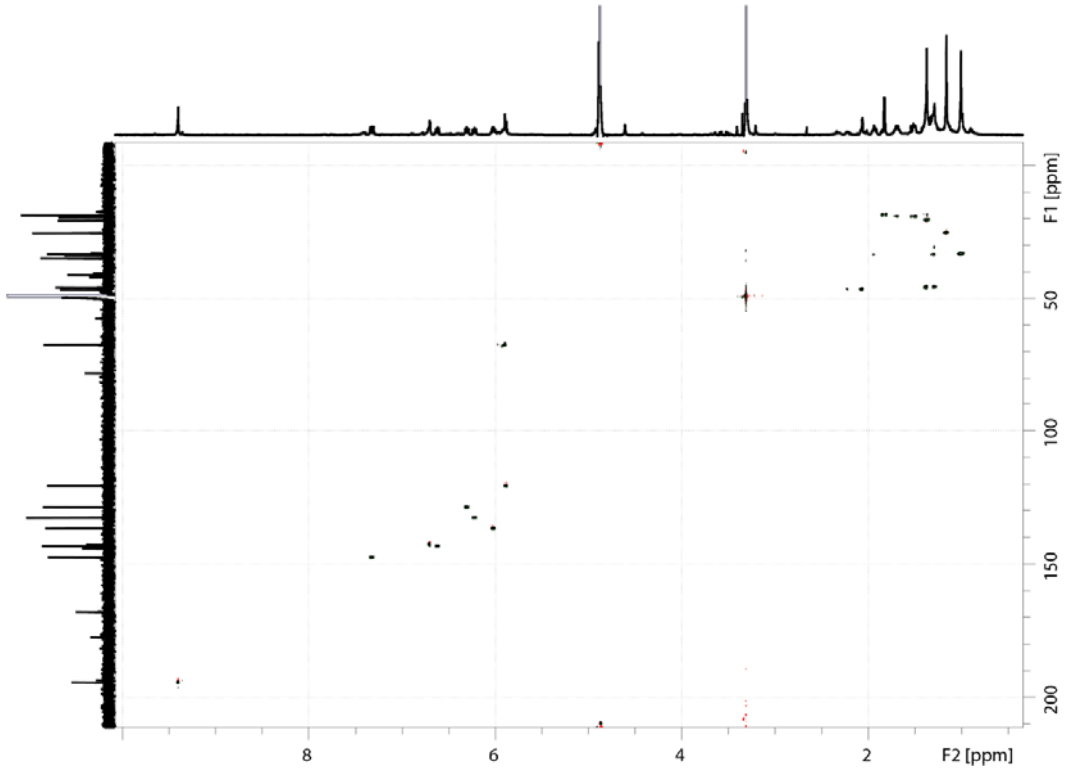

Figure B.37: HSQC NMR spectrum (700 MHz, MeOH-d_4) of **3.5**

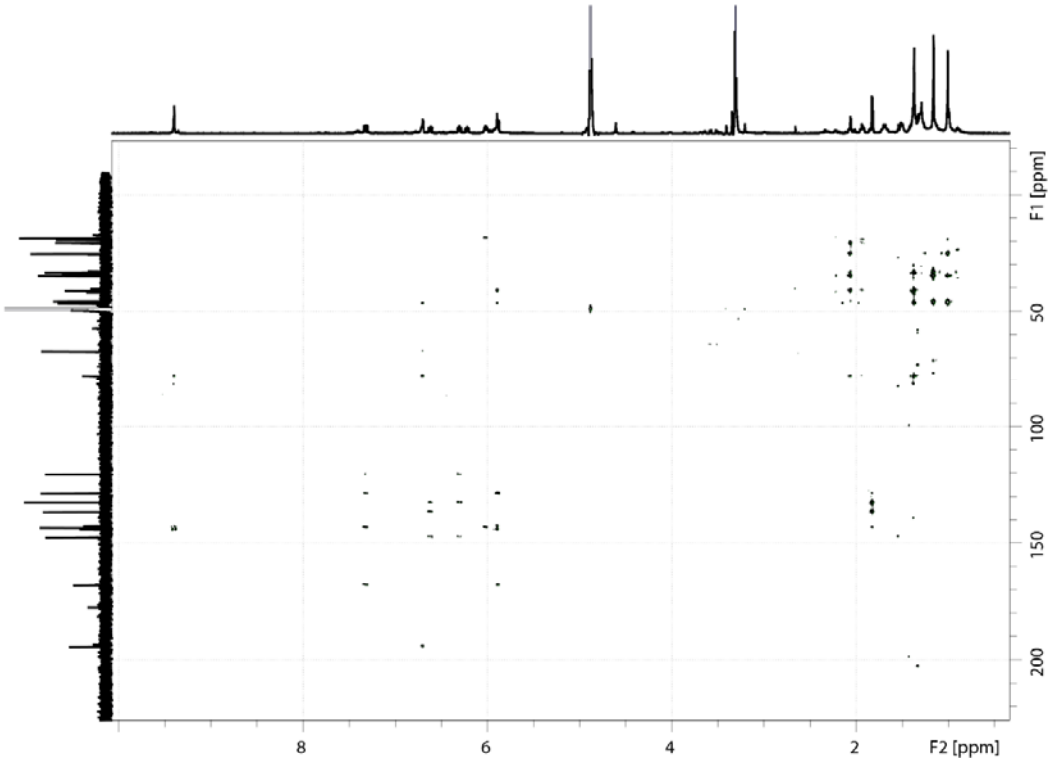

Figure B.38: HMBC NMR spectrum (700 MHz, MeOH-d_4) of **3.5**

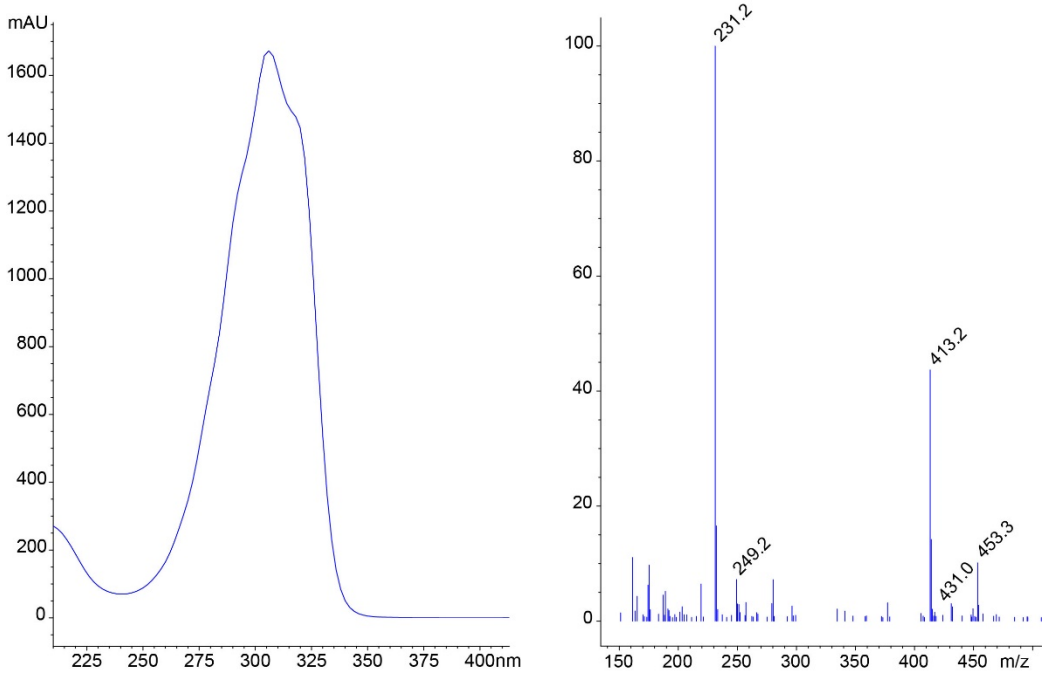

Figure B.39: UV and low-resolution mass spectrum of **3.2**Me

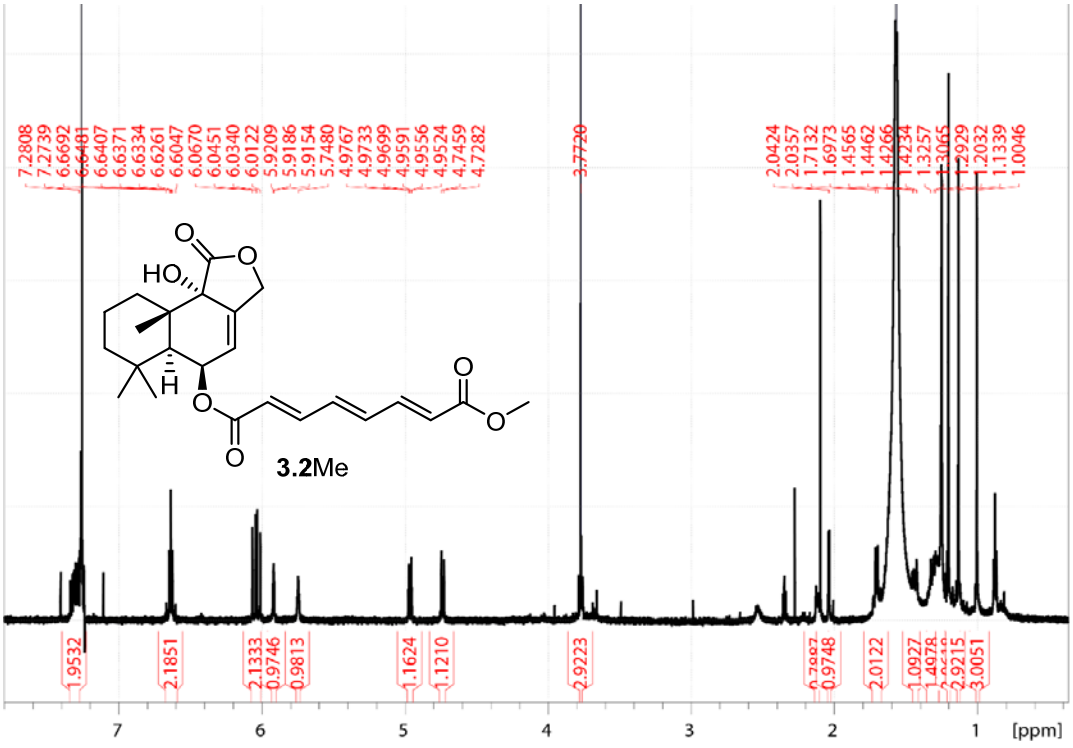

Figure B.40: ^{1}H NMR spectrum (700 MHz, $CDCl_3$) of **3.2**Me

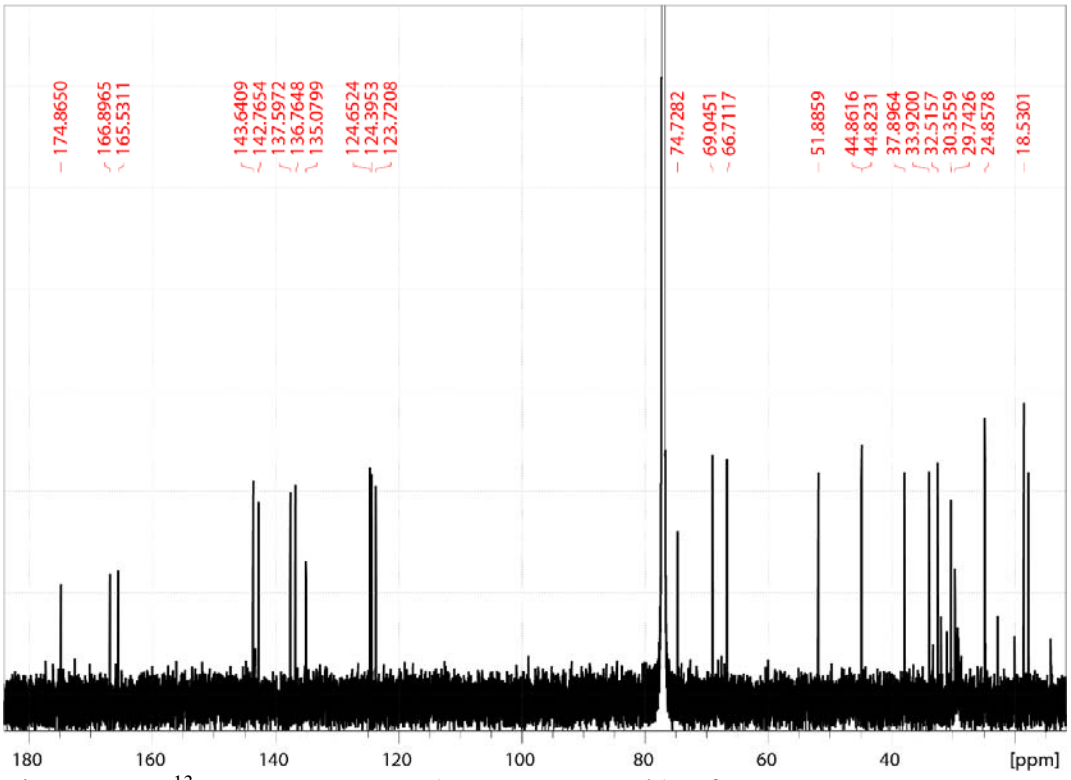

Figure B.41: ^{13}C NMR spectrum (176 MHz, $CDCl_3$) of **3.2**Me

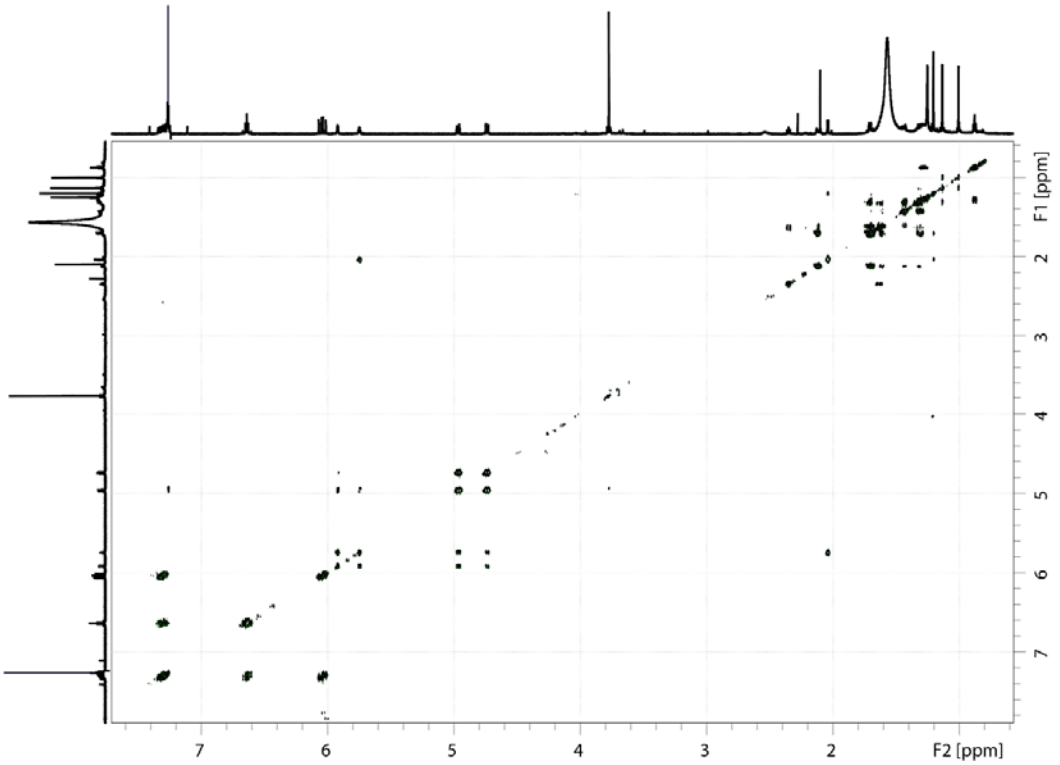

Figure B.42: COSY NMR spectrum (700 MHz, $CDCl_3$) of **3.2**Me

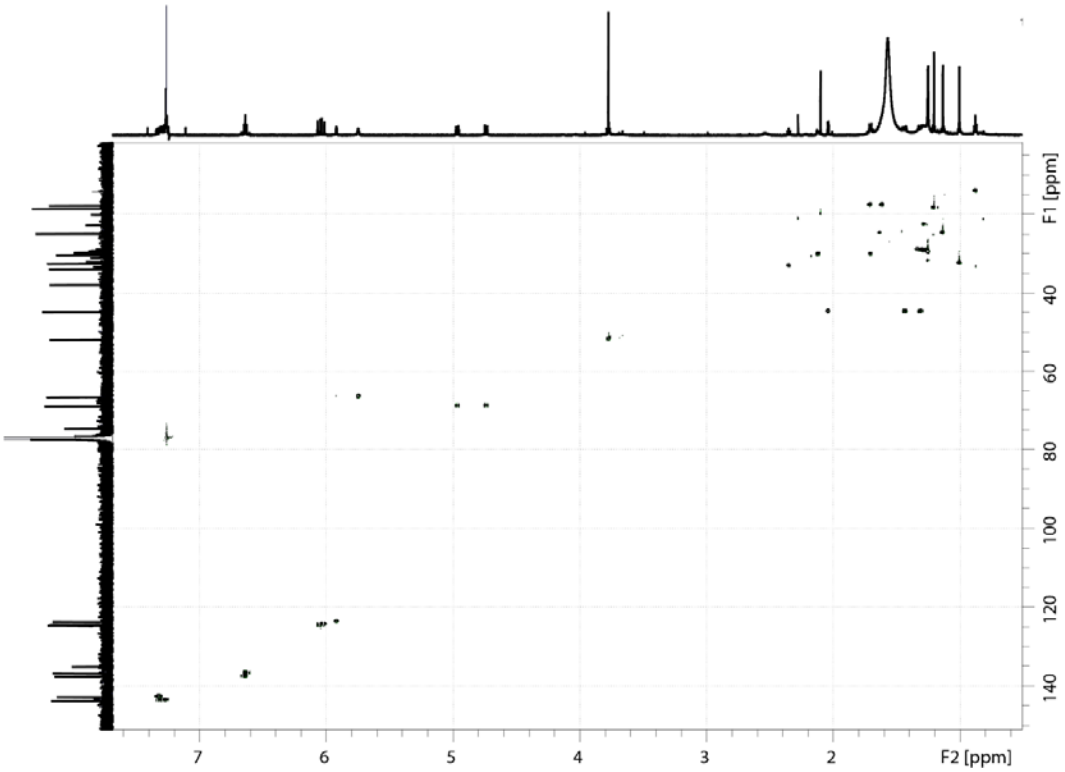

Figure B.43: HSQC NMR spectrum (700 MHz, $CDCl_3$) of **3.2**Me

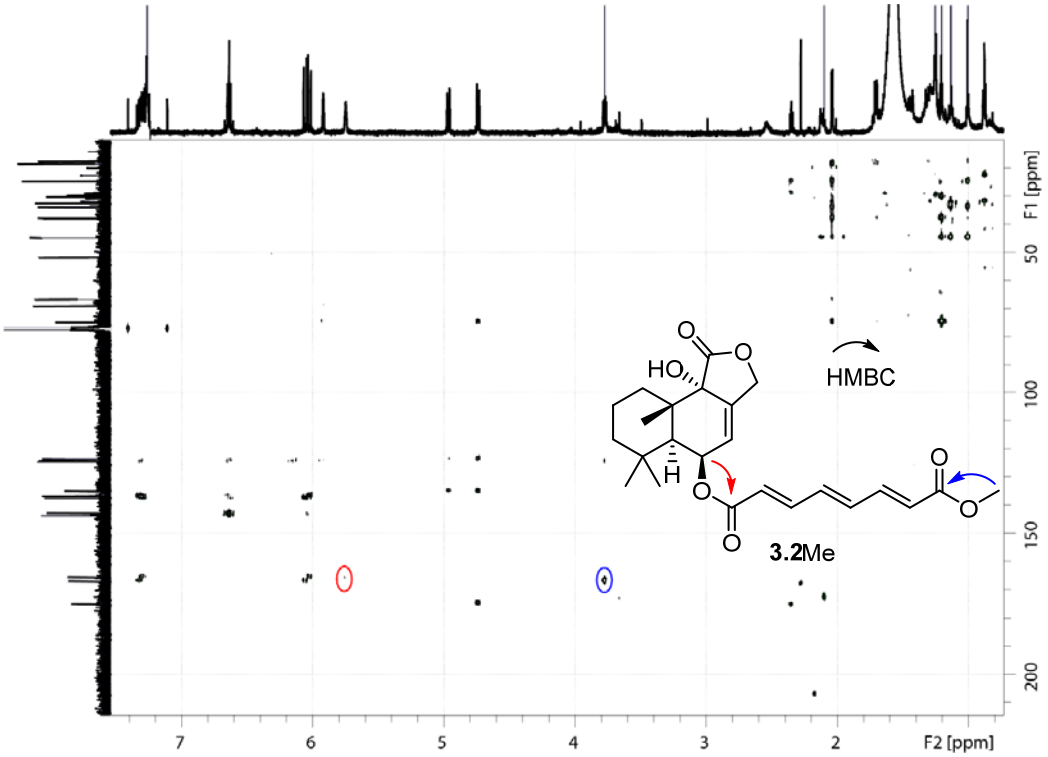

Figure B.44: HMBC NMR spectrum (700 MHz, $CDCl_3$) of **3.2**Me showing key correlations

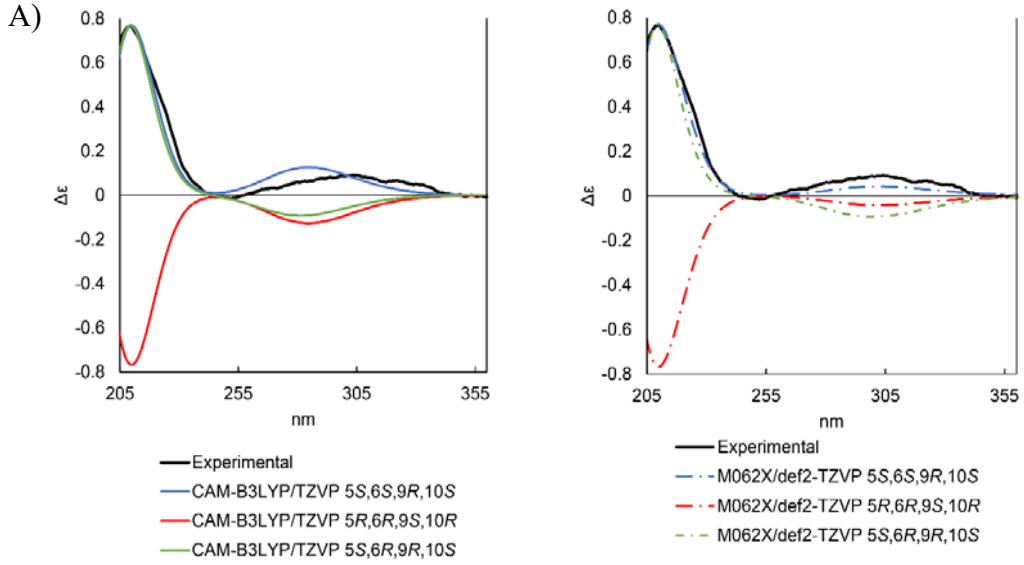

Figure B.45: A) Experimental ECD spectrum of **3.1** (black) in methanol with computed spectra of the enantiomers 5*S*,6*S*,9*R*,10*S* and 5*R*,6*R*,9*S*,10*R* along with the diastereomer 5*S*,6*R*,9*R*,10*S* at the CAM-B3LYP/TZVP level of theory. Blue solid line: 5*S*,6*S*,9*R*,10*S* (shift: 7 nm; σ = 0.42 eV); red solid line: 5*R*,6*R*,9*S*,10*R* (shift: 7 nm; σ = 0.42 eV); green dotted line: 5*S*,6*R*,9*R*,10*S* (shift: 5 nm; σ = 0.43 eV). B) Experimental ECD spectrum of **3.1** (black) in methanol with computed spectra of the enantiomers 5*S*,6*S*,9*R*,10*S* and 5*R*,6*R*,9*S*,10*R* along with the diastereomer 5*S*,6*R*,9*R*,10*S* at the M062X/def2-TZVP level of theory. Blue dashed line: 5*S*,6*S*,9*R*,10*S* (shift: 8 nm; σ = 0.43 eV); red dashed line: 5*R*,6*R*,9*S*,10*R* (shift: 8 nm; σ = 0.43 eV); green dotted line: 5*S*,6*R*,9*R*,10*S* (shift: 7 nm; σ = 0.45 eV)

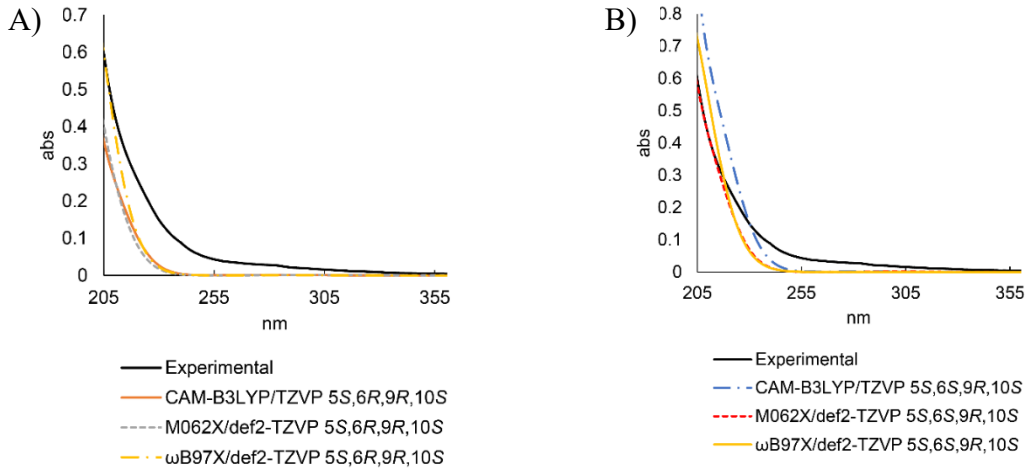

Figure B.46: A) Experimental UV spectrum of **3.1** (black) in methanol with computed spectra of 5*S*,6*R*,9*R*,10*S* configuration at multiple levels of theory B) Experimental UV spectrum of **3.1** (black) in methanol with computed spectra of 5*S*,6*S*,9*R*,10*S* configuration at multiple levels of theory

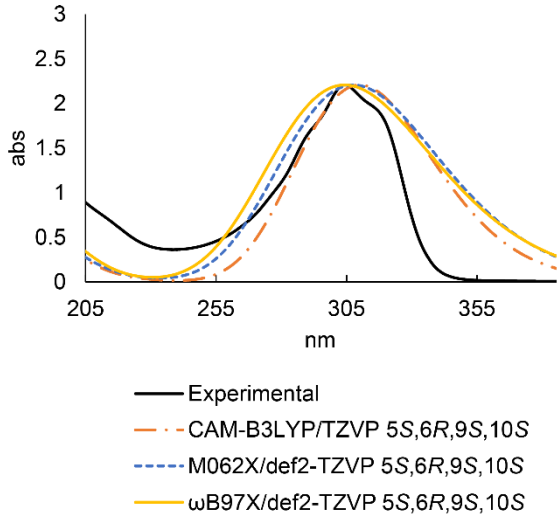

Figure B.47: Experimental UV spectrum of **3.2** (black) in methanol with computed spectra of 5*S*,6*R*,9*S*,10*S* configuration at multiple levels of theory

Appendix C: Supporting Information for Chapter Four

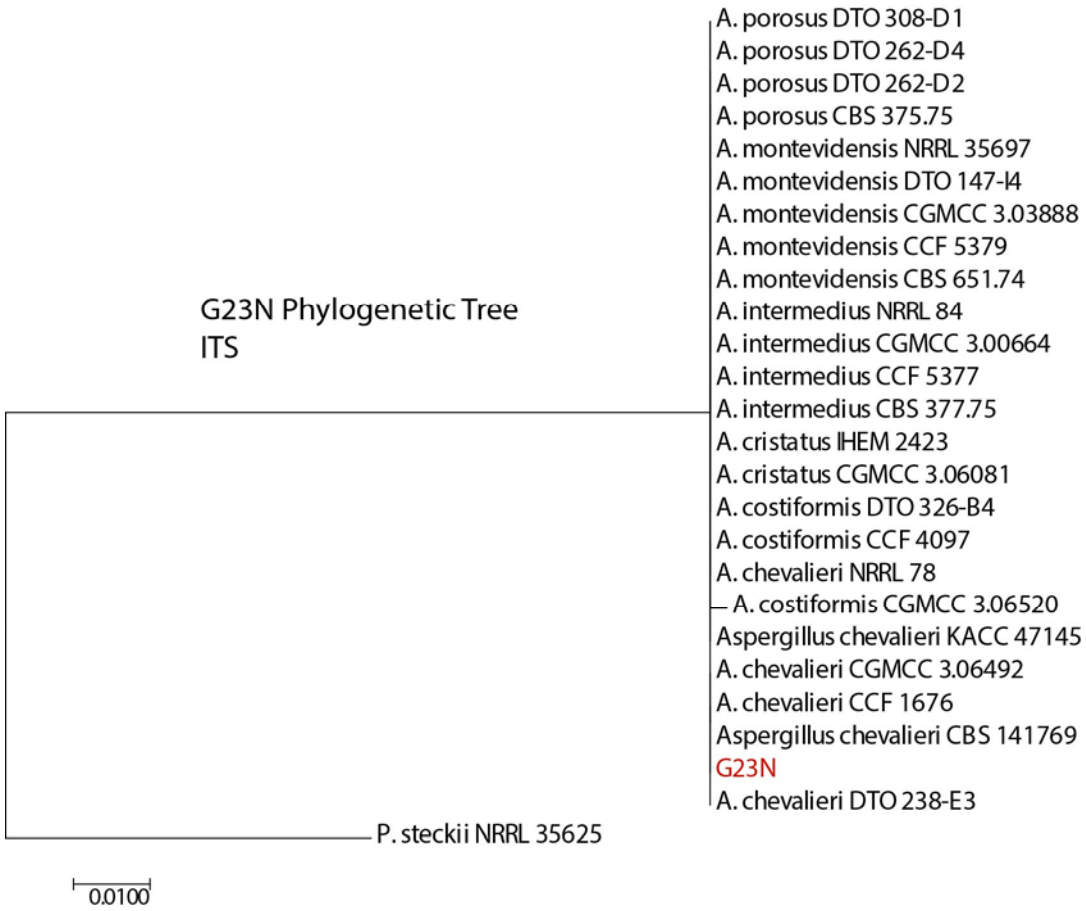

Figure C.1: Phylogenetic tree based off ITS gene fragment

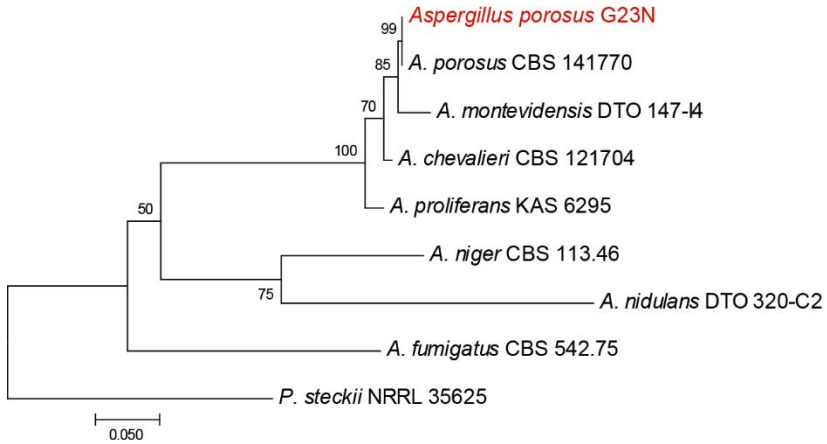

Figure C.2: Phylogenetic tree based off partial beta-tubulin gene fragment

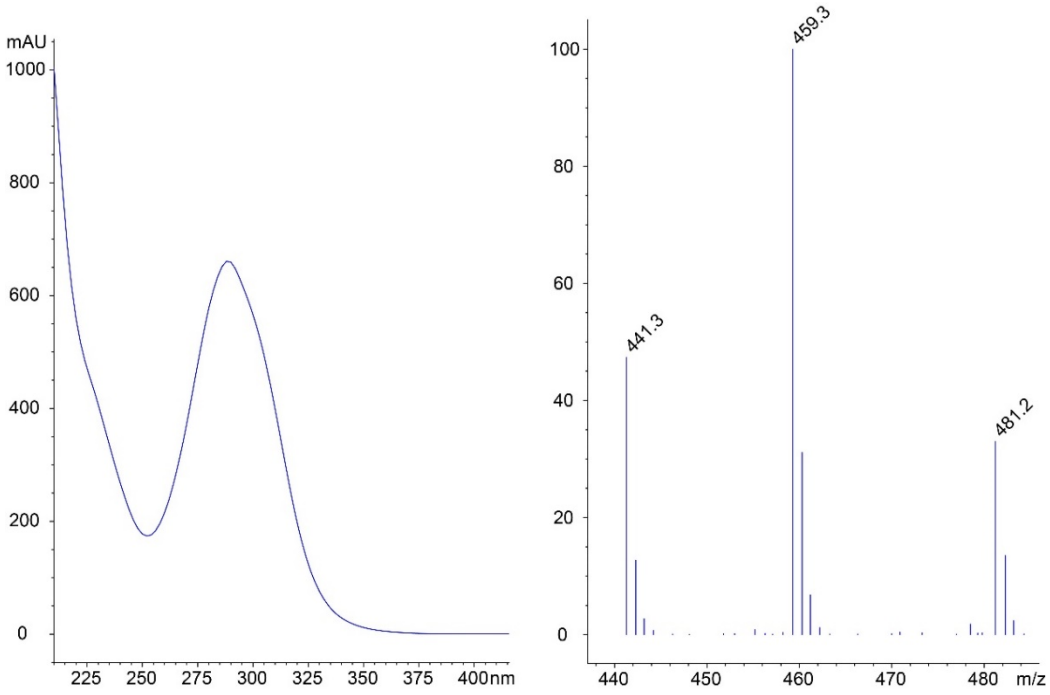

Figure C.3 UV and ESI positive mode low-resolution mass spectrum of **4.1**

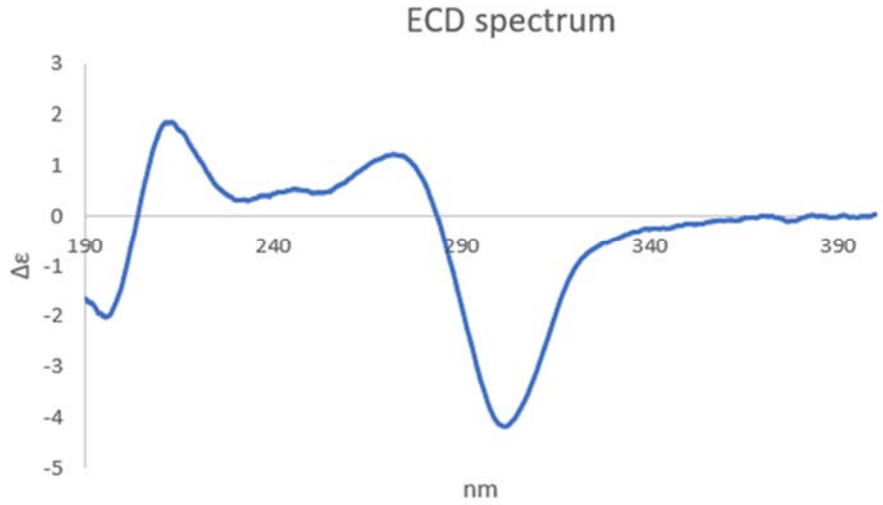

Figure C.4: ECD spectrum of **4.1**

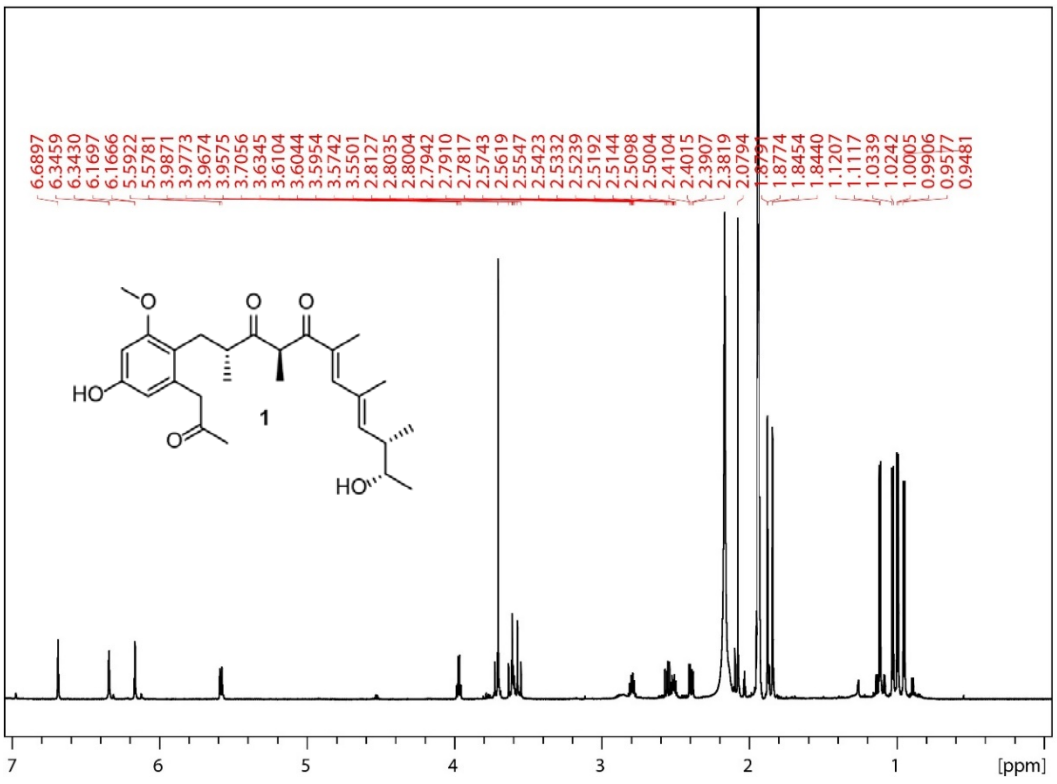

Figure C.5: ^{1}H NMR (700 MHz, CD_3CN) of **4.1**

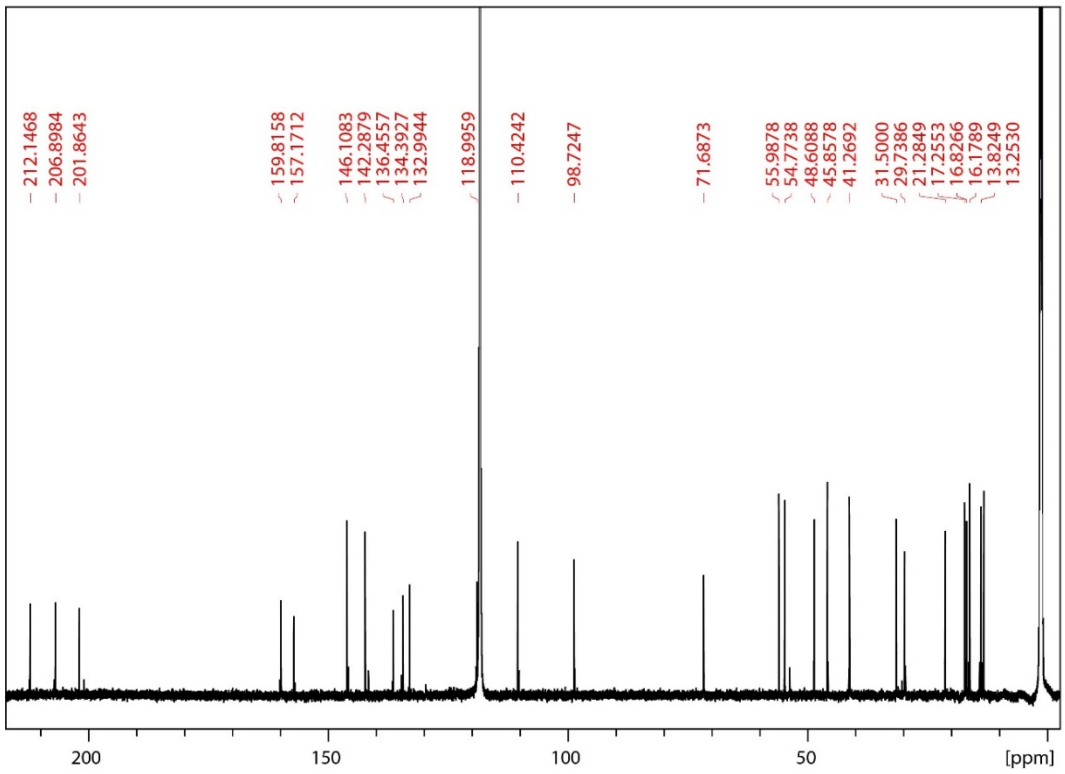

Figure C.6: ^{13}C NMR (700 MHz, CD_3CN) of **4.1**

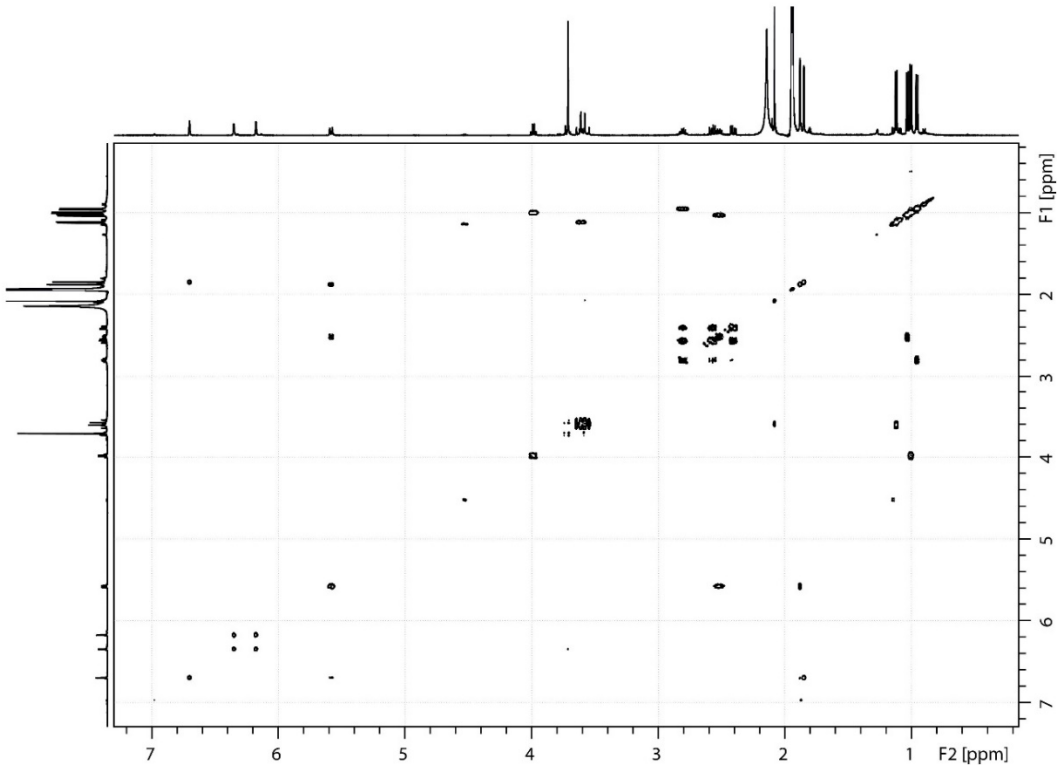

Figure C.7: COSY NMR Spectrum (500 MHz, CD_3CN) of **4.1**

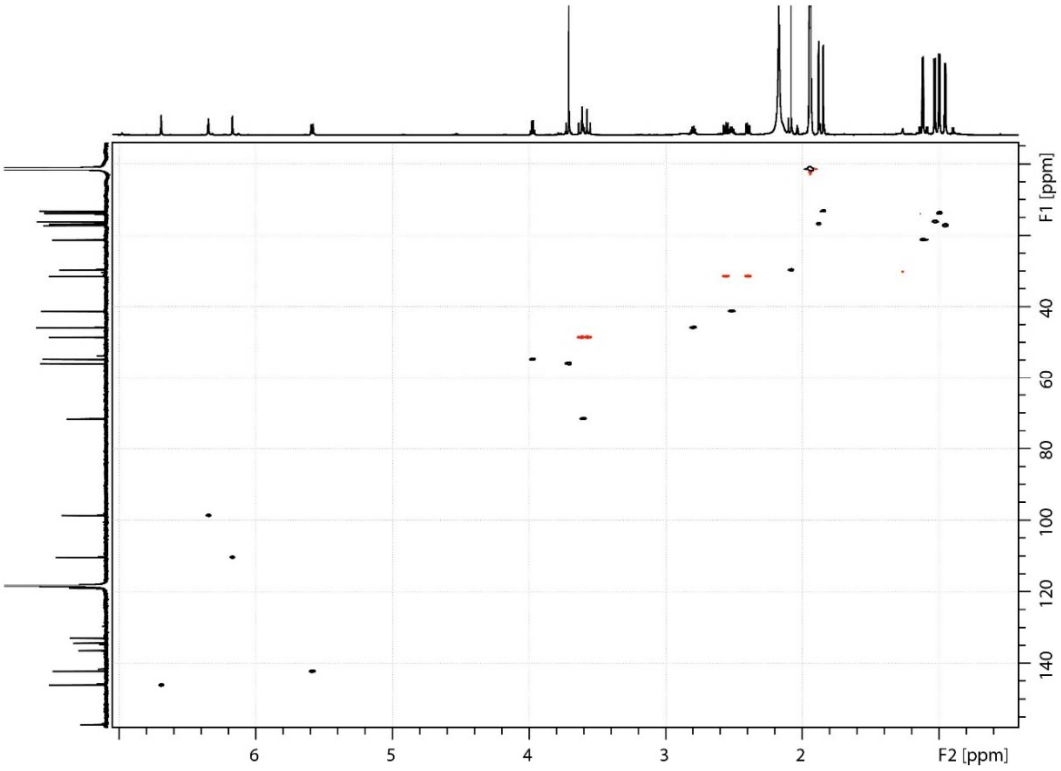

Figure C.8: HSQC-DEPT NMR Spectrum (700 MHz, CD_3CN) of **4.1**

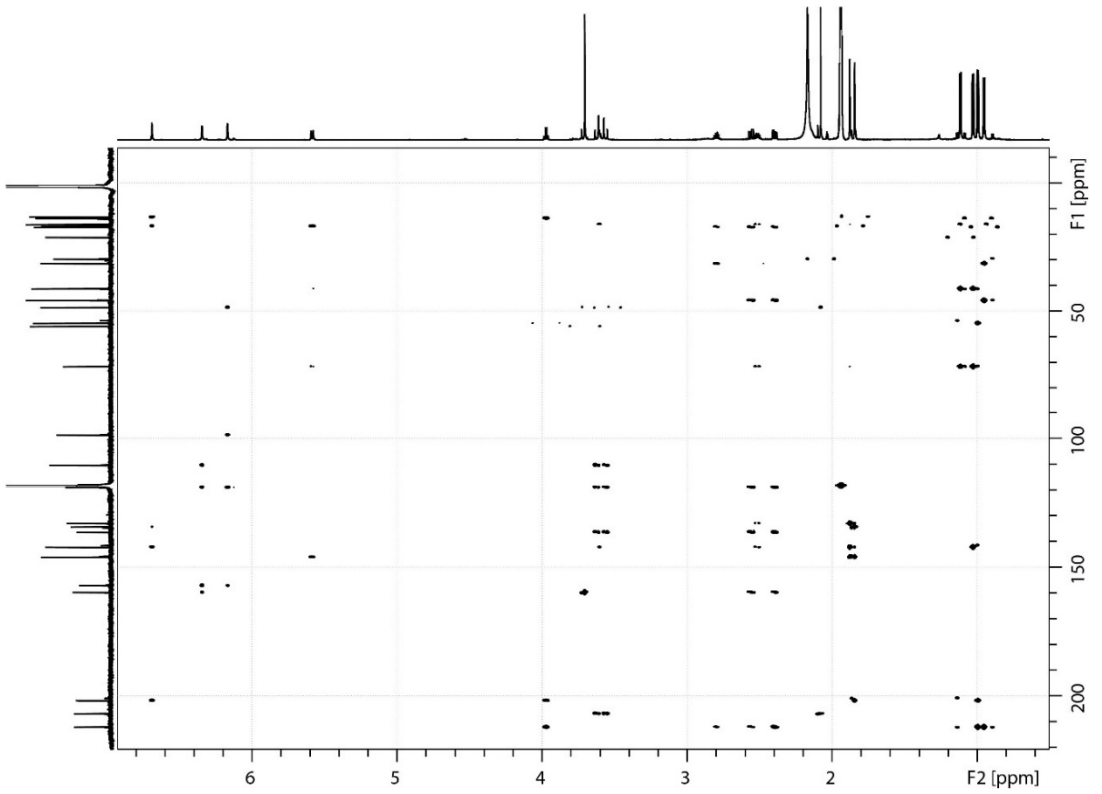

Figure C.9: HMBC NMR Spectrum (700 MHz, CD_3CN) of **4.1**

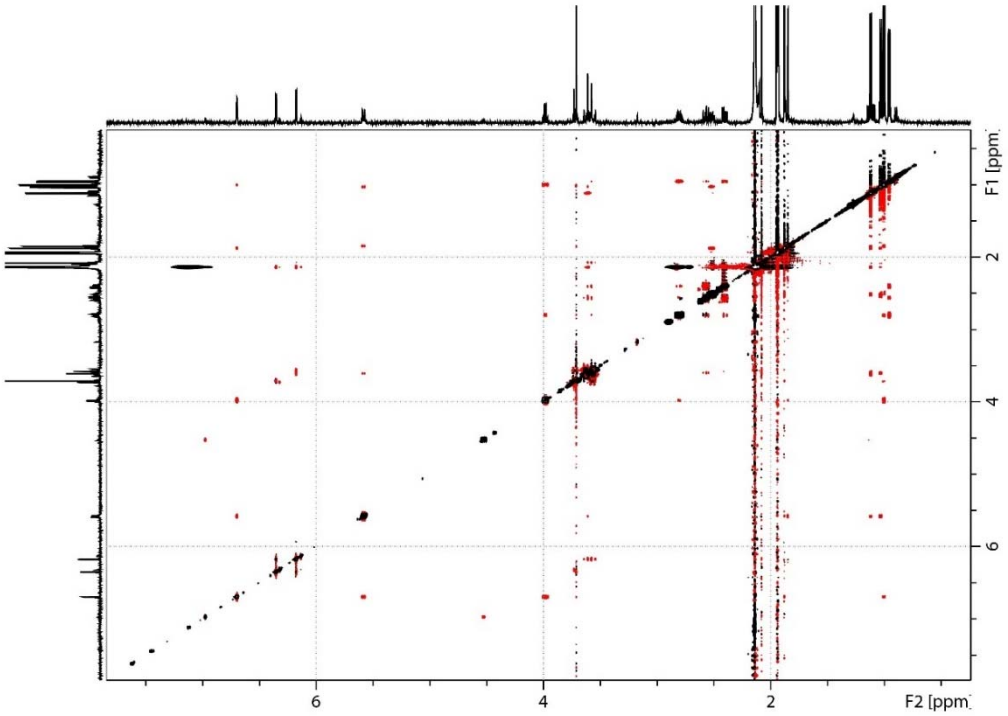

Figure C.10: NOESY NMR Spectrum (500 MHz, CD_3CN, Mixing time = 800 μsec) of **4.1**

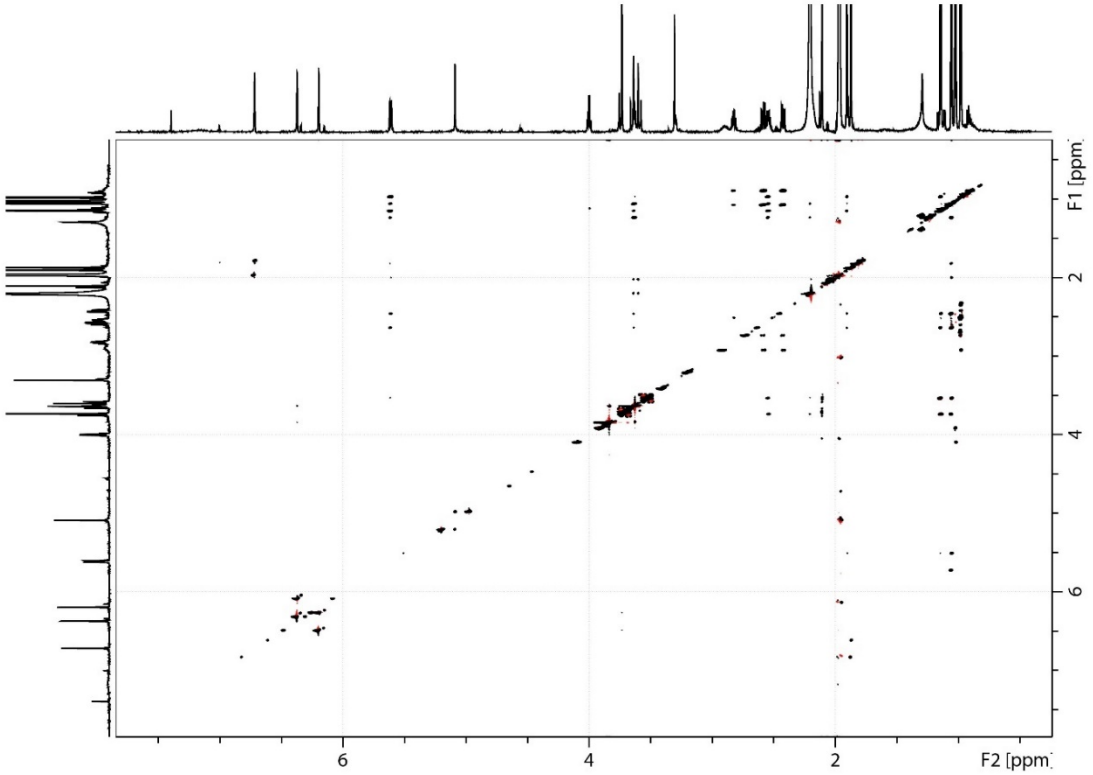

Figure C.11: HETLOC NMR Spectrum (700 MHz, CD_3CN, O1P = 4.7 ppm, O2P = 70.0 ppm) of **4.1**

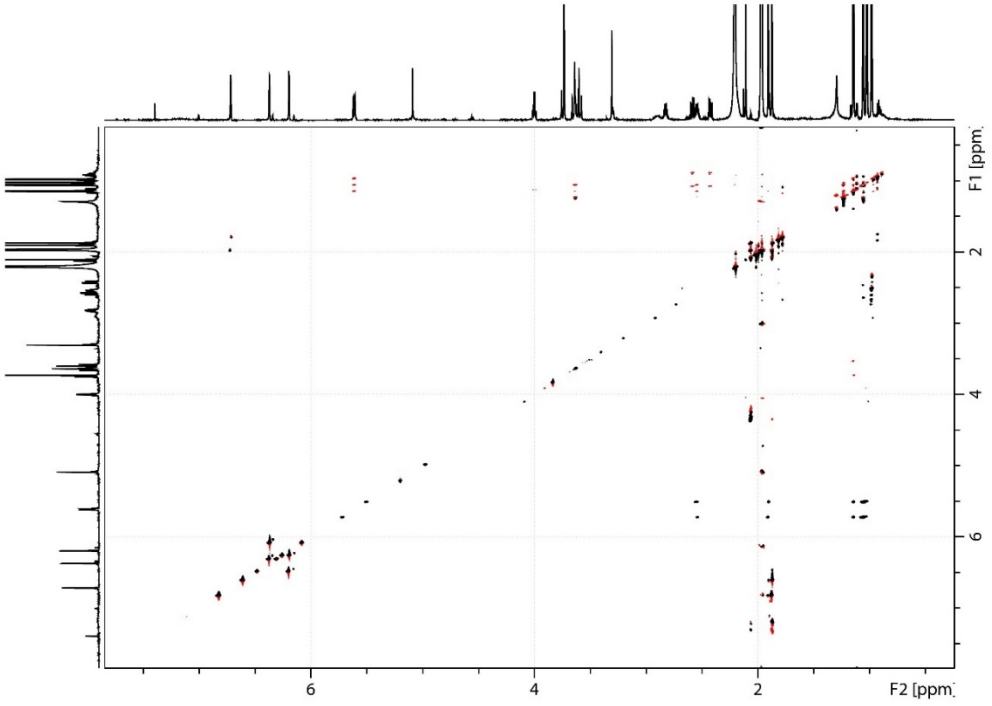

Figure C.12: HETLOC NMR Spectrum (700 MHz, CD_3CN, O1P = 4.7 ppm, O2P = 140.0 ppm) of **4.1**

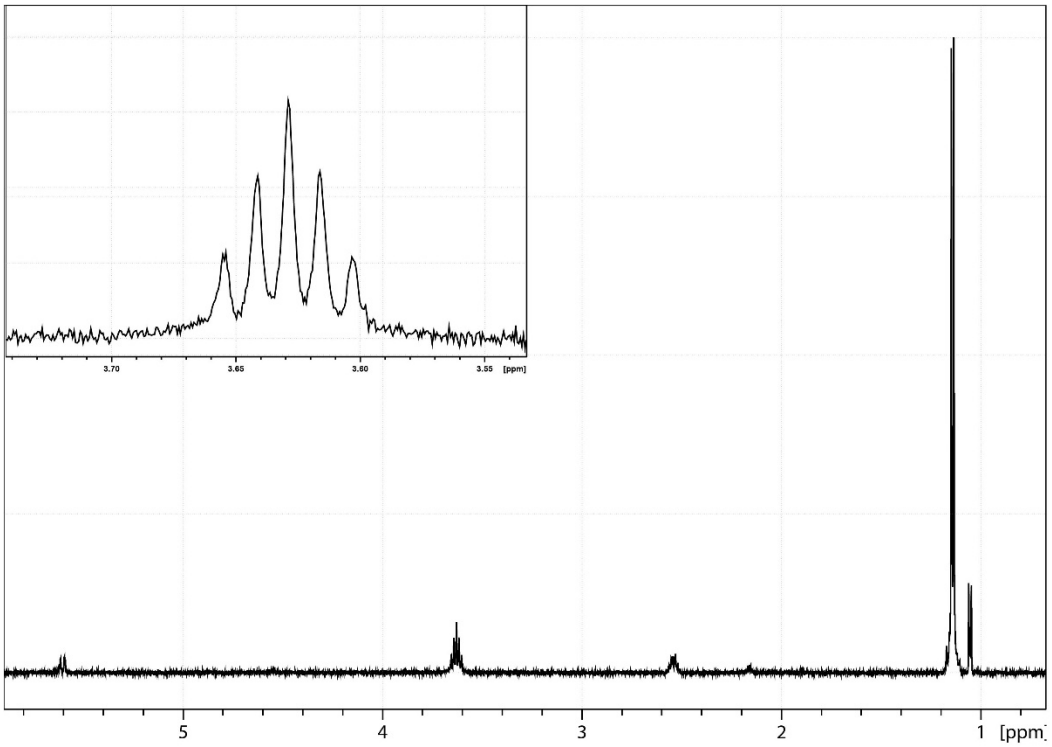

Figure C.13: 1D selective TOCSY NMR Spectrum (500 MHz, CD_3CN, O1P = 1.12 ppm) of **4.1**

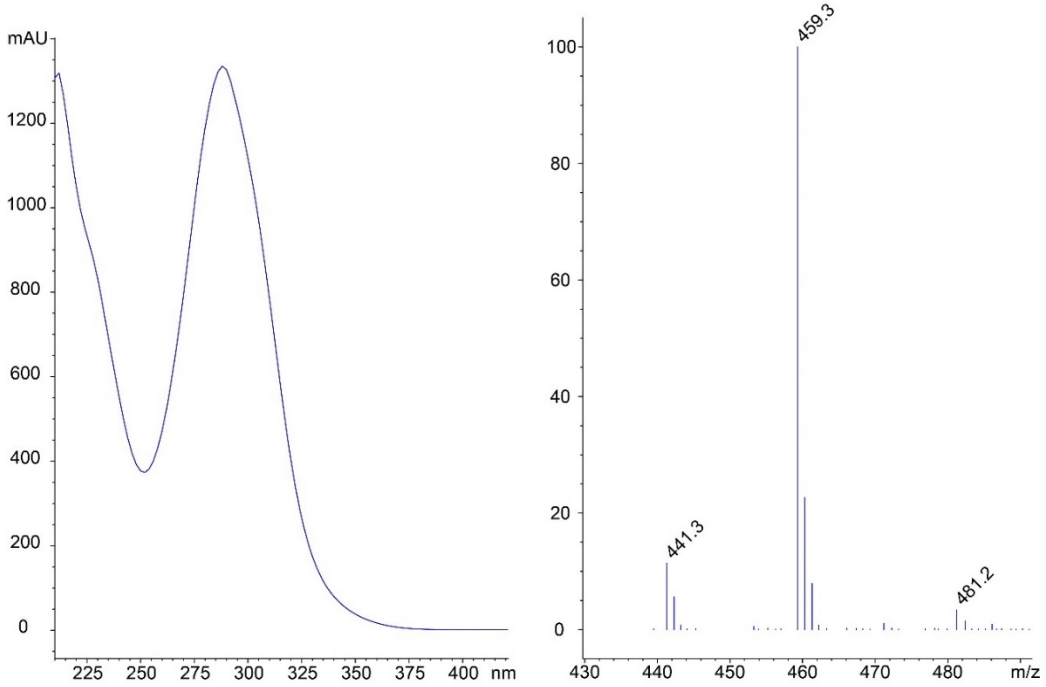

Figure C.14: UV and ESI positive mode low-resolution mass spectrum of **4.2**

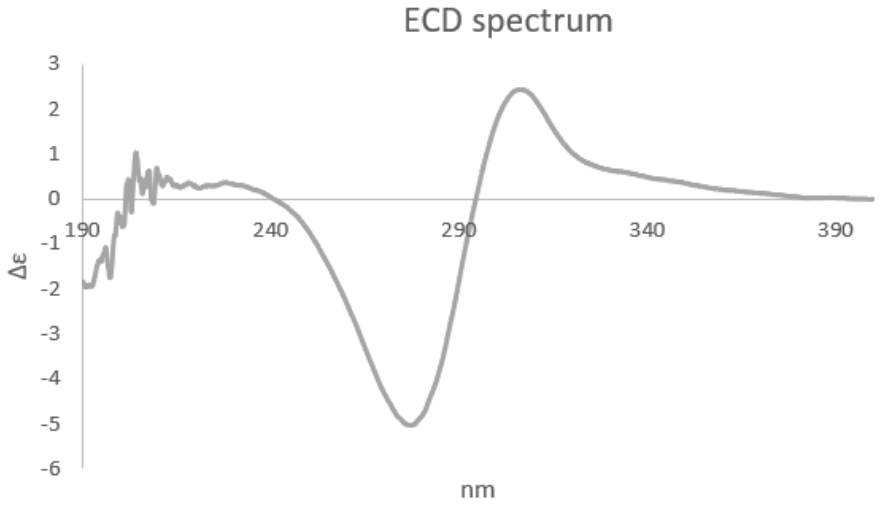

Figure C.15: ECD spectrum of **4.2**

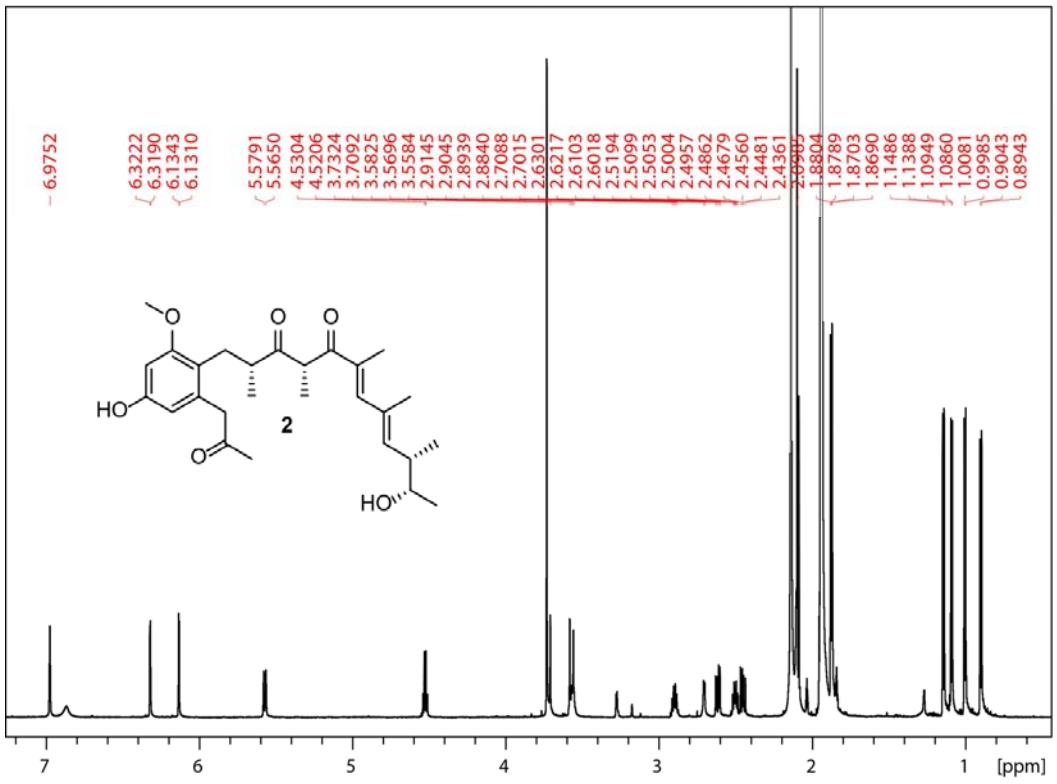

Figure C.16: ^{1}H NMR (700 MHz, CD_3CN) of **4.2**

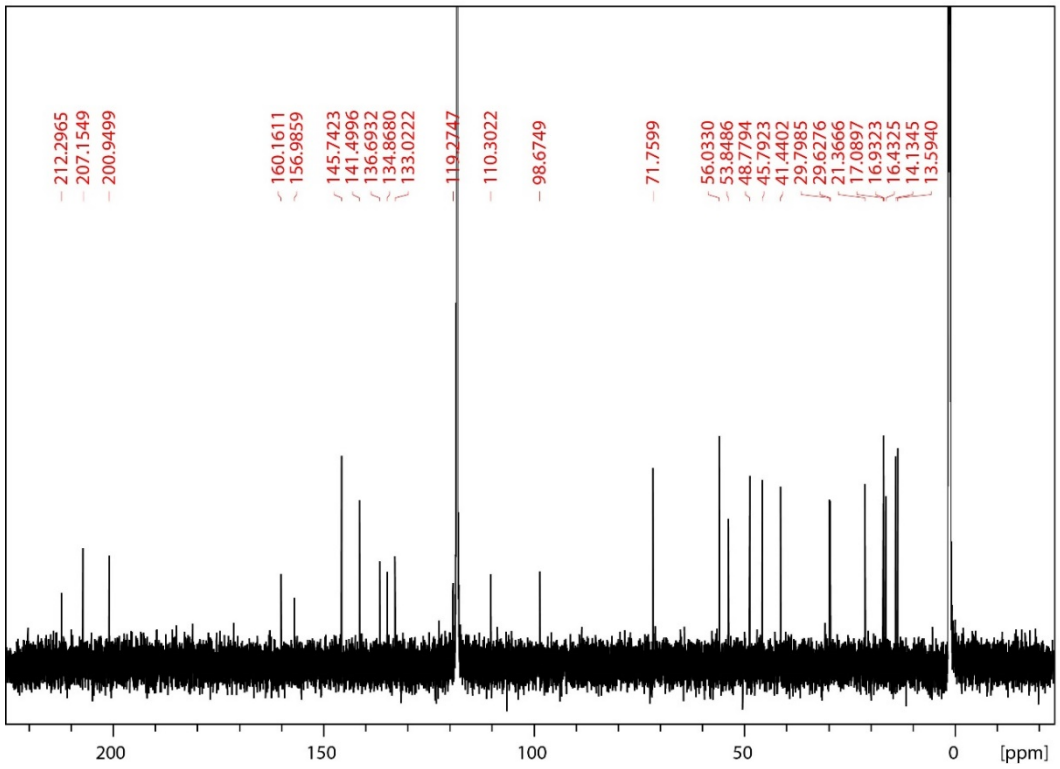

Figure C.17: ^{13}C NMR (700 MHz, CD_3CN) of **4.2**

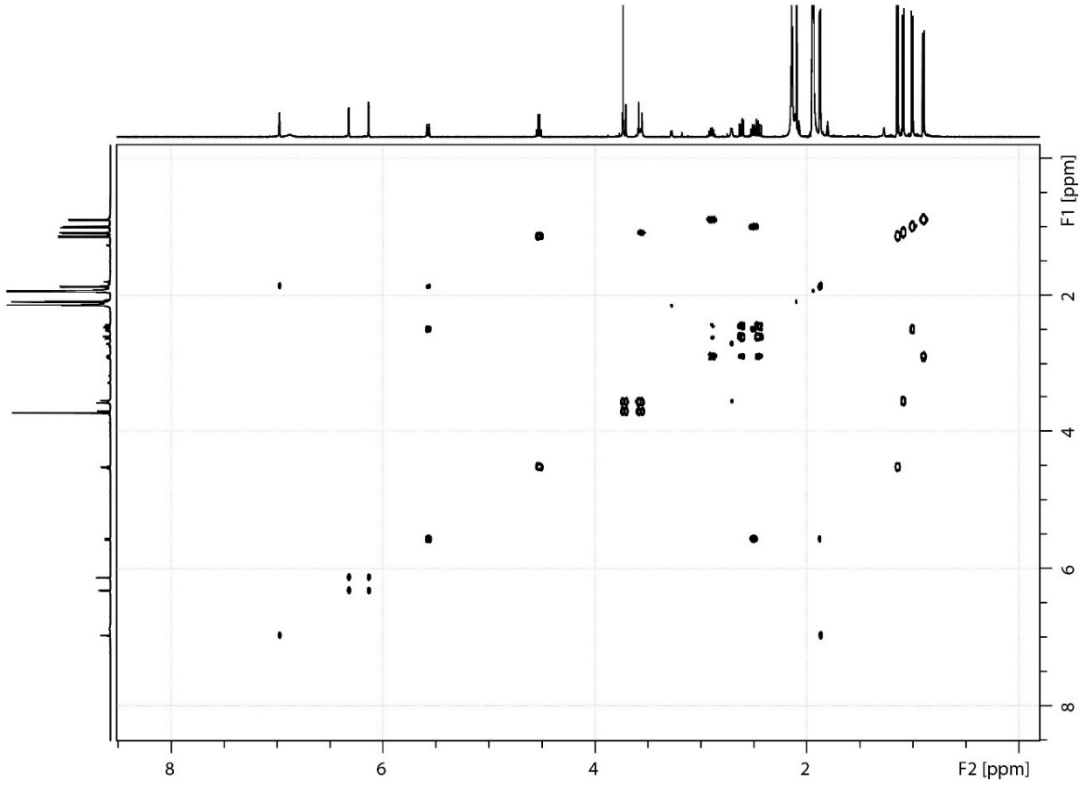

Figure C.18: COSY NMR (500 MHz, CD_3CN) of **4.2**

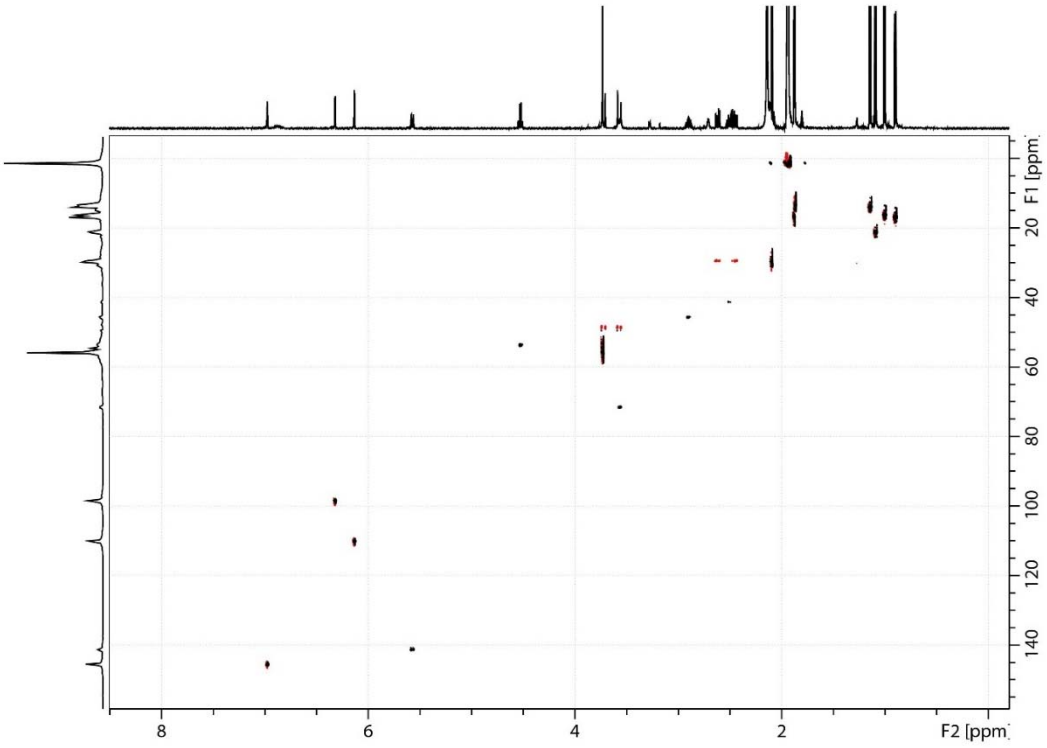

Figure C.19: HSQC-DEPT NMR (500 MHz, CD_3CN) of **4.2**

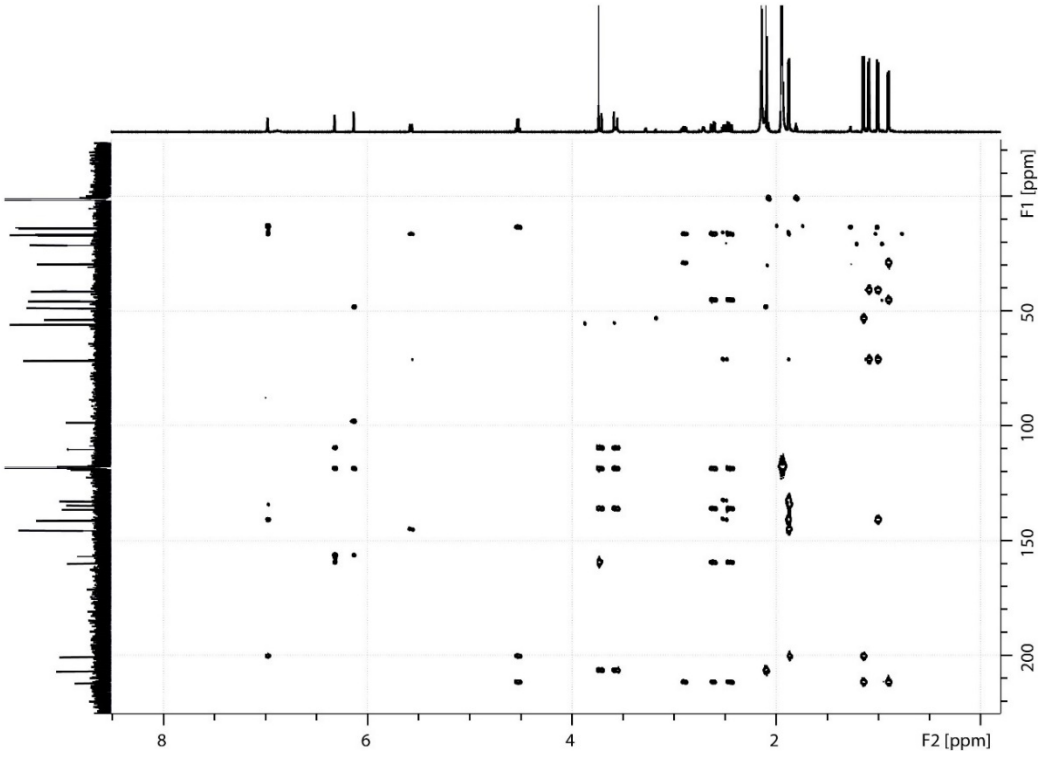

Figure C.20: HMBC NMR (500 MHz, CD_3CN) of **4.2**

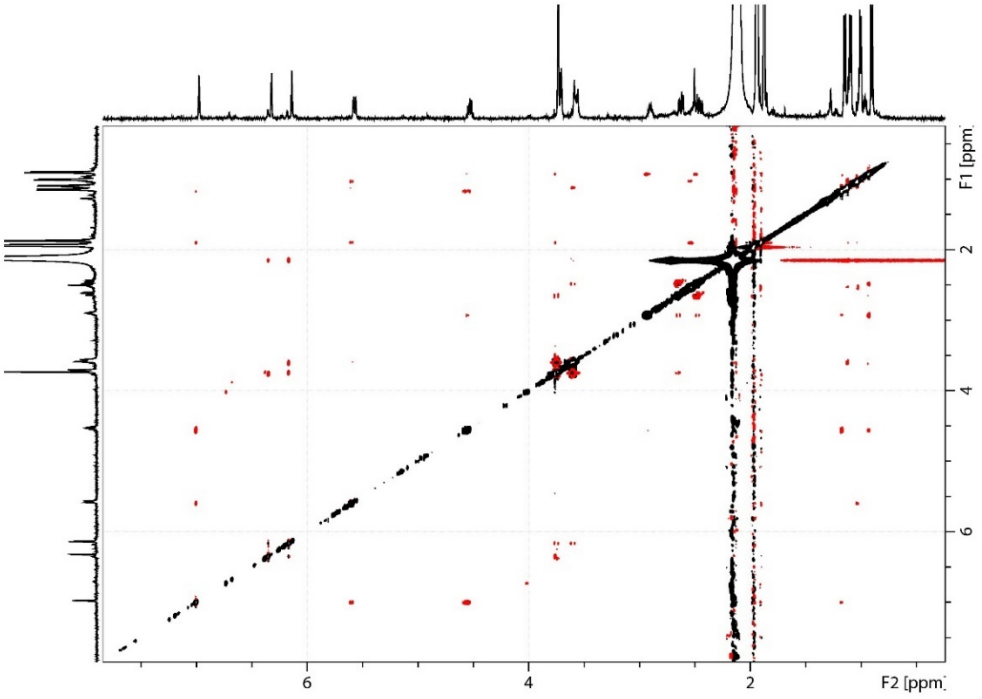

Figure C.21: 2D-NOESY NMR (500 MHz, CD_3CN, Mixing time = 800 μsec) of **4.2**

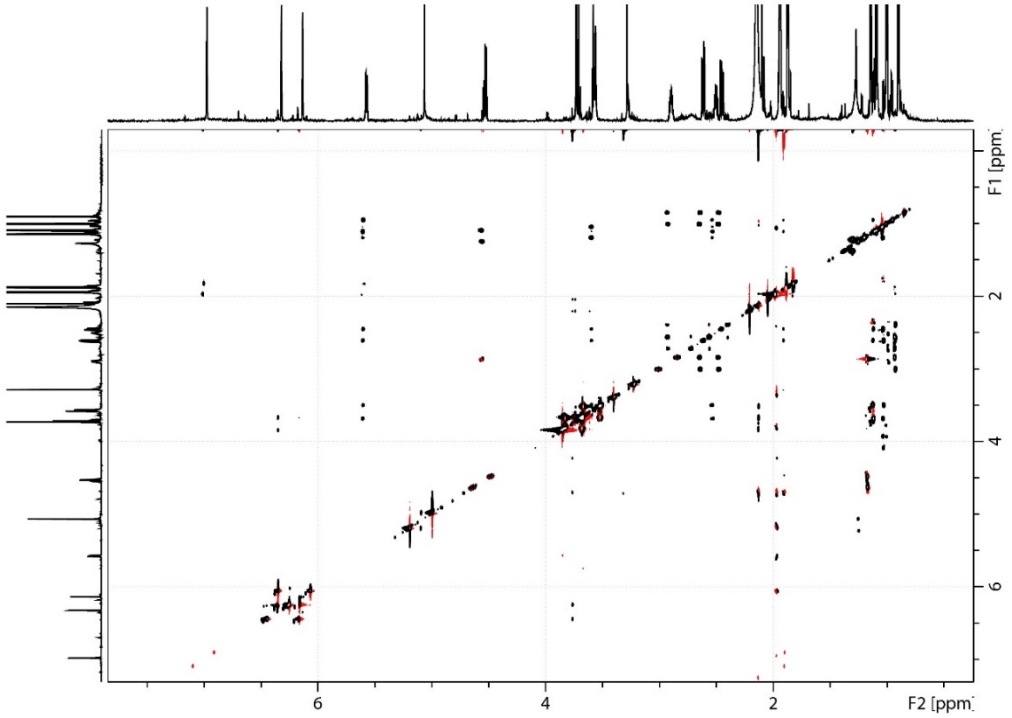

Figure C.22: HETLOC NMR Spectrum (800 MHz, CD_3CN, O1P = 4.7 ppm, O2P = 75 ppm) of **4.2**

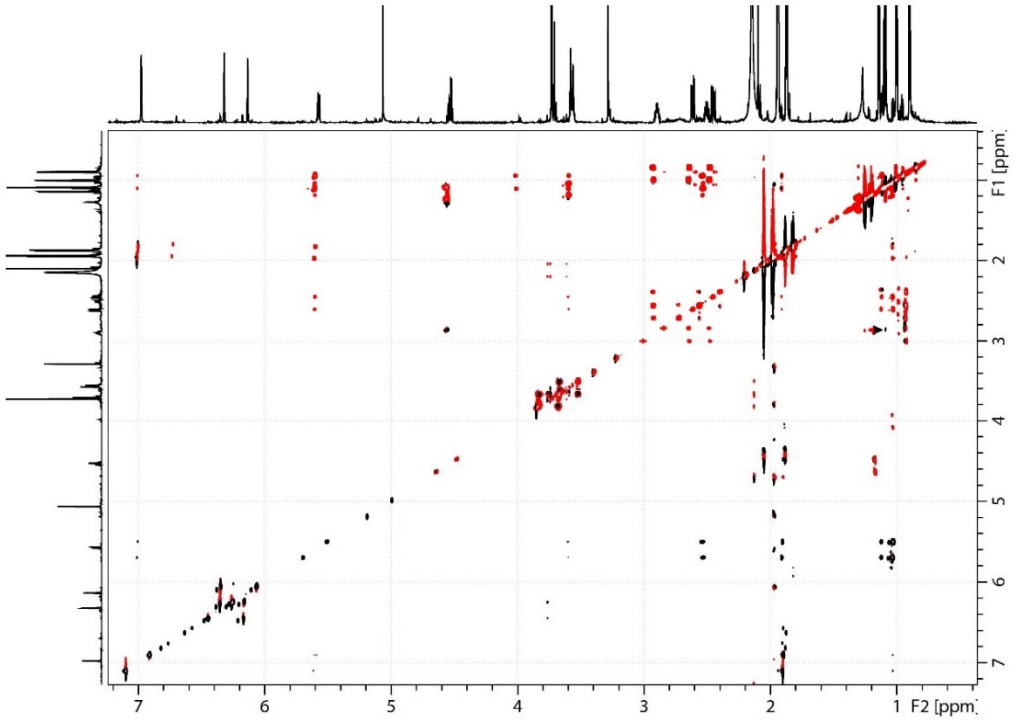

Figure C.23: HETLOC NMR Spectrum (800 MHz, CD_3CN, O1P = 4.7 ppm, O2P = 140 ppm) of **4.2**

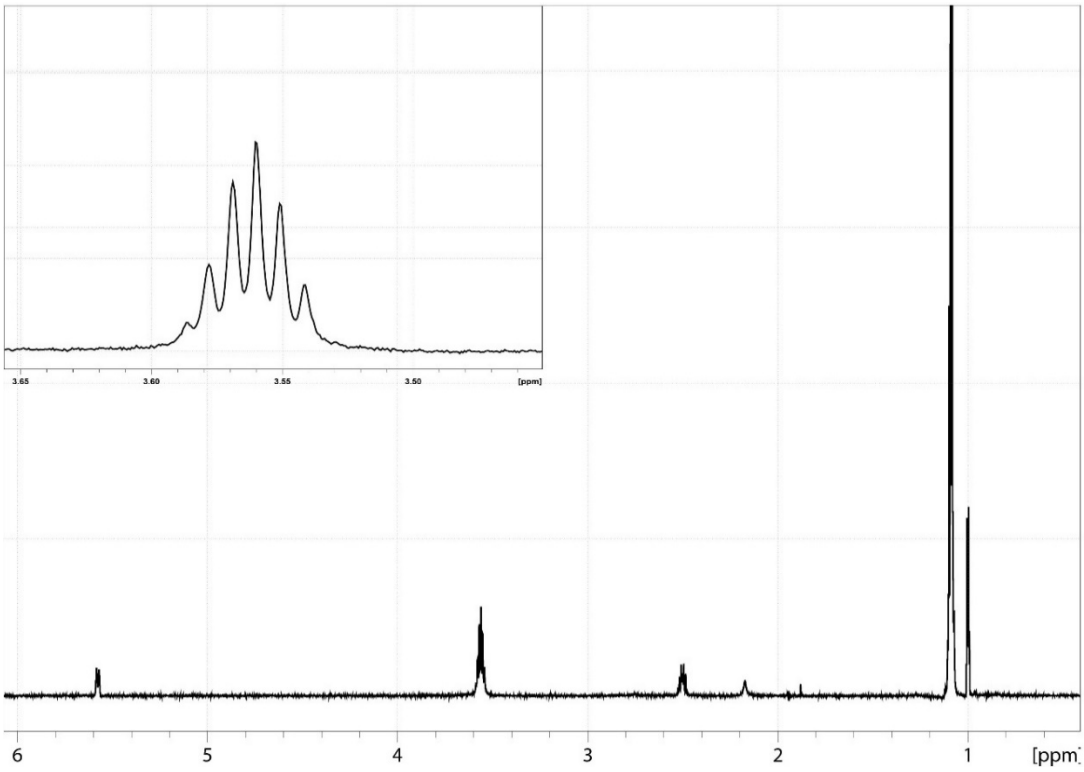

Figure C.24: 1D selective TOCSY NMR Spectrum (700 MHz, CD_3CN, O1P = 1.09 ppm) of **4.2**

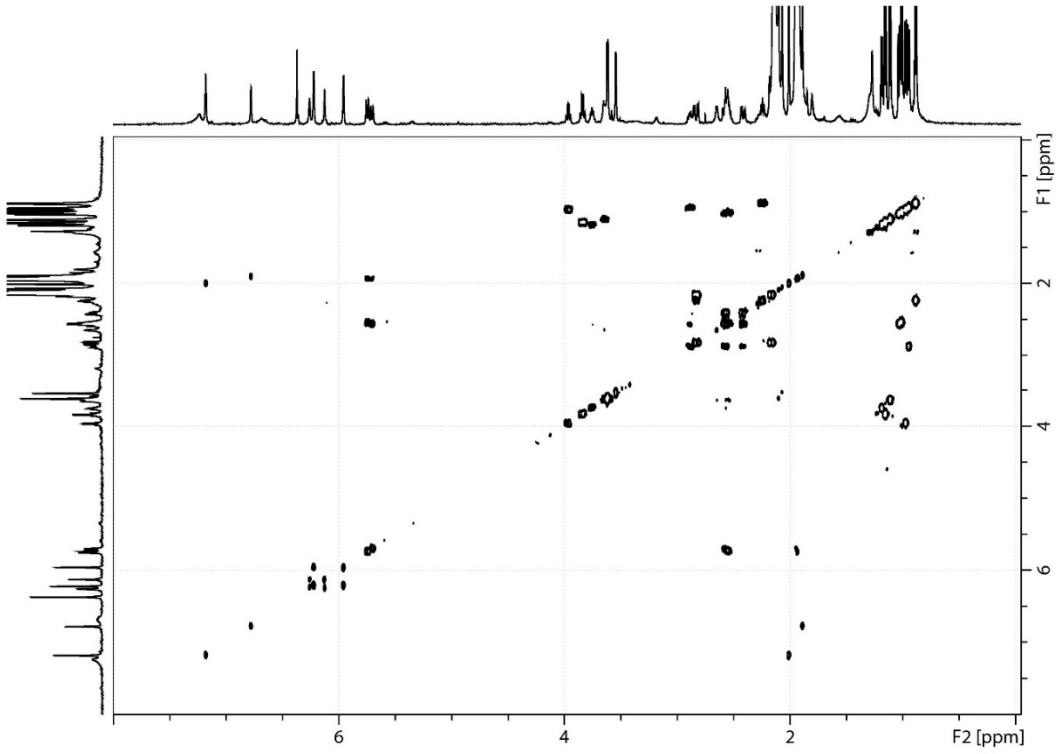

Figure C.25: COSY NMR (500 MHz, CD_3CN) of mixture of **4.3a** & **4.3b**

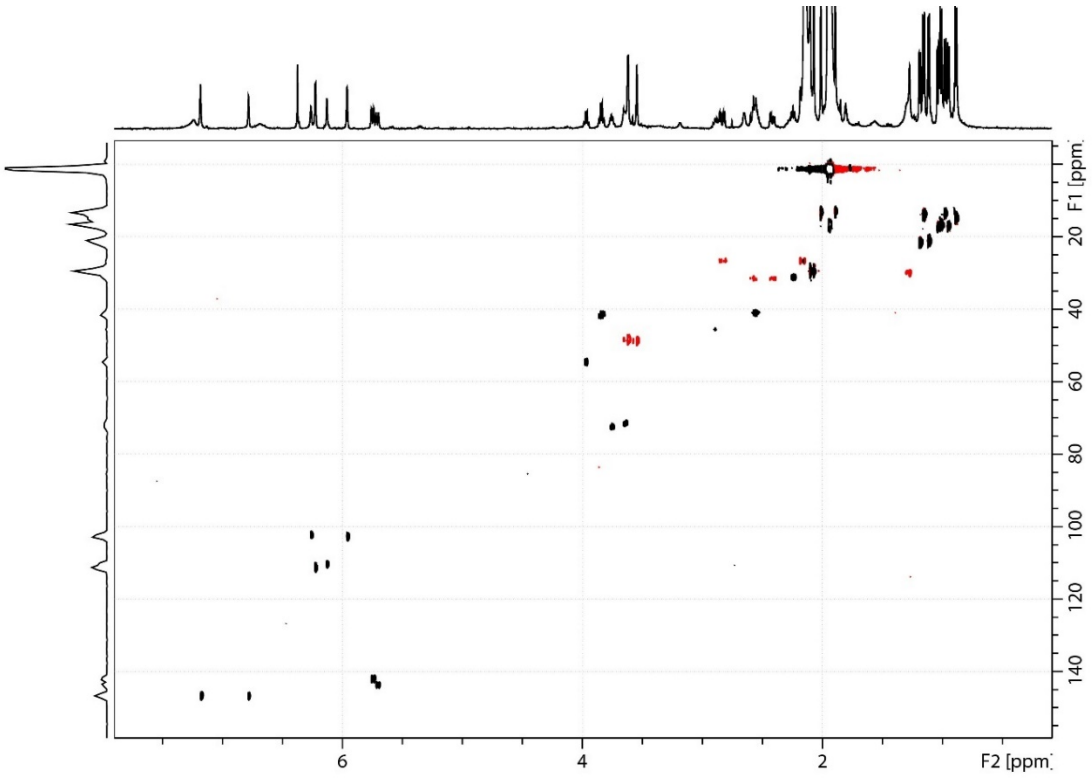

Figure C.26: HSQC-DEPT NMR (500 MHz, CD_3CN) of mixture of **4.3a** & **4.3b**

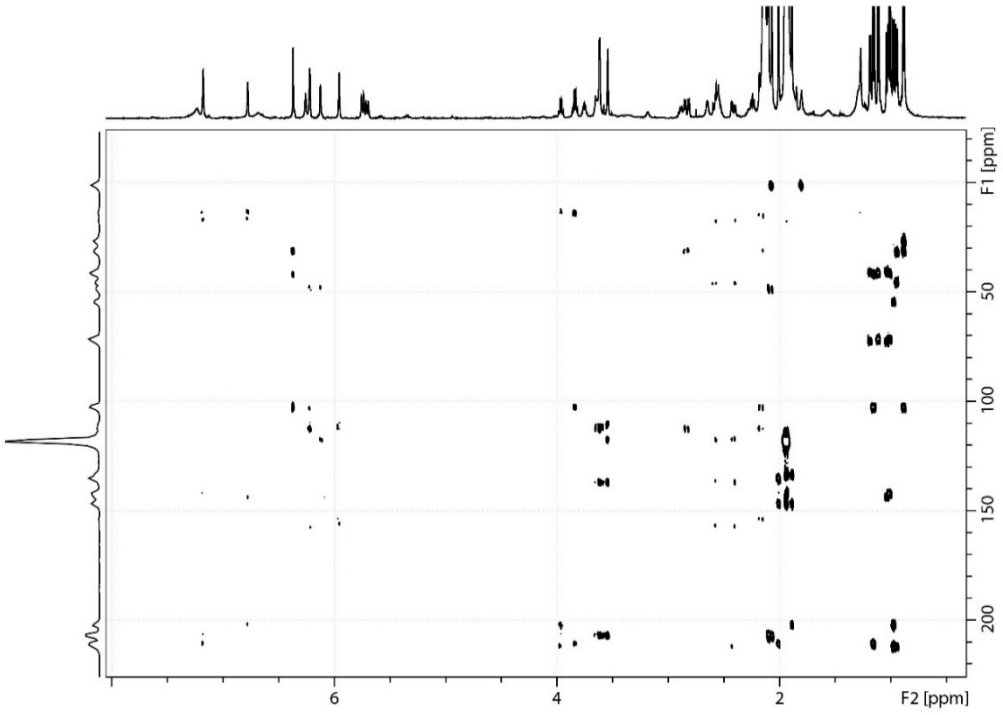

Figure C.27: HMBC NMR (500 MHz, CD_3CN) of mixture of **4.3a** & **4.3b**

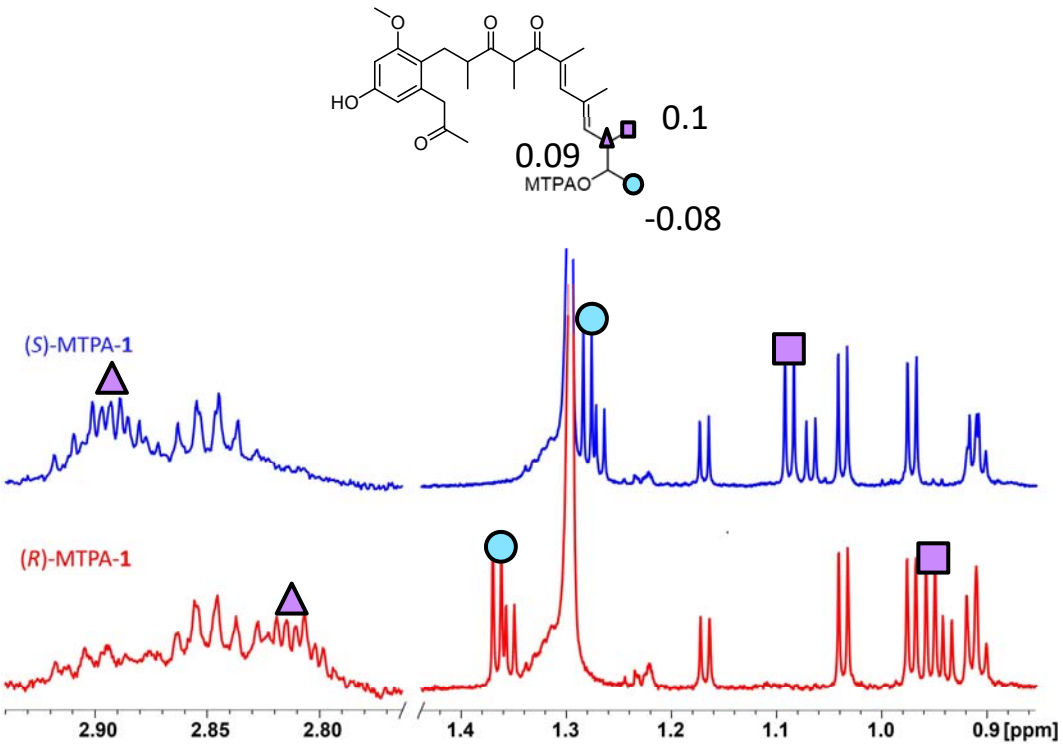

Figure C.28: Key regions of ^{1}H spectrum of Mosher's ester analysis of **4.1**

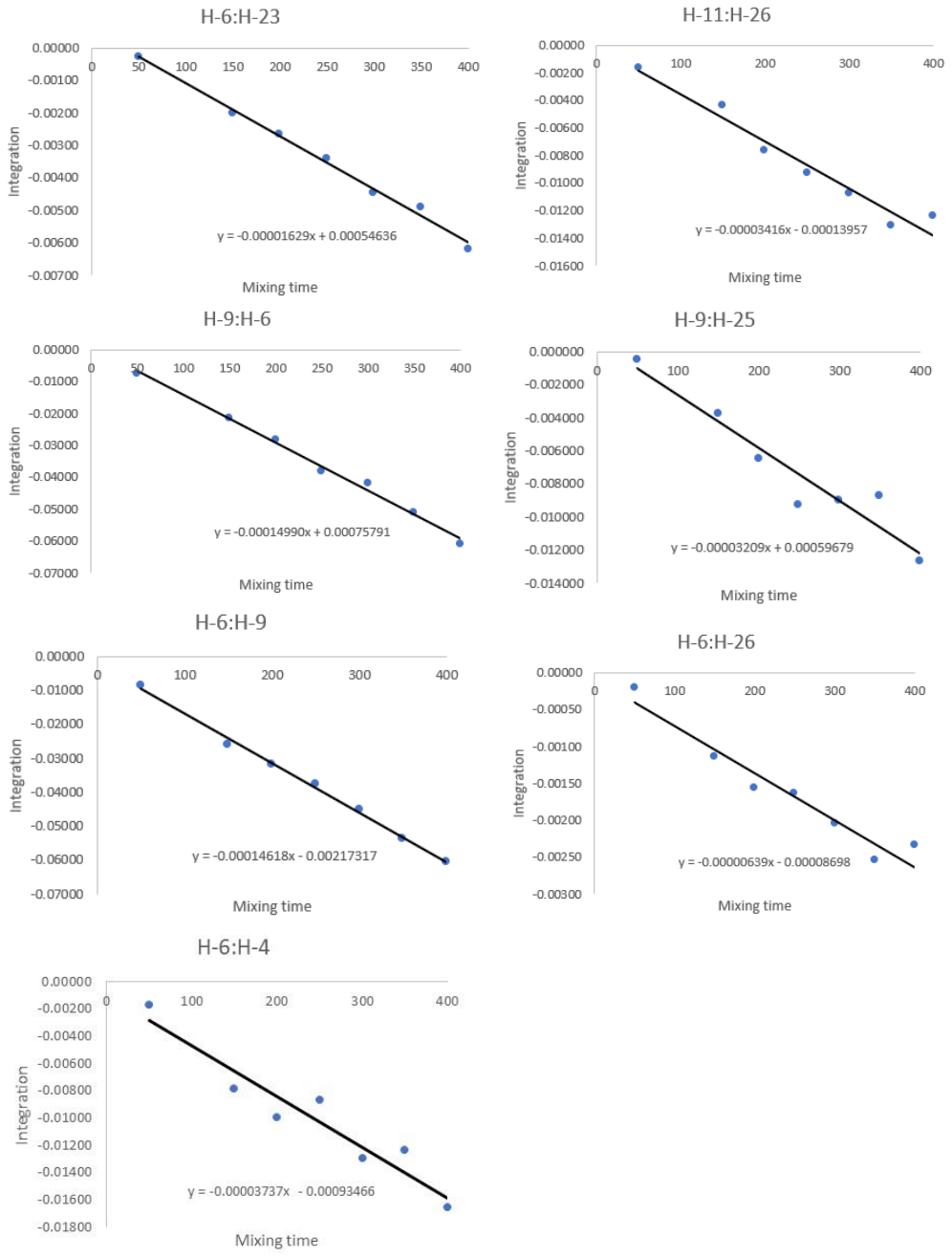

Figure C.29: PANIC (Peak Amplitude Normalization for Improved Cross-relaxation) plots were used to obtain NOE distances between H6-H9, H6-H4, H6-Me26, and H6-Me23

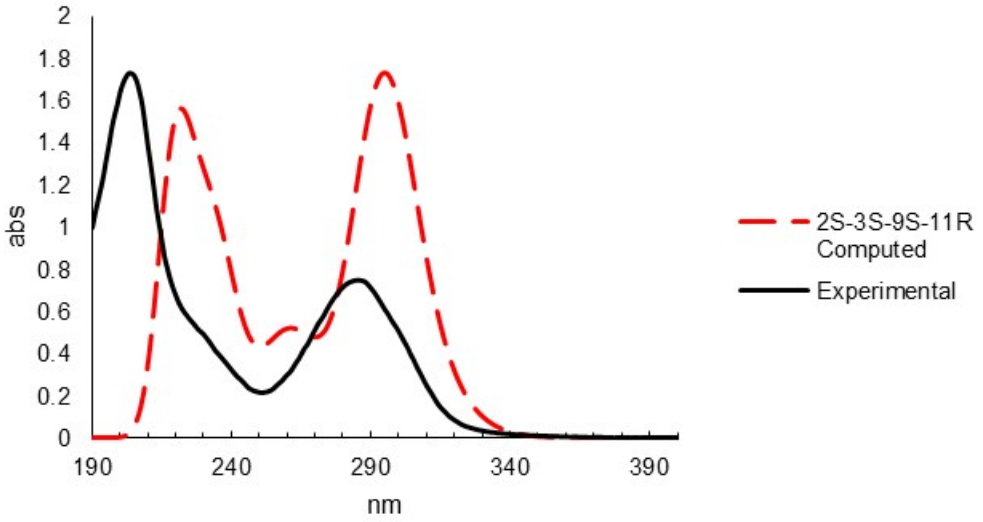

Figure C.30: Comparison of UV spectra of **4.1** to computed spectra at the wB97XD/def2-TZVP level with conductor-like PCM (CPCM) in acetonitrile

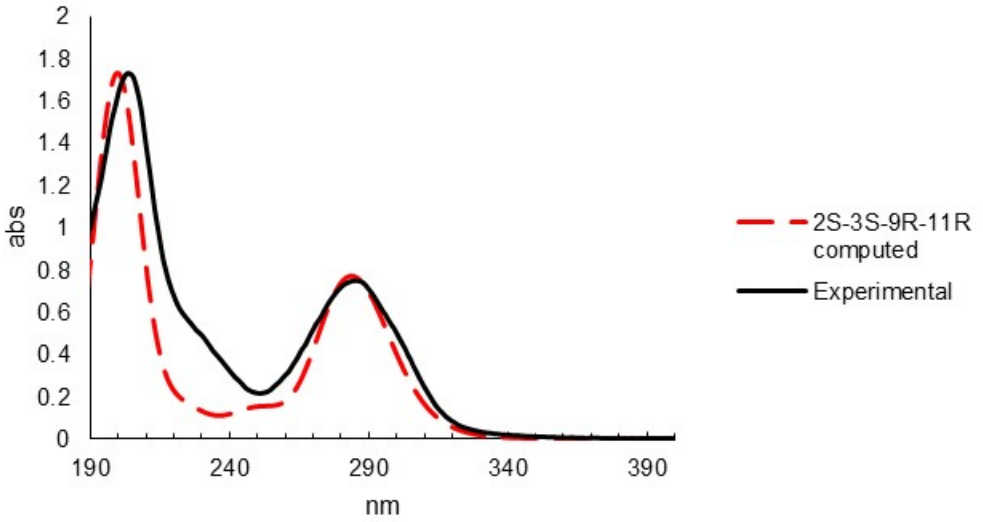

Figure C.31: Comparison of UV spectra of **4.2** to computed spectra at the cam-B3LYP/TZVP level with integral equation formalism PCM (IEFPCM) in acetonitrile

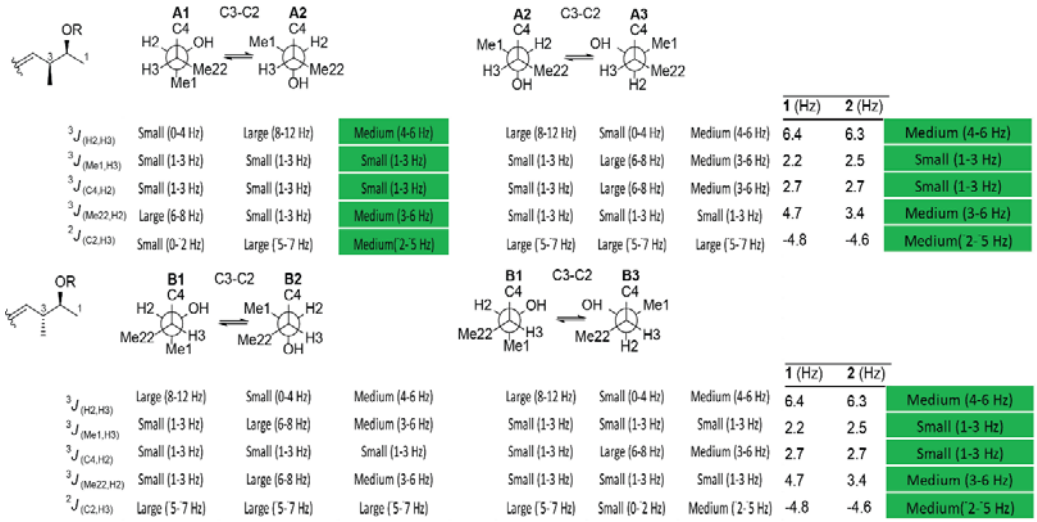

Figure C.32: *J*-based analysis including all conformer pairs that produce a medium $^3J_{(H2\text{-}H3)}$

conf.	rel. kcal solv.	rel. kcal gas
4	0.00	1.00
10	0.79	0.00
6	2.91	1.10
2	9.85	9.54
43	6.85	7.35
1	25.14	17.34

Table C.1: Relative DLPNO-CCSDT single point energies (with and without CPCM solvation in acetonitrile) for all conformers of **4.1** contributing to Stereofitter ensembles (see Table C.2)

conformers in ensemble	ratio	χ^2	AIC
2,43	0.497:0.503	4.35	6.35
1,2	0.482:0.518	5.70	7.70
2,4,43	0.495:0.084:0.421	4.18	8.18
2,6,43	0.493:0.058:0.449	4.27	8.27
2,10,43	0.496:0.053:0.451	4.28	8.28

Table C.2: Conformer numbers, ensemble ratios, χ^2, and Aikake Information Criteria values for Stereofitter solutions for **4.1**